2017

Osteogenic Potential of Poly (l-lactic acid) Scaffolds Prepared by Thermally Controlled Methods on Human Adipose Derived Stem Cells

Harish Chinnasami Shanmugam
Louisiana State University and Agricultural and Mechanical College, hchinn1@lsu.edu

OSTEOGENIC POTENTIAL OF POLY (L-LACTIC ACID) SCAFFOLDS PREPARED BY THERMALLY CONTROLLED METHODS ON HUMAN ADIPOSE DERIVED STEM CELLS

A Dissertation

Submitted to the Graduate Faculty of the
Louisiana State University and
Agricultural and Mechanical College
in partial fulfillment of the
requirements for the degree of
Doctor of Philosophy

in

The Department of Mechanical and Industrial Engineering

by
Harish Chinnasami Shanmugam
B.E., Mechanical Engineering, Anna University, 2010
August 2017

Acknowledgements

It is a pleasure to thank the many people who made this dissertation possible. I would like to start by thanking my advisor Dr. Ramachandra V Devireddy. His passion, inspiration and guidance, has helped me learn and complete my research in a pleasant and straightforward manner. I sincerely thank him for providing the necessary resources and motivation, which has nurtured my research aptitude. I would like to thank my committee members Dr. Ingmar Schoegl, Dr. Todd Monroe, Dr. Manas Gartia and Dr. Dennis Landin for dedicating their time and crucial guidance to help me complete my dissertation.

I would like to thank Dr. Daniel Hayes who helped me understand the basic concepts of tissue engineering and its significance in future research. I sincerely thank Dr. Jeffery Gimble at LaCell, New Orleans, LA for providing us with sufficient human adipose stem cells, which were vital to my experiments. I would like to thank Dr. Kenneth Matthews from Physics Department, LSU who taught and guided me to use his X-ray micro-tomograph at his Radioisotope Imaging Laboratory. I thank Dr. Ted Gauthier for lending me many of the equipments like autoclave, freeze-dryer, plate reader etc., without which my experiments would have been impossible.

Many of my colleagues, lab-mates and friends have provided academic, intellectual and moral support during my doctoral program. I thank Ammar Qureshi, George Idicula, Anoosha Forghani, and so many other people with whom I have worked in past years at LSU. I wish to thank Forum Shah for practically teaching me various aseptic methods in cell culture. I especially thank my lab-mate Mulla Shahensha Shaik, who helped me solve many roadblocks over the course of my experimental projects.

Last but not least I would like to thank my parents and family back in India, for providing me with much needed emotional support during my doctoral program. Finally, I'd like to thank my parents Shanmugam Chinnasami and Shanthi Aiyasami for providing me with unconditional love at every stage of my life. I would like to dedicate my doctoral dissertation and all my future achievements to my parents.

This research was supported by Economic Development Assistantship (EDA) granted by LSU Graduate School. I would like to thank them for their support.

Table of Contents

List of Tables

List of Figures

Abstract

Thermally Induced Phase Separation (TIPS) method was used to make porous three-dimensional PLLA scaffolds. The effect of imposed thermal profile during freezing of the PLLA in dioxane solution on the scaffold was characterized by their micro-structure, porosity (%), pore-sizes distribution and mechanical strength. The porosity (%) decreased considerably with increasing concentrations of PLLA in the solution, while a decreasing trend was observed with increasing cooling rates. The mechanical strength increases with increase in PLLA concentration and also with increase in the cooling rate for both types of solvents. Therefore, mechanical strength was increased by higher cooling rates while the porosity (%) remained relatively consistent. Scaffolds made using higher concentrations of PLLA (7% and 10% w/v) in solvent, showed better mechanical strength which improved relatively with increasing cooling rates. This phenomenon of enhanced structural integrity with increasing cooling rates was more prominent in scaffolds made from higher initial PLLA concentrations. Human adipose derived stem cells were cultured on these scaffold (7 and 10% w/v) prepared by TIPS at all cooling rates to measure the cell proliferation efficiency as a function of their micro-structural properties. Mean pore-sizes played a crucial role in the cell proliferation than % porosity since all scaffolds were > 88 % porous. The viability of human adipose tissue derived adult stem cells cultured on 7% PLLA scaffolds cooled at 10˚C/min was also shown to be comparable with corresponding culture conditions without scaffolds for a period of 42 days. Scaffolds made from 10% PLLA in dioxane and cooled at 10°C/min favored cell proliferation compared to scaffolds made from other parameters. This structurally characterized scaffolds for bio-response was used for osteogenic studies and found that PLLA scaffolds are ‘osteoinductive’ when cultured in stromal media in vitro. Osteo-conductivity of PLLA on hASCs was further enhanced with osteo-inductive media.

Chapter 1 : A Review of Biomaterials used in Scaffolds for Osteochondral Grafting

1.1. Introduction

A remarkable phenomenon of human skeletal system is its restorative healing capacity with immobilization [1]. However incomplete healing can occur in specific sites of injuries at lower limb joints. This leads to a condition called psuedoarthrosis, where complete bone fusion to its original form is impossible without surgical implantation of external grafts [2]. Three-dimensional scaffolds are used to make tissue engineered bone grafts for treating traumatic defects by surgical implantation [3] and by controlled drug delivery [4]. In rare cases bone grafting was used to treat tumors by curettage and cementation methods [5]. Scaffolds used in making such implantable grafts is that it should micro and macro-structurally mimic the recipient host tissue. Moreover, the scaffolds material should be bio-compatible providing no cytotoxicity as well as facilitating in vivo integration after implantation. The pore-size and porosity play a crucial role in cellular growth and differentiation of progenitor cells (stem cells) [6]. A viable bone graft should possess the following integral properties: *Osteo-induction*: Induce the differentiation of osteo-progenitor cells (stem cells) into osteogenic lineages; *Osteo-conduction*: Favorably influence the proliferation of osteoblasts and blood vessel incursion leading to the formation of osteoid; and *Osteo-genic*: The implanted graft material should itself integrate with the host bone simultaneously maintaining the viability of cells.

First described bone grafting was in 1668. A cranial defect of an injured soldier was repaired using dog's skull [7]. An ever-increasing demand for bone grafting has followed since then (due to trauma, tumor excision, spinal fusion etc.,) calling for expanded research for skeletal reconstructions. Musculoskeletal defects restricted the lives of over 1.5 million Americans in 2015

and the numbers have only increased during the intervening years [8]. About 2.2 million bone grafting procedures are done worldwide annually [9]. Many of these disorders require surgery to accelerate or improve bone repair. One common example is spinal fusion surgery recommended to treat back pain secondary to scoliosis, spinal stenosis, degenerative disc disease, infectious processes, tumors, and trauma. At present, the "gold standard" for spinal fusion repair is autologous bone, usually harvested from the iliac crest of the individual [10]. Nevertheless, this is far from a perfect solution.

Autografts (previously known as homografts) are the most osteogenic material containing live osteocytes, increasing the chances of fusion. Although autografting may seem like a convenient ideal method for bone grafting, they are limited by numerous practical disadvantages. High chance of morbidity in the donor (iliac crest, rib, fibula etc.,) as well as host (injured) sites. Rates of psuedoarthrosis are from 5 to 35% in the healed site. These are only further complicated by low availability, risk of blood loss and transfusion, increased surgical time and cost [11]. In 30% of patients, the donor site becomes infected, bruised, fractured, or painful following the surgery [12]. Indeed, when a patient requires autograft bone for multiple spinal fusions, the iliac crest may not provide sufficient material [13]. While there are alternative materials available all face a common limitation; none display osteogenic capability. Allograft bone from cadavers can be sterilized, stored, and used in the operating room as needed. These materials can be pre-shaped for specific use or powdered, allowing them to be applied as a paste at the surgical site [14]; however, allografts can cause inflammation, elicit an immune response, and have been an infectious source in a limited number of cases [15]. Because allograft bone is sterilized, it no longer contains viable native bone forming cells (osteoblasts, osteocytes) and lacks osteogenic properties. In clinical trials, allograft bone is inferior to autograft bone in multilevel spinal fusions [16].

A group in National University of Singapore collaborating with Temasek Polytechnic has developed, calibrated, and patented a novel PCL-Ceramic (HA/TCP) using Fused Deposition Modelling (FDM) technique. These FDM fabricated implants are being used as burr hole plugs in cranioplasty and to re-generate iliac crest after autograft was taken. Clinical outcomes were positive with no patients developing adverse side-effects a year after surgery [17]. Therefore, it is extremely important to have better understanding of various factors involved in tissue engineering a viable bone graft. This review reports some commonly used materials and methods intended to make bone grafts and their *in vivo* outcome on some mammalian species.

1.2. Scaffold Materials: Ceramics and Polymers

Ceramics like Tri-calcium phosphates (TCP) ($Ca_3(PO_4)_2$) have been used in bone repair for the past 80 years [18]. The stoichiometry of TCP is similar to amorphous precursor to inorganic composition of bone. A significant advantage of α and β-tricalcium phosphates is its solubility in water, enhancing in vivo degradation [18]. However, βTCP does not dissolve in vivo at physiological pH levels. It requires acidic pH levels caused by cell activity [19]. α and β-tricalcium phosphates have similar chemical composition, however they have different crystallographic structures, making αTCP more soluble in water. αTCP is obtained by heating βTCP at high temperatures (1150°C) followed by quenching [20]. Most common bone scaffolds made from βTCP has porosity ranging 35 - 50 % and pore-sizes ranging 100 - 300 μm [21].

Hydroxyapatite (HA) ($Ca_{10}(PO_4)_6(OH)_2$ - crystal unit) is another commonly used calcium orthophosphate compounds [18]. This preference is due to its stoichiometric similarity to minerals naturally present in bones. A variety of bone substitutes made of HA are available commercially like Pro Osteon 500R (Interpore Cross International, Irvine, CA, USA), Bio-Oss® (Geistlich

Pharma North America Inc., Princeton, NJ, USA) and Endobon® (Zimmer Biomet, Palm Beach Gardens, FL, USA) [22]. Pro Osteoan 500R is made by de-mineralizing natural coral exoskeletons and hydrothermal conversion of calcium carbonate into calcium phosphate. Incomplete conversions result in external HA and internal calcium carbonate which are more resorbable [23]. The resorption rates of HA in vivo is very low at 5 - 15% per year [21].

HA are comparatively more crystalline than βTCP. Hence scaffolds made from HA has higher mechanical strength comparable to cancellous bone. However, βTCP promotes in vivo degradation. To combine the advantages of these two compounds, composites of βTCP and HA (biphasic calcium phosphates) are used as scaffold materials. The resorption of the implants depends on the composition of βTCP : HA. Most common compositions of either of these compounds are 40 - 60 %. Some commercially available bone substitutes are Triosite (Zimmer Biomet, Palm Beach Gardens, FL, USA) and BCP bone void filler (Medtronic Sofamor Danek USA, Inc., Memphis, TN, USA) [18].

Basically, sintering process or a minor modification of the same is used to make pure ceramic scaffolds. The micro-structural property in such methods are partially controlled by using a negative mold made of industrial foam like polyurethane. This mold will be simultaneously removed during the heating process. A combination of gel casting and polymer sponge mold was used to make porous HA scaffolds by sintering at 1350°C for 2 hours [24] by Ramay et al,. Alternatively, phase separation method was adopted by Fukasawa et al., by freeze-drying water based ceramic slurry [25]. In general, the pore sizes of such scaffolds were in the order of few hundred μm to few millimeters. But the porosity will be as low as 30 - 40 %. This combined with the low bio-degradability of materials like HA, led the scientists to study bio-degradable polymers for bone grafts.

Polymers can be divided into two major categories: naturally available polymers like polysaccharides (starch, alginate, chitin/chitosan, hyaluronic acid derivatives) or proteins (soy, collagen, fibrin gels, silk) [26] and synthetic bio-degradable polymers (PLA, PGA and PCL). This book chapter will focus synthetic bio-degradable polymers, due to its compatibility to bone graft synthesis. Scaffolds made using synthetic polymers can be produced under controlled conditions with predictable and reproducible mechanical (compressive/tensile strength and modulus) and structural properties (pore-sizes, pore shapes and porosity (%)). Moreover, using synthetic polymers, averts the risk material impurities and toxins in the bone graft, which leads to immune rejections in the host.

Some commonly used synthetic polymers used to make tridimensional scaffolds for bone tissue engineering are saturated poly-α-hydroxy esters namely, poly (lactic acid) (PLA) and poly (glycolic acid) (PGA), as well as poly (lactic-co-glycolide) (PLGA) copolymers [27]. PLA exists in three forms: l-PLA (PLLA), d-PLA (PDLA), and racemic mixture of d,l-PLA (PDLLA).

PGA is a simplest linear aliphatic polyester. This was first synthesized as an absorbable suture material under the trade name Dexon. PGA is not soluble in most organic solvents, due to their high crystallinity (46-50%) except highly fluorinated organic solvents such as hexafluoro isopropanol [28]. Jeon et al., 2008 [29] cultured hASCs on 2D and 3D PLGA scaffolds (200-300μm pore size) fabricated by solvent casting and particulate leeching technique, in osteogenic media. Mineralization in extracellular matrix and expression of late bone marker genes (bone sialoprotein and osteocalcin) were observed after 2 weeks of osteogenic induction.

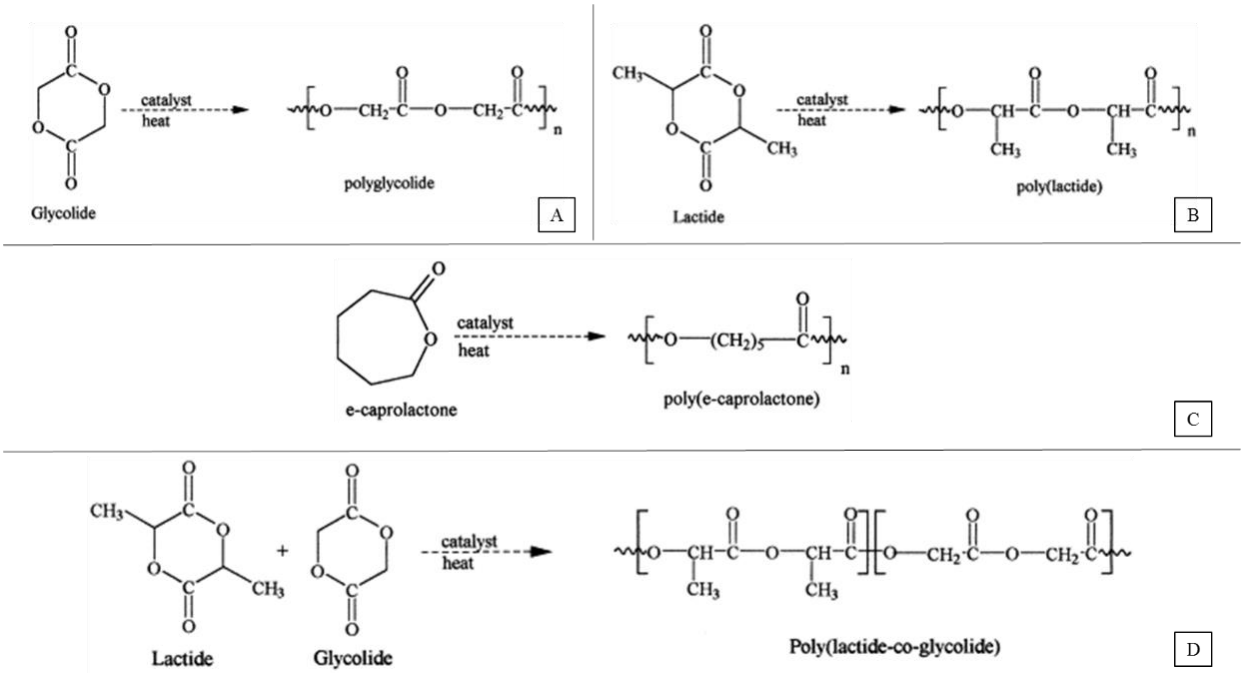

Figure 1.1. Synthesis of (A) Poly (glycolic acid) (PGA), (B) Poly (l-lactic acid) (PLLA), (C) Poly (ε-caprolactone) (PCL) and (D) Poly (lactic-co-glycolic acid) (PLGA) (Adapted from Ref. [30])

PLA is a biodegradable thermoplastic aliphatic polyester derived from renewable resources, such as corn starch, tapioca roots or sugarcane. Poly-lactic acid is in fact a polyester and not a polyacid. Poly-L-lactide (PLLA) is the product resulting from polymerization of L,L-lactide (also known as L-lactide). PLLA has a crystallinity of around 37% (Poly-L-lactic acid and Poly-D-Lactic acid are semi-crystalline), a glass transition temperature 60–65 °C, a melting temperature 173–178 °C and a tensile modulus 2.7–16 GPa [31]. PLLA is soluble in chlorinated solvents, hot benzene, tetrahydrofuran, and dioxane.

Table 1.1. Bio-degradation and mechanical properties of synthetic polymers (adapted from Ref. [32])

Polymer	Bio-degradation time (months)	Compressive* or tensile strength (MPa)	Modulus (GPa)
PDLLA	12 - 16	Pellet: 35 - 150* Film or disk: 29–35	Film or disk: 1.9–2.4
PLLA	> 24	Pellet: 40 – 120* Film or disk: 28 – 50 Fiber: 870 – 2300	Film or disk: 1.2 – 3.0 Fiber: 10 – 16
PGA	6 - 12	Fiber: 340 – 920	Fiber: 7 – 14
PLGA	Adjustable: 1 - 12	41.4 – 55.2	1.4 – 2.8
PCL	> 24	-	-

A specific advantage of using these synthetic polymers is its natural bio-degradability. After surgical implantation, these materials undergo a hydrolytic degradation in vivo through de-esterification (hydrolysis of ester bonds). The resulting monomeric products (lactic and glycolic acids) undergo natural pathways to be excreted from the body. PLA is known to be cleared through tri-carboxylic acid cycle. Bio-degradation time of PLGA can be adjusted significantly by adjusting the lactic and glycolic acid component ratio [33]. PGA undergoes faster degradation at lower pH levels [34].

Poly(ε-caprolactone) (PCL), an important member of the aliphatic polyester family, has been used to entrap antibiotic drugs. Thus, a composite of PCL and antibiotic drugs can be considered as an

effective drug-delivery system [35]. These composites can be used in the treatment of bone defects by enhancing bone ingrowth and regeneration. The degradation mechanism of PCL is similar to that of PLA undergoing a hydrolytic degradation of ester bonds. However, the degradation time for PCL is higher compared to other polymers taking up to several years in some cases [36].

The degradation times given in Table 1 represents a collection of observed data so far from various literatures. However, the actual degradation times of the grafts in vivo would depend on a lot of factors such as: pore morphology, porosity (%), mechanical strength, crystallinity, molar mass (Mw) and polydispersity (Mw/Mn). In general, the degradation rates are as follows [32]:

PGA > PDLLA > PLLA > PCL

When using, PLA and PGA or its other forms (PLLA, PDLA, PLGA) as scaffold materials for bone tissue engineering, there is always a risk of bulk degradation causing the implant to fail pre-maturely. This quick degradation causes an influx of acidic by products which may lead to inflammatory responses in the host tissue [37].

1.3. Scaffold Fabrication Methods

1.3.1. Solvent-Casting and Particulate Leaching Technique

In this method of fabricating scaffolds, water soluble salt (e.g. sodium chloride, sodium citrate) particles are mixed into a biodegradable polymer solution. The solvent is then removed by lyophilization. The salt particles are leached out to obtain a porous structure. The advantages of this method are: simple operation, ability to control pore size and porosity by varying the salt/polymer ratio and particle size of the added salt [38].

1.3.2. Gas-Foaming Process

In this method, solid polymer disks are saturated with high pressurized CO2. Releasing CO2 gas from the polymer system causes thermodynamic instability. This makes the CO2 bubbles to grow inside the composite forming a 3D porous polymer structure. By this technique scaffolds of ~ 93% porosity and pore size of ~100μm can be fabricated. No organic solvents are used in this method. The disadvantage in this method is that interconnectivity of pores is too low [39].

1.3.4. Electrospinning Technique

A polymer solution or melt is induced with an electric potential. At a critical voltage, the charge imbalance overcomes the surface tension forming a polymer jet. This jet is directed onto a substrate as the solvent evaporates and polymer fibers are formed. Localized control on the micro-structure of the porous scaffold can be achieved. Only disadvantage of this method is it is very tedious to make a 3D scaffold of considerable thickness. Scaffolds made by this process are usually sheets with thickness in microns [40].

1.3.5. Thermally Induced Phase Separation (TIPS)

This is a simple procedure in which, the polymer is first dissolved in a solvent at a higher temperature. Liquid–liquid or solid–liquid phase separation is induced by lowering the temperature until the composite is frozen. Frozen solvent is sublimated by maintaining low pressure and temperature leaving a porous polymer scaffold. The pore morphology of the scaffolds varies depending on the concentration of the polymer solution and induced thermal profile during freezing process. Usually scaffolds fabricated by this method have good mechanical properties. Ma et al., 2001 [41] observed that PLLA scaffolds fabricated using this technique has a

compression modulus about 20 times higher than that of the scaffold fabricated using other methods. This method usually generates scaffolds with a pore size of 30–150 μm [41].

1.3.6. Solid Freeform Fabrication (SFF)

Computer-aided design (CAD) models are used to tridimensionally print a polymer scaffold of pre-design micro and macro structures. One early form of SFF known as Rapid Prototyping Technique (RPT) was first developed and published by Bredt et al., 1990 in Massachusetts Institute of Technology, Cambridge, MA, USA [42]. Polymer jet is targeted on a substrate similar to ink-jet printing, forming complex 3D scaffolds of sequential layers. Scaffolds using low molecular weight PLLA was used to print scaffolds of tensile strength up to 17 MPa [43]. However, the practical disadvantage of this method thick layers of scaffold material which are determined by the thickness of the polymer jet. This essentially decreases the overall porosity (%) of the scaffold. Coupling SFF method with other conventional scaffold fabrication process (solvent - casting, phase separation, gas foaming) could give an ideal scaffold with distinguishable micro and macro-porous structures at the same time increasing the porosity. In 2002, Xiong et al., from Tsinghua University, Beijing, China, developed such a combination method. PLLA/TCP/dioxane composites were printed using low-temperature deposition method (LDM). By this method, the measured porosity values were about 90% [44]. These PLLA/TCP composite scaffolds loaded with bovine bone morphogenic protein (bBMP) was implanted into to repair 20 mm segmental defects in canine radiuses. The defect was found to be completely cured at 24 weeks after implantation. Long fabrication time and high costs of manufacture are critical limiting factors for using this technique. This is the reason, majority of in vitro and clinical studies for bone grafting uses conventional scaffold fabrication techniques.

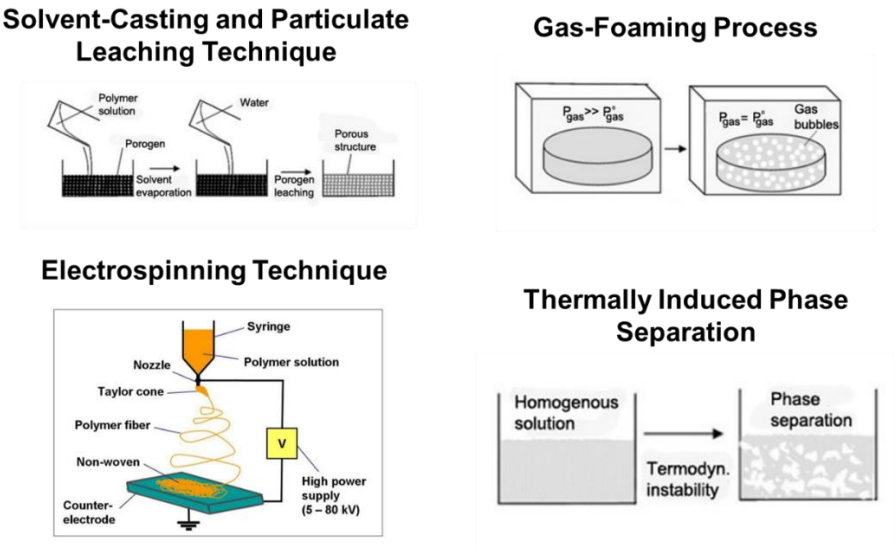

Figure 1.2. Schematic illustrations of basic scaffold fabrication techniques. (Adapted from Ref. [45])

1.4. Structural Requirements of a Scaffold

Vascularization remains a problem for successful fusion of larger grafts (order of mm in dimensions) in vivo. Implanted bone grafts depend on blood vessels for nutrients, oxygen and growth factors during the initial stages of fusion. The three-dimensional architecture (pore-size, porosity and inter-connectivity of pores) of the scaffold used should facilitate spontaneous vascular ingrowth, failing which may lead to cell death due to hypoxia in the interior portions of the graft [46]. Necessity of graft implantation occurs primarily to treat large sized defects (order of mm). Hence it is implied that the micro-structural properties of scaffolds should resemble that of cancellous bone also.

Table 1.2. Structural properties of scaffolds made from various techniques

Scaffold material / Fabrication method	Pore-size		Porosity (%)		Compressive Modulus (MPa)	
	Min	**Max**	**Min**	**Max**	**Min**	**Max**
Non-3D printed ceramic scaffolds [47-49]	300 μm	1 mm	25	80	3	50
Polymers / Gas foaming [50, 51]	10 μm	100 μm (439 μm with salt leeching)	67	97	0.15	0.3
Ceramics / Gas foaming [52, 53]	100 μm	400 μm	46.8	78.4	100	1800
Polymers / Electro-spinning [54, 55]	0.11 μm (fiber dia)	1.19 μm (fiber dia)	-	-	1.09	20
Polymers / TIPS [56, 57]	50 μm	100 μm	71	91	0.15	6.2
Cancellous bone [58]	300 μm	600 μm	75	85	100	300
Cortical bone [58, 59]	10 μm	50 μm	5	10	18,000	22,000

From Table. 2, it can be observed that, very few synthetic polymer based fabrication techniques provides the necessary pore-sizes. However, porosity values are sufficiently higher which may cause more uniform degradation in vivo. In terms of mechanical strength, it will be necessary to rely on other support structures to with stand the compressive/tensile stresses at the defect site. Loads within a human intra vertebral disc can reach a maximum of 4MPa [60]. The young's modulus of a human cortical bone is ~35 GPa and cancellous bone varies between 50-500 MPa

[61]. However the % porosity and mean pore-size of most synthetic polymer scaffolds are comparable to that of a cancellous bone (90%) [62, 63] and pore size (~ 50 μm) [64]. Using these scaffolds in conjunction with calcium phosphate cements (CPC) may be the solution [65]. Though biologically inert [11], CPC is extensively used to harden material/fillers to treat minor skeletal defects [66].

1.5. Current Bone Tissue Engineered Scaffold Models

In recent years, extensive research is being done on scaffold assisted bone regeneration using synthetic materials. Using BMSCs (Bone Marrow Stem Cells) or osteoblasts on synthetic materials on mammals (mouse, rats and rabbits) is the common model of invitro study [67, 68]. In 2004, Lendenckel et al. successfully treated and healed a calvarial defect of a 7-year old girl using hASCs due to lack of enough autologous cancellous bone from iliac crest [69]. Still ethical reasons prevent testing the scope of hASCs combined with a synthetic material on treating skeletal defects in human species [70].

1.5.1. Synthetic Polymer Models

On-site delivery of bone marrow stem cells (BMSCs) using a porous polyethylene glycol–polyurethane (PEG–PU) scaffold to the injury site bearing the therapeutic potency of BMSCs. Though no differentiation pathways were performed, this study re-emphasizes the retention of stem cells characteristics in vivo by measuring Oct-4, Sox-2, Klf-4, c-Myc along with nestin, CD49f, CD29, CD73, CD44 and Sca-1 gene expressions [71, 72]. PCL scaffolds were manufactured by electrostatic fiber spinning method by making a polymer solution of PCL in chloroform. Mesenchymal Stem Cells (MSCs) derived from bone marrow of neonatal rats (3 – 7 days old) were loaded on the scaffold (pre-soaked in purified collagen) by mechanically pressing

the cell pellet on the scaffold. The electro spun PCL scaffolds exhibited mineralized bone tissue formation and three-dimensional cell penetration. The shape-ability of such tissue engineered bone grafts in surgical applications for treating defect sites was emphasized [40].

Three-dimensional 75:25 PLGA scaffolds were fabricated by solvent casting particulate leeching method. 12.5 mm in diameter and 6 mm in height. Porosity of 79%. MSCs loaded on top of the scaffolds were cultured in a spinner flask and a rotating wall vessel in addition to static conditions. This was done to study if mitigated nutrient transfer from the media outside the scaffold boundary influenced cell proliferation and differentiation inside the scaffolds. Interestingly, spinner flask showed comparatively higher cell proliferation and significantly high calcium deposition (representing high expression of ALP and OC genes) compared to static culture. On the other hand, rotating wall vessel setup exhibited relatively lower cell proliferation and differentiation. However, in all three culture systems, inhomogeneous cell distribution was observed with high cellular density on the surface and considerably lower density on the interior. This indicated that the micro-structural properties of the scaffold itself could determine the three-dimensional cellular growth inside the scaffolds [73].

In situ forming scaffolds eliminate the complexity of fabricating complex geometries ex vivo. Poly (methyl methacrylate) (PMMA) bone cements are the most widely used injectable and in situ forming materials in orthopedics. Hydrogel disks (10 mm diameter and 1 mm thick before swelling) were fabricated with 10 wt% PEGDA in phosphate buffered saline (PBS) with the addition of no Acr-PEG-RGD, 0.5 mM Acr-PEG-RGD, 5.0 mM Acr-PEG-RGD, and 5.0 mM Acr-PEG-RDG. Osteoblasts were seeded onto sterile disks at a density of 5×10^4 cells/cm^2 [74]. Commercially available PLGA scaffolds (GC corporation, Itabashi-ku, Tokyo, Japan) of 5 mm diameter and 1.5 mm thick were used to heal large cartilage defects in rabbit knees. These scaffolds

were loaded with BMSCs obtained from isolated from the humeral head of each rabbit and cultured in vitro overnight before surgically implanting into the defect areas of the same rabbits. After 4 and 12 weeks of implantation, the defect sites were histologically analyzed. It was found that the implant had fused successfully into the host bone providing architectural support. However in vivo chondrogenesis was hinted without dedicated study for gene markers [75].

Membranes made from nanofibers of PLGA was fabricated by electrospinning technique by dissolving PLGA in N,N-dimethylformamide (Junsei, Tokyo, Japan) and tetrahydrofuran (Junsei) solution at 25% (wt). Lactic acid / glycolic acid content ratios were 75 : 25, 50 : 50 and a blend of 75 : 25 and 50 : 50. Chondrocytes isolated from porcine articular cartilages were cultured on these polymer membranes to study their cellular response in terms of cell proliferation and cytotoxicity. ECM formation (indicative of chondrogenesis) was evaluated by measuring glycosaminoglycans (GAG) content. Chondrocytic phenotype was aspired to be maintained bymeans of mechanical stimulation as intermittent hydrostatic pressure (IHP). The mechanical strength (tensile modulus, ultimate tensile stress/strain) of these nanofibers based scaffolds were comparable with human skin and lower than cartilage. Faster degradation of 50 : 50 PLGA scaffolds were observed which may be attributed to the hydrophilic nature of glycolic acid content [76].

A custom hybrid poly-(lactic-co-glycolic acid) (PLGA)–gelatin/chondroitin/hyaluronate (PLGA–GCH) scaffold was developed to evaluate its chondrogenic potential relative to PLGA scaffolds. PLGA scaffolds were developed by low-temperature deposition method (LDM) [44]. The idea was to hybridize PLGA scaffolds with GCH miming the hyaline cartilage ECM composition (15–20% collagen type II, 5–10% chondroitin sulfate, 0.05–0.25% hyaluronan). Cell proliferation and ECM formation was significantly higher in PLGA-GCH hybrid scaffolds than control PLGA at 24 days in vitro. At 24 weeks post-operation, the hyaline repair was more tenacious and ill-demarcated in

PLGA–GCH group at the repair interface [68]. PLGA scaffolds were fabricated by molding and leeching process combined with sieved NH_4HCO_3/NaCl (1:1) particulates of two different size ranges (125–180 and 300–500 μm) and chloroform. Three groups of such scaffolds were surface modified with 0.2% (V/V) pig-skin collagen type I (Life Technologies, Grand Island, NY), 2% (W/V) chitosan (Mol. Wt.: 880,000; degree of deacetylation: 90%) (Kiotek, Taiwan) and 10% (W/V) N-succinyl-chitosan solutions. The results showed that collagen increased sell attachment and proliferation while decreasing osteogenic differentiation compared to the chitosan and N-succinyl-chitosan modifications [77].

PLGA scaffolds of 7mm in diameter and 4mm in thickness with 90% porosity were prepared by solution-casting/salt-leaching method. In vitro degradation analysis shows that it lost around 60% of its original mass at 20 days. Cell attachment study shows that only 37% of the initial loaded cells attached to the scaffolds at day 1. After 2 weeks, calcification was observed in vitro for osteogenic induction medium. Critical size osseous defects of 12 × 5 mm were made on the mandible of 12 mature White New Zealand rabbits (2.5 kg). Tissue engineered PLGA/MSCs composites were implanted into the defects in the experimental group and just PLGA scaffold in the control group. After 6 or 12 weeks, all rabbits were euthanized for histological examinations of healed sites. It was observed that the defects can be completely cured with tissue engineered PLGA/MSCs graft after 3 months of implantation. On the contrast, blank PLGA showed very little healing [78]. PLGA and PLGA/PVA scaffolds were developed by melt-molding and particulate leeching method. In vitro and In vivo degradation were focused in this study. Hydrophilic addition of PVA fosters the degradation rate of these scaffolds both in vivo and in vitro for short term. However, during long term (4 weeks), the total degradation between the test samples of PLGA and PLGA/PVA wetted and pre-wetted were not significant [79].

Bone marrow stem cell knitted PLGA scaffolds were used to treat tendon defects in New Zealand White rabbits with single sutures as control. Histological examinations were done after 2, 4, 8 and 12 weeks of implantation. In vitro cultures of BMSc combined with PLGA shows. Type I and type III collagen fiber formation was observed in in vitro cultures of BMSCs combined with PLGA and at 4 weeks post-surgery in New Zealand White rabbits [80]. Blended 3D scaffolds of PCL/PLGA were fabricated using Solid Free Foam technology. Compressive strength was determined as the maximum stress (0.8 MPa) from where the linearity of stress-strain curve deflects. Compressive stress modulus of such scaffolds was 12.9 MPa and the porosity was 69.6%. MC3T3-E1 cells were cultured on these scaffolds with standard culture media (DMEM, 10% FBS) for 15 days with consistent cell proliferation [81].

PLGA scaffolds were fabricated by solid-liquid phase separation method for oriented micro-porous structures or non-oriented micro-porous structures using NaCl particles as porogeny. In the oriented group pores were parallelly longitudinal in the vertical section and uniformly distributed in the cross section. In the non-oriented group pores where spherical and non-homogenous in sizes. There was no significant difference between volume or porosity of scaffolds between the two groups. However, scaffolds of oriented porous structures show increased compressive modulus (~7MPa) relative to non-oriented porous samples (~3MPa). Also, oriented porous structures had more homogeneous cellular growth than the non-oriented porous structures in vitro. Thickness and volume shrinkage was observed to be lesser in oriented group than non-oriented group fabricated by NaCl porogens. Additionally, oriented groups had more cartilage specific ECM deposition after 12 weeks of in vivo implantation in nude mice. These crucial results emphasize the importance of homogeneity of pore sizes and structures in tissue engineered scaffold [82].

Table 1.3. Current osteo-chondrogenic models

	Scaffold Material	Cell type	Species	Cell loading density	Study type	Pathways	Gene markers	Period of culture	References
Polymers	PLLA	BMSCs	Male human	5 × 105 / scaffold	In vitro	Chondrogenesis	SOX-9, COL1A1, COL2A1, Aggrecan	4 weeks	[60]
	(PEG)–PLLA	MC3T3-E1 cells	Mouse calvaria	6 × 105 / scaffold	In vitro	-	-	4 weeks	[83]
	mPEG-PCL gel	hADSCs	Fisher rat	2.5 × 105 / scaffold	In vitro / In vivo	OS	ALP	3 weeks (In vitro), 4 weeks (In vivo)	[84]
	polyethylene glycol–polyurethane (PEG–PU)	BMSC	C57BL/J6 mice	5 × 105 / scaffold	In vitro / In vivo	Engraftment	Sca-1, CD11b, CD29, CD133 and CD140a	10 days	[72], [71]
	PLGA	Chondrocytes	Newborn swine	5 × 107 / cm3	In vitro / In vivo	-	-	12 w (In vitro), 12 w (In vivo)	[82]
	PCL	BMSCs	Lewis rats	4 × 106 / scaffold	In vitro	OS	ECM, Calcification	4 weeks	[40]
	75:25 PLGA	MSCs	Male Sprague–Dawley rats	106 / scaffold	In vitro	OS	ALP, OC	21 days	[73]
	Poly (ethylene glycol)-diacrylate (PEGDA)	Calvarial Osteoblasts	Rats	5×10^4 / cm^2	In vitro	OS	-	4 weeks	[74]
	PLGA	BMSCs	Male Japanese white rabbits (3–4 kg)	1×10^7 cells / cm^3	In vitro / In vivo	Chondrogenesis	-	12 h (In vitro), 12 w (In vivo)	[75]
	PLGA/PVA	-	Male Sprague-Dawley rats (200–250 g)	-	In vivo	-	-	4 weeks	[79]
	Modified PLGA	Osteoblastic stromal cells	Sprague-Dawley rats	7×10^4 / scaffold	In vitro	OS	ALP, Ca deposition	14 days	[77]
	PLGA	MSCs	White New Zealand rabbit	10^5 / scaffold	In vitro / In vivo	OS	Ca deposition	20 d (In vitro), 12 w (In vivo)	[78]
	PCL/PLGA	MSCs (MC3T3-E1)	Mouse	-	In vitro	-	-	15 days	[81]
	PLGA	Chondrocytes	Porcine	5×10^4 / scaffold	In vitro	-	ECM	14 days	[76]
	PLGA–GCH	BMSCs	Mature New Zealand white rabbits (2.5 - 3 kg)	10^7 / scaffold	In vitro / In vivo	Chondrogenesis	ECM	8 h (In vitro), 24 w (In vivo)	[68]
	PLGA	BMSCs	Female New Zealand White rabbits	1×10^7 / graft	In vivo	Tenogenesis	-	12 weeks	[80]
Polymer-Ceramics	Poly(caprolactone) (PCL) (nanofibers), hydroxyapatite (HAP)	L-929 fibroblast cells	Mouse	5×10^3 / scaffold	In vitro	OS	ALP	5 days	[85]
	PLLA/Apatite/Collagen	Saos-2	Female Human	1×10^5 / scaffold	In vitro	-	ALP	8 days	[86]
	nano-HA/ collagen/PLA	Osteoblasts	Rat calvaria	5×10^4 / cm^2	In vitro / In vivo	-	-	16 weeks	[87]
	PolyHIPE Polymer	Osteoblasts	Rat	300×10^5 / scaffold	In vitro	OS	-	35 days	[88]
	poly-ε-caprolactone (PCL)/CaP	BMSCs	Human	3×10^5 / scaffold	In vitro	OS	Ca deposition. OC, collagen - I	8 weeks	[89]
	PLGA/HA	Calvarial Osteoblasts	Rat	2.0×10^6 / scaffold	In vitro / In vivo	-	Ca deposition	8 weeks	[90]

Scaffolds of dual-sized pore structures were fabricated by incorporating montmorillonite (MMT) (a family of phyllosilicates (2:1) that comprise of two tetrahedral silica thin layers with a central octahedral sheet of magnesia) into a PLLA solution. To obtain the final scaffolds, electrospinning and salt leaching/gas foaming methods were adopted in this study. It was observed that the degradation of scaffolds in terms of weight loss and molecular weight decrease of PLLA was enhanced by the presence of MMT over a course of 40 days. Particularly, the molecular weight underwent a sharp decrease from 110,000 to 10,000 from 5 to 15 days. However, there were no significant difference between pure PLLA scaffolds and MMT infused nanocomposite models in decrease of molecular weight over a period of 40 days. Significant difference in weight loss was observed with PLLA/MMT nanocomposite scaffolds [91].

PLLA scaffolds were formed by solvent casting and particulate leaching, simultaneously incorporating NaCl particles as porogens. The median pore diameter of such scaffolds was 62.44mm and the porosity was 90.4%.

Human bone marrow stem cells were cultured on these scaffolds aimed for a viable clinical application as a treatment for either osteoarthritic cartilage injury or the degenerate inter vertebral disc (IVD). It was found that differentiated BMSCs in combination with SOX-9 transfection would establish tighter chondrocytic phenotype. Additionally, pre-differentiated BMSCs when cultured on PLLA scaffolds, synthesize and similar matrix molecules as in vivo [60].

Macro-porous poly(l-lactic acid) (PLLA) scaffold was fabricated from a PLLA–dioxane–water ternary system with added polyethylene glycol (PEG)–PLLA using thermally induced phase separation (TIPS) method. Cloud-point temperatures of various compositions of (PEG)-PLLA was observed to increase with increasing concentrations of PLLA. MC3T3-E1 cells (osteoblast-like

cells derived from mouse calvaria) were cultured on these three-dimensional constructs for 28 days. Addition of amphiphilic diblocks helped in the fabrication of interconnected scaffolds without segregation or sedimentation. Such macro-porous scaffolds induced high cell proliferation for the culture period studied [83]. PLLA scaffolds of 95.65% porosity were fabricated by solid-liquid phase separation method, with no controlled cooling profiles before sublimation process. A subset of these scaffolds were immersed/coated with simulated body fluid (SBF) or simulated body fluid with collagen (SBFC). Saos-2 osteoblast-like cells were loaded and cultured on these scaffolds to measure their viability and ALP activity at 8 days. Scaffolds made with apatite coating and composite coating expressed more ALP activity and viability than PLLA [86].

1.5.2. Polymer-Ceramic Models

PLLA scaffolds fabricated by thermally induced phase separation method were hybridized with nano-hydroxy apatite (NHAP) or micro-hydroxy apatite (MHAP) at different compositions of NHAP. Two different quenching temperatures were used before sublimation to study their structural integrity as well as different composition of solvent (dioxane/water). The compressive modulus of the scaffolds increased as expected with increasing NHAP/MHAP concentrations. But 100% dioxane had the highest compressive modulus (~8.5 MPa) compared to water substitutions in solvent [92].

To mechanically strengthen nano-hydroxyapatite/collagen (nHAC) composite, a novel nano-HA/collagen/poly(lactic acid) (nHAC/PLA) was developed by adding PLA to the mixture. A combination of molding and solid liquid phase separation method was adopted at a quench temperature of -20°C before lyophilization. The compressive modulus of these composite scaffolds was highest (~45MPa) when PLA composition was 10% in solvent. PLA concentration

of 8% and 12% had a modulus of 20 MPa and 40 MPa respectively. The ultimate compressive strength of 8, 10 and 12% PLA were 1.3, 1.5 and 1.85 MPa respectively. These scaffolds were loaded with osteoblasts derived from calvaria of neonatal rats before implanting into 15 mm segmental defect in the right forelimb of New Zealand adult rabbits (2.5–3 kg). The porous scaffolds mimicking the natural cancellous bone in terms of composition and microstructure was found to be biologically active when implanted in vivo [87].

Mineralization of Shish-Kebab structure of Hydroxyapatite on poly(e-caprolactone) (PCL) nanofibers following NFSK (Noncoherent Frequency Shifting Key) pattern by incubating in calcium induced cell culture medium and SBF (Simulated Body Fluid). A comparative tensile strength analysis of aligned and randomly oriented mats was done for PCL, NFSK and mineralized NFSK models. Results showed that the randomly oriented structures showed lower ultimate strength for all models. Aligned mineralized NFSK had the highest young's modulus (22.5 MPa) followed by aligned NFSK (10 MPa), followed by aligned PCL nanofibers (2.5 MPa). Fibroblasts (L-929) cells were cultured on these pre-mineralized structures to characterize its cytotoxicity and morphological changes. NFSK scaffolds showed similar cytocompatibility as PCL nanofibers [85]. A porous construct was developed by high internal phase emulsion (HIPE) polymerization technique. Pore-surfaces were coated with hydroxyapatite for enhanced bio-compatibility. Rat osteoblasts were seeded and cultured for up to 35 days to measure the cell proliferation and formation of bone nodules (extracellular matrix with related minerals) which characterizes functionally mature osteoblasts [88].

1.6. Conclusion

Traditionally, bone implants made from ceramic materials have been implanted into patients. But in recent years, polymers like poly (L-lactic acid) and poly (glycolic acid) are studied extensively for scaffold fabrication for bone grafts. This is mainly due to their high bio-compatibility and simple degradation by hydrolysis after implantation. Every aspect of the scaffold fabrication, from the choice of material to the technique will impact the characteristic of the final scaffold. Currently most of the clinical studies involving osteo-chondrogenic models overlook the aspect of mechanical stability. Ultimate strength and compressive/tensile modulus are vital factors when engineering a skeletal graft. Solvent-Casting and Particulate Leaching Technique is a simple operation which gives ability to control pore size and porosity by varying the salt/polymer ratio and particle size of the added salt. Using Gas-Foaming technique, scaffolds of high porosity and pore size, but low connectivity can be fabricated. By electro-spinning method, large porous inter-connected scaffolds can be fabricated. But the thickness is limited to microns. Three-dimensional printing gives localized control over the micro-structure of the scaffolds. Ultimately, the tissue of interest dictates the characteristics required of a scaffold. More clinical studies are needed to further evaluate the potential of polymer-ceramic models or as a viable bone graft. In the case of grafts engineered towards a musculoskeletal incorporation, mechanical stability of the graft is of vital importance. It should be noted that few studies from the osteo-chondrogenic models have focused on the mechanical stability, strength and stiffness of the engineered constructs. Tissue engineering is a rapidly growing field with the use of bio-degradable synthetic polymer and their compounds becoming increasingly feasible in vivo studies. This is further supported by the influx of progenitor cells and access to them. In the case of human beings, adipose derived stem cells are relatively easy to avail, and they are known for their pluripotency. Extensive in vitro as well as in

vivo studies have been done on hASCs being differentiated into osteoblasts and implanted into live mammals (rats, rabbits, etc.,). In scaffold assisted bone tissue engineering thorough investigation and characterization of the scaffold to be used for cell culture is a necessity. This study is dedicated to characterizing a three-dimensional porous PLLA scaffold combined with hASCs as a viable bone graft model.

Chapter 2 : Controlling the Cooling Rates of PLLA : Dioxane

2.1. Introduction

Several methods have been reported to fabricate scaffolds using synthetic biodegradable polymers. Thermally induced phase separation method uses thermal energy and latent heat of the solvent to induce crystallization resulting in the phase separation of the polymer [93-96]. The key advantage in using this technique is that the micro-structural properties of the resulting scaffold can be adjusted depending on the thermal profile imposed on the polymer/solvent solution during the phase separation process. A large portion of research in adjusting these thermal profiles has been focused on the quenching temperature or the final temperature of these solution or the total time the solution was left exposed to these temperatures before the lyophilization process [86, 92, 97, 98] and Poly (l-lactic acid) (PLLA) or any of its isomers were the choice of synthetic material in most of these works [99-101]. The main scope of this chapter was to study the cause and effect of various temperature profiles on the micro and macro structural property of the subsequent scaffolds. Utilizing the thermal conductivity difference of varying materials (copper = 401 W/m/K, aluminum = 237 W/m/K and glass = 1.2 W/m/K), an attempt to induce phase separation at different cooling rates on polymer/solvent solution was made. In situ temperature gradient of the polymer/solvent solution was recorded and their effect on the resulting scaffolds are reported.

2.2. Materials and Methods

PLLA (mol. wt. 100,000; density 1.2 g/cc) was obtained from SurModics Pharmaceuticals (Birmingham, AL) with trade name 100 L 7A.

2.2.1. Fabrication of Copper and Aluminum vials

Copper and Aluminum vials of inner diameter 13.5mm and outer diameter 15.5mm were manufactured in ME Machine Shop in Louisiana State University, Baton Rouge, LA. The total length was 44 mm. This was done to maintain standard wall dimensions of the metal vials to that of the commercially purchased borosilicate glass vials (Kimble® 60831D-1544 Titeseal®). However, the dimensions of the bottom portion of the both the metal vials had to be changed as shown in Fig. 2.2 due to lack of better manufacturing process in Me Machine Shop, LSU.

Figure 2.1. Manufactured aluminum (left) and copper (right) vials

2.2.2. Preparation of PLLA-Dioxane Solution

The PLLA-Dioxane solution was formed by dissolving 7 % wt/vol of PLLA in anhydrous 1,4-Dioxane (Sigma, USA) at 323 K with constant stirring for 2 hours to form a clear solution. This

solution was transferred into cylindrical vials (borosilicate glass or aluminum or copper) of internal diameter 13.5 mm, keeping the volumes consistently at 5 mL. These solutions were stored at room temperature for 48 hrs before the phase separation process.

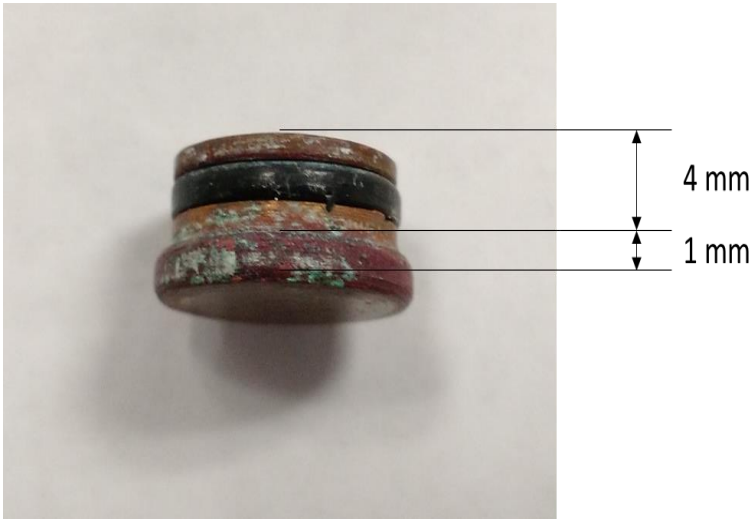

Figure 2.2. Bottom plug of the copper vial (similar to the aluminum vial)

2.2.3. Design of the Floating Block using Expanded Polystyrene (EPS)

A cooling block to hold the aluminum, copper and glass vials was shaped using EPS. This block directly floats above the liquid nitrogen in an EPS vessel while the solution in the vials undergo phase separation during the controlled cooling process. The design of this block as shown in Fig. 2.3, facilitated maintaining the bottom surface of the vials at a constant height of 38 mm directly above liquid nitrogen (-160°C). This ensured the only variables controlling the imposed thermal profiles was the thermal conductivity of the material of the vial.

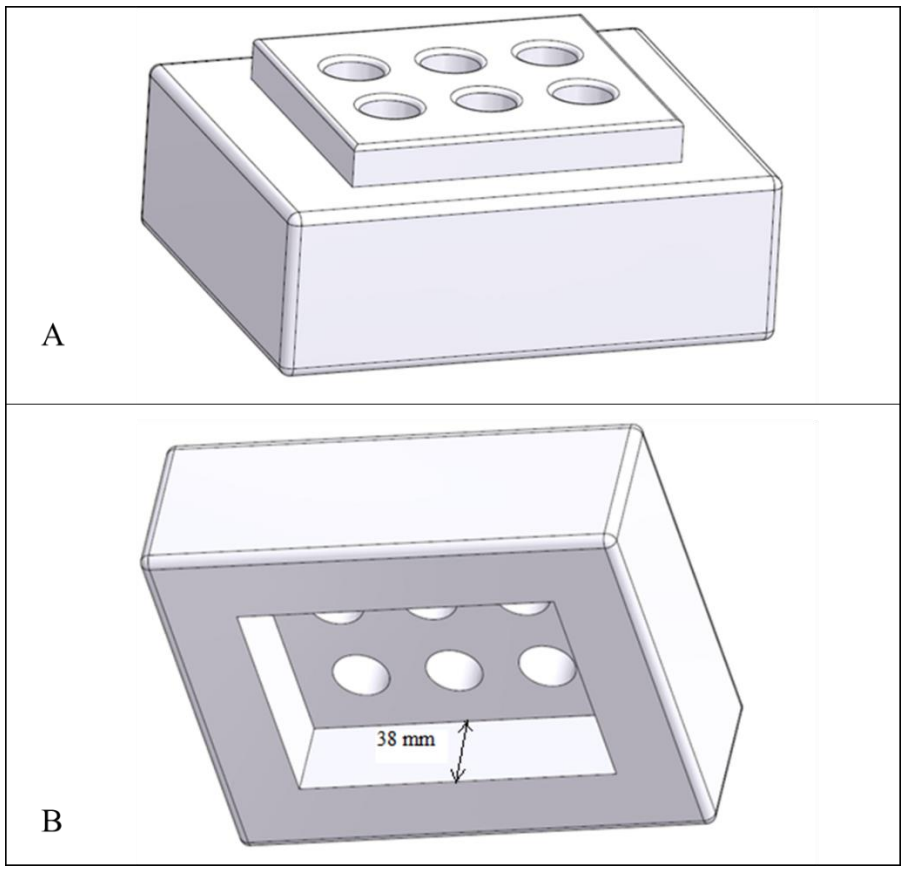

Figure 2.3. Isometric views showing (A) top surface and (B) bottom surface of the floating block

2.2.4. Controlled Phase Separation Process

The vials with 4 mL or 5 mL 7% (wt/vol) PLLA : Dioxane solution was placed on the floating block and allowed to float on the liquid nitrogen surface to undergo cooling, nucleation of 1,4-dioxane causing phase separation of PLLA. The in situ temperature profile of the solution was recorded simultaneously using a type K thermocouple (Omega, CT, USA) connected to a data logger (Vaisala Veriteq SP - 1700 - 51 W), every 10 seconds for 90 mins.

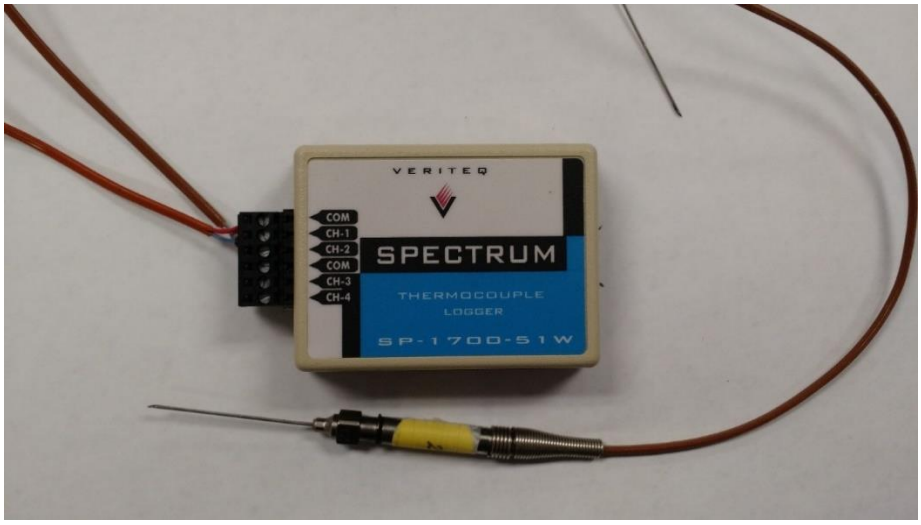

Figure 2.4. Data logger used to measure and record instantaneous temperature during phase separation process

2.2.5. Lyophilization Process

The frozen PLLA-Dioxane solution in the vials were transferred to a Labconco Fast-Freeze Flask. The Fast-Freeze Flask was connected to the FreeZone Plus 2.5 Liter Cascade Console Freeze Dryer (Labconco Corporation Kansas City, Missouri, USA) for 48 hours to sublimate the solvent (Dioxane or Dioxane-Ethanol). The console freeze dryer maintained the frozen PLLA-Dioxane/Ethanol vials at 0.037 bar and -55°C to generate 3D porous PLLA scaffolds. The frozen and freeze-dried porous scaffolds were extracted from the vials and typically range in size from 15 to 16 mm in height and approximately 12 mm in diameter (somewhat smaller than the internal diameter of the cylindrical capsule due to shrinkage during the sublimation process).

2.2.6. Micro-structural Characterization

The cross-sectional microstructure of the frozen and freeze-dried porous scaffolds was analyzed using Scanning Electron Microscopy (SEM) at a distance of 5 - 10 mm from the bottom scaffold surface. Additionally, the microstructures of the frozen and freeze-dried porous scaffolds were also obtained along the vertical cross sections. The surfaces of the 3D porous scaffolds to be characterized were coated with 15 nm's of Platinum using EMXS550X Sputter Coater (Electron Microscopy Sciences, Industry Road, Hatfield, PA, USA). JEOL JSM-6610LV Scanning Electron Microscope (Jeol, Dearborn Rd, Peabody, MA, USA) was then used to scan and capture the scaffold micro-structural images.

2.2.7. Pore Diameter and Porosity

Pore-sizes were measured at various random locations (~20) from the SEM images using JEOL JSM-6610LV software. Porosity of the scaffold was calculated by gravimetric method as follows [102]:

$$Scaffold\ density\ \left(\rho_{scaffold}\right) = \frac{mass}{volume}$$

$$Porosity\ (\%)\ = \left[1 - \frac{\rho_{scaffold}}{\rho_{PLLA}}\right] \times 100$$

2.3. Results and Discussion

2.3.1. Temperature profiles

Instantaneous in situ temperatures (°C) were plotted relative to time (mins) for aluminum, copper and glass vials. After 90 mins of cooling, the samples in coper, aluminum and glass vials cooled

to about -25°C, -30°C and -80°C respectively. Standard deviations are plotted for replicate samples (n = 4). Temperatures become momentarily steady at the freezing point of anhydrous 1,4-dioxane (4 mL) around 10°C during cooling process. The average cooling rate of glass vial was the highest at 1 °C/min. However, the average cooling rates of PLLA/dioxane copper and aluminum vials was almost equal (copper at 0.41°C/min; aluminum at 0.48°C/min). This was contradictory to the expected results since copper has the highest thermal conductivity of the tested materials.

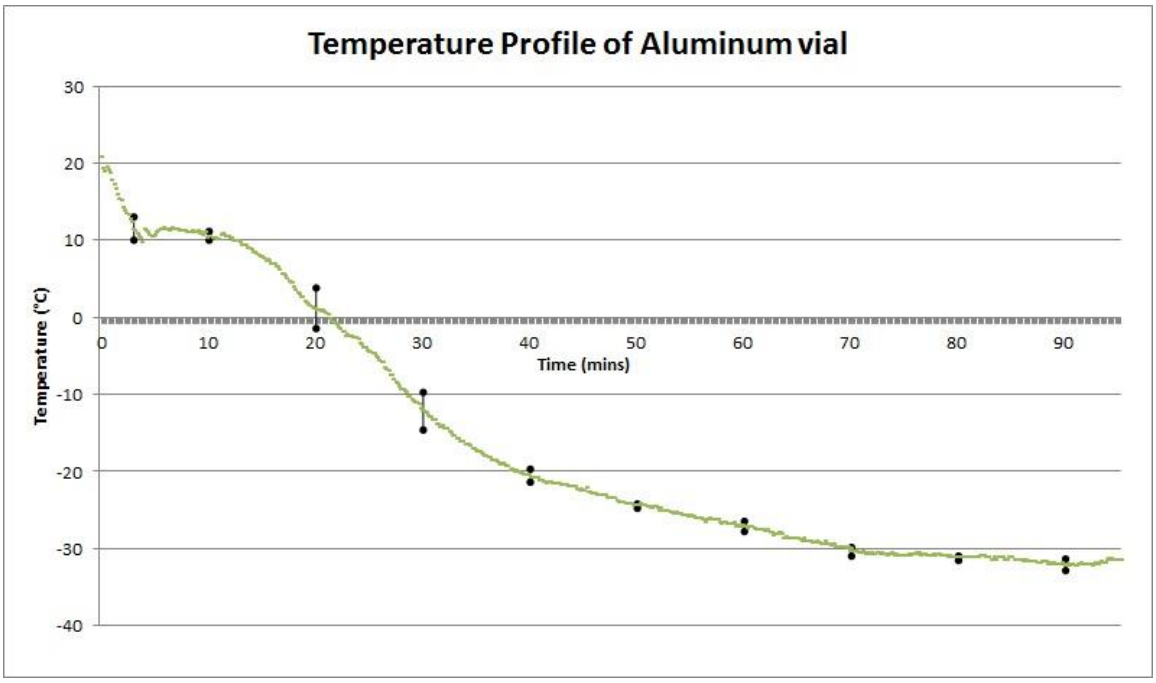

Figure 2.5. Temperature profile of PLLA/dioxane in aluminum vial with standard deviations (n = 4)

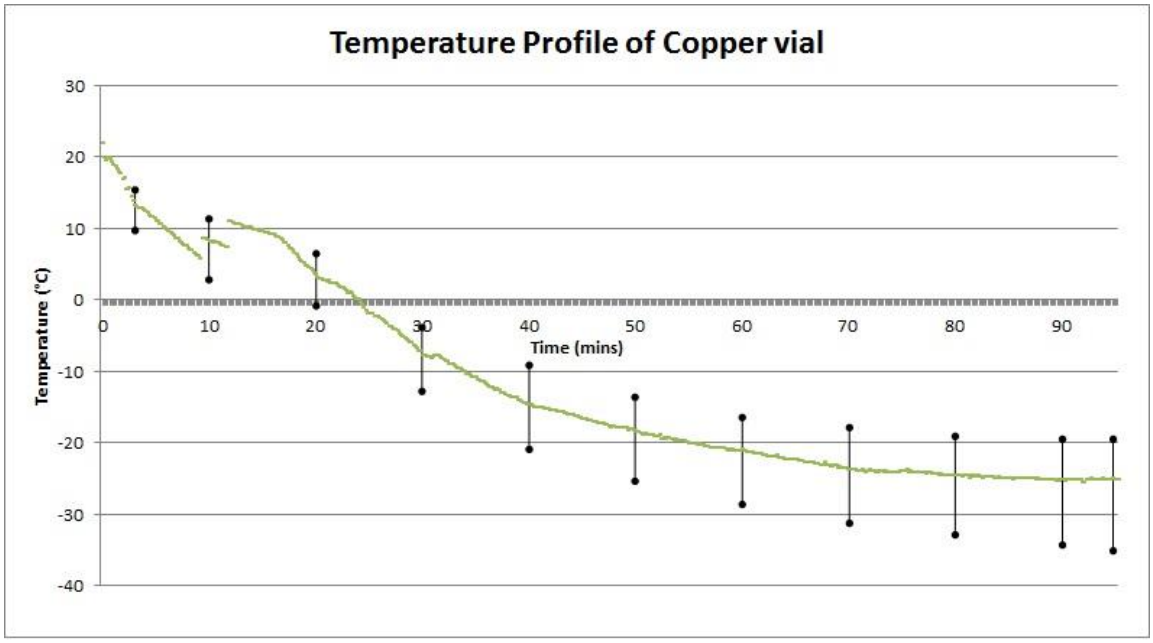

Figure 2.6. Temperature profile of PLLA/dioxane in copper vial with standard deviations (n = 4)

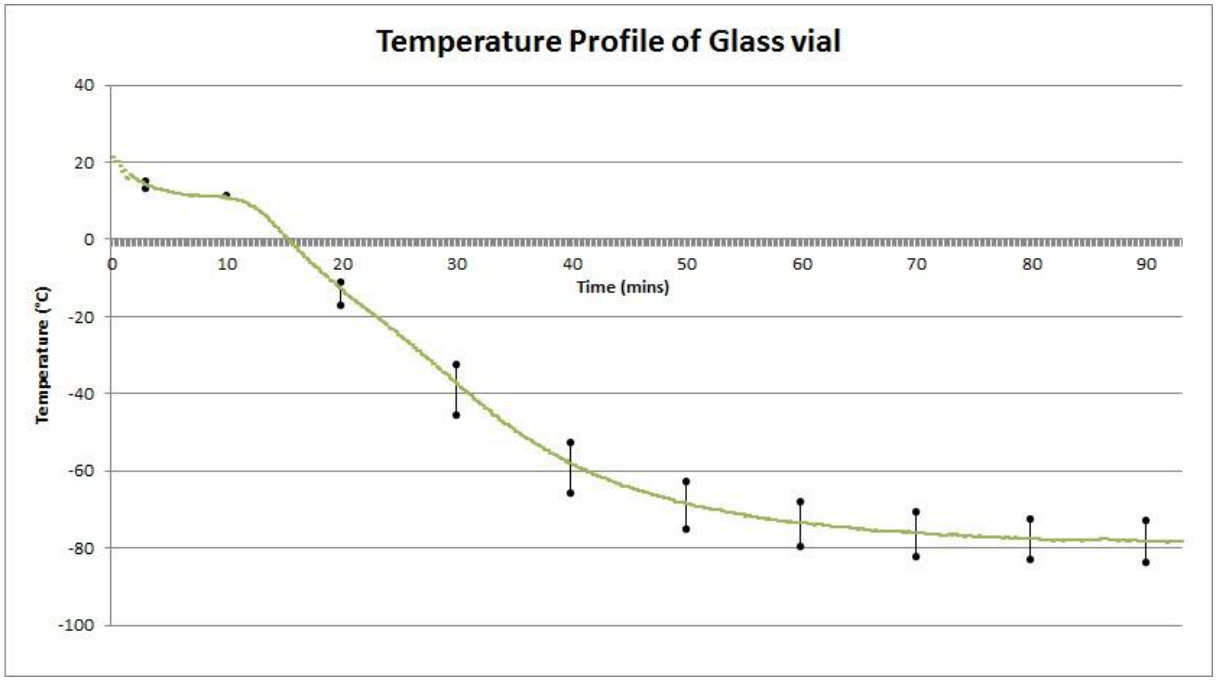

Figure 2.7. Temperature profile of PLLA/dioxane in glass vial with standard deviations (n = 4)

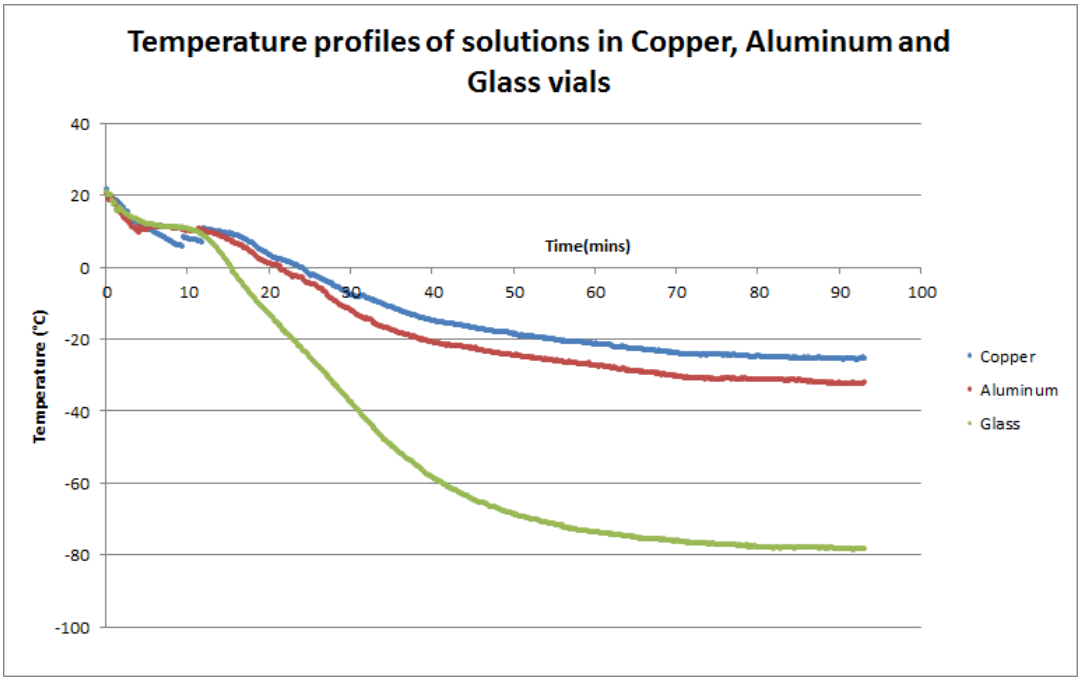

Figure 2.8. Comparison of mean temperature profiles of PLLA/dioxane in vials of all materials studied

The discrepancy in the resulting cooling rates could be due to the structure of the vial itself affecting the imposed thermal profile. At such high temperature differences, minor factors like rubber seal (as seen in Fig2.2) in the bottom plug could be influencing the resulting cooling rates.

2.3.2. Porosity (%)

The resulting scaffolds from aluminum vials had the highest mean porosity of 90.255%. Scaffolds from copper and glass vials had a mean porosity of 90.15% and 89.77% respectively. However, none of these values were significantly different from each other with p-values of 0.68, 0.27 and 0.14 between Al-Cu, Cu-glass and glass-Al respectively.

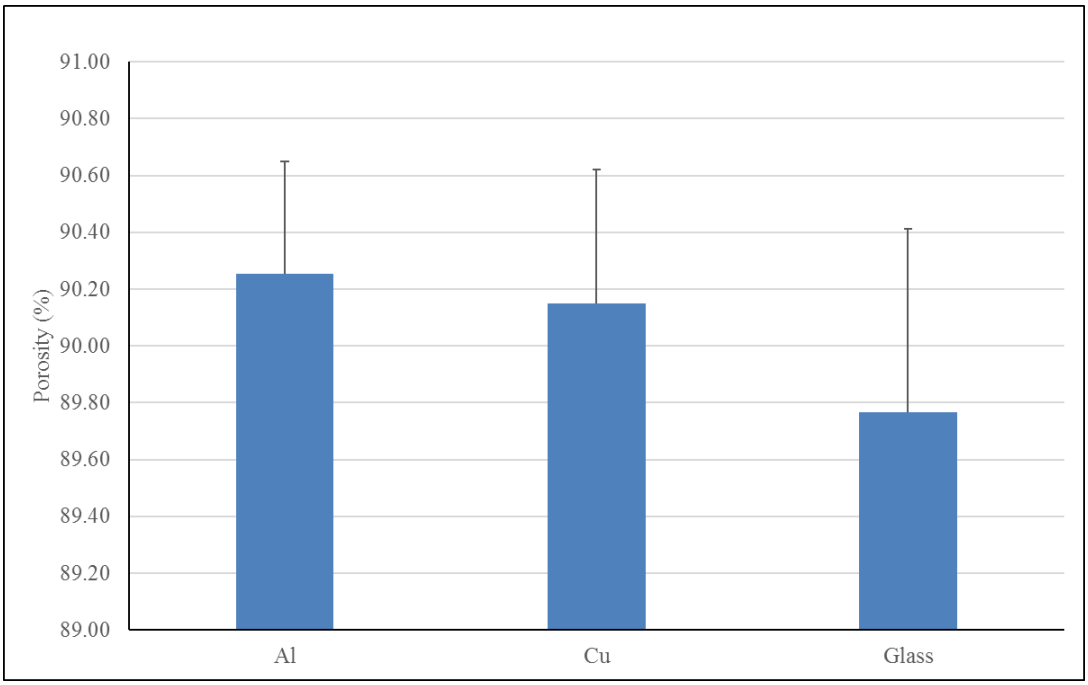

Figure 2.9. Porosity (%) of scaffolds made from Al, Cu and glass vials

2.3.4. SEM Images and Pore Sizes

The SEM image of scaffolds from copper vials showed that the pores were largely spherical shaped and compartmentalized in the central are of the scaffold (Fig. 2.11). Visually, no sign of porous interconnectivity was observed. However, there were long striated, spindle shaped pore structures near the outer periphery of the scaffold. The micro-structural image of scaffold made using aluminum vial also showed a similar but an emphasized trend with longitudinal porous structures near the peripheral region and spherical compartmentalized pores in the central region (Fig. 2.10).

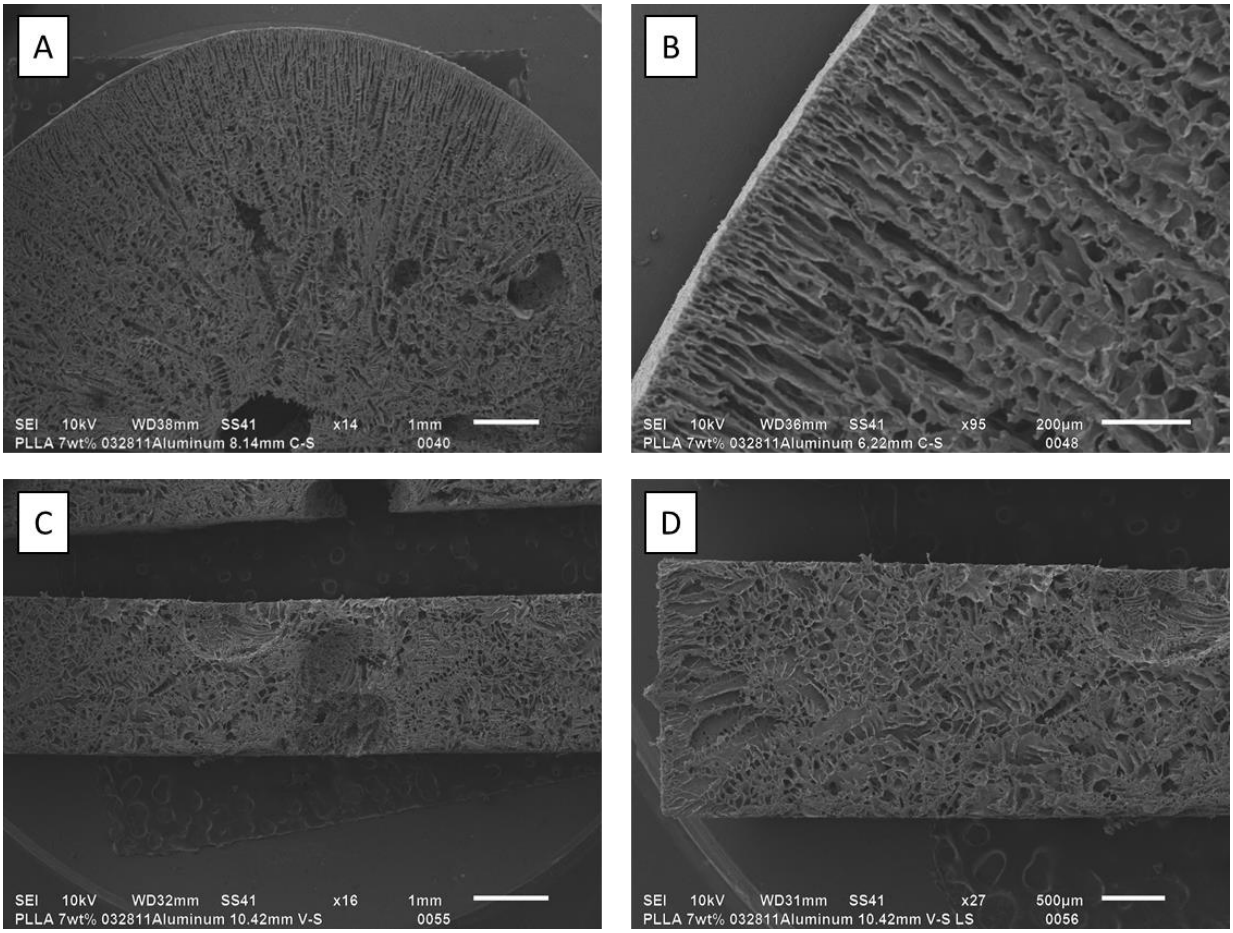

Figure 2.10. SEM image of scaffold made from aluminum vials representing the cross-section perpendicular to the axis (A, B) and vertical section parallel to the axis (C, D)

Micro-porous structures of scaffolds made from aluminum vials were very elongated spindle shaped. Though the length of the pores were larger than 200 µm, the width of the pores were approximately 10 - 20 µm. Since the average size of a human adipose stem cell is about 10 µm, such constricted longitudinal pores may not be an ideal structural property for cell growth.

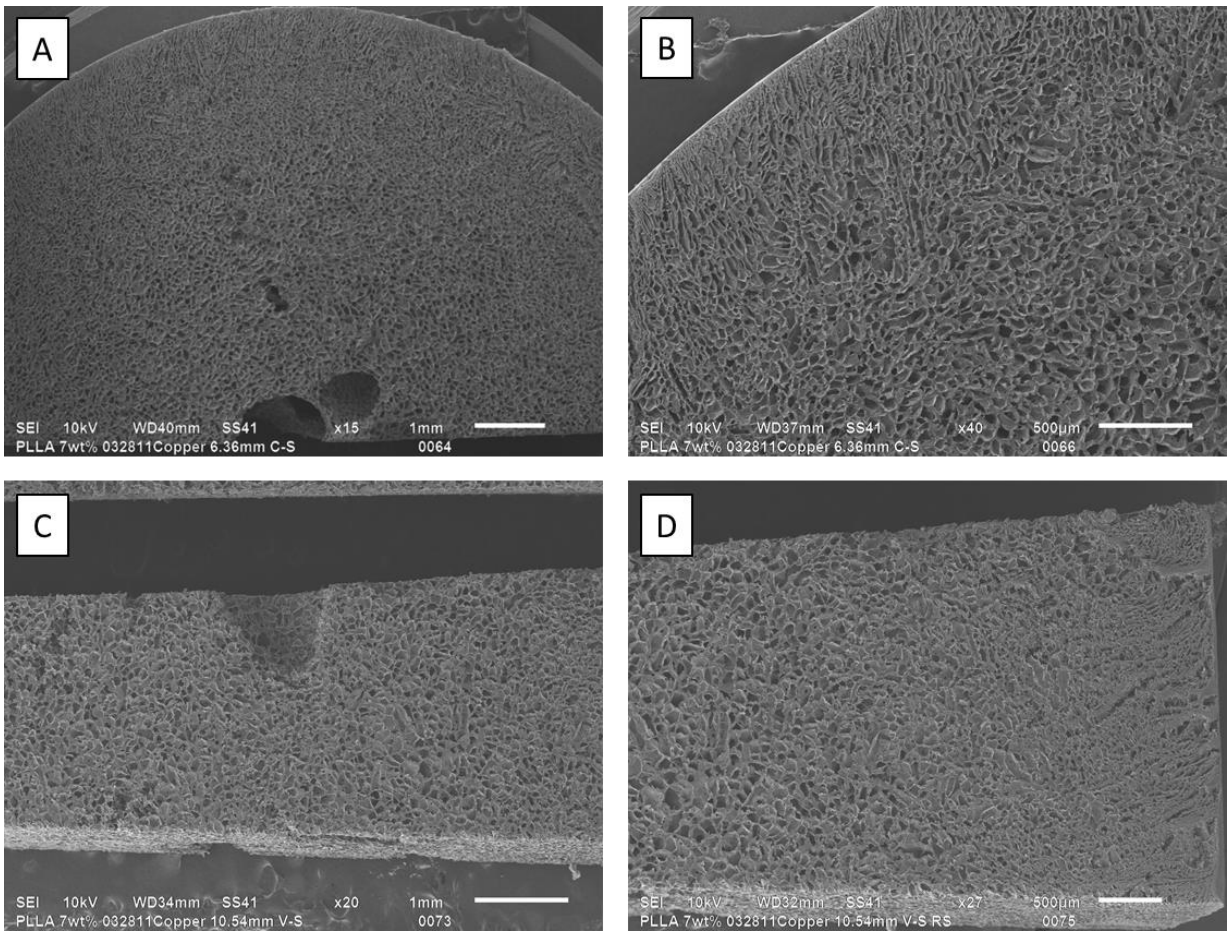

Figure 2.11. SEM image of scaffolds made from copper vials representing the cross-section perpendicular to the axis (A, B) and vertical section parallel to the axis (C, D)

Scaffolds made from copper vials exhibited a homogenous distribution of spherical porous structures on both horizontal and vertical sections. Some longitudinal porous structures were found in proximity to the walls of the capsules i.e., in the outer peripheral region of the scaffolds. Spherical shaped pores over a large central region may indicate poor interconnectivity of pores. Scaffolds made from glass vials on the other hand had patterns of regular spindle shaped porous structures alternating in all directions on the horizontal section. The vertical section shows a pattern of porous structures propagating inside from the outer periphery as shown in Fig 2.12 (C, D).

However, near the center, the pore structures propagate in a vertical direction, tilting towards the walls of the glass capsules. This suggests that there is unidirectional cooling only in the central region of the scaffold and the cooling from the walls play a major role near the outer periphery. The scaffolds made from glass vials showed very little presence of spherical compartmentalized pores. Therefore, scaffolds made from glass vials suggests having more interconnectivity among porous structures.

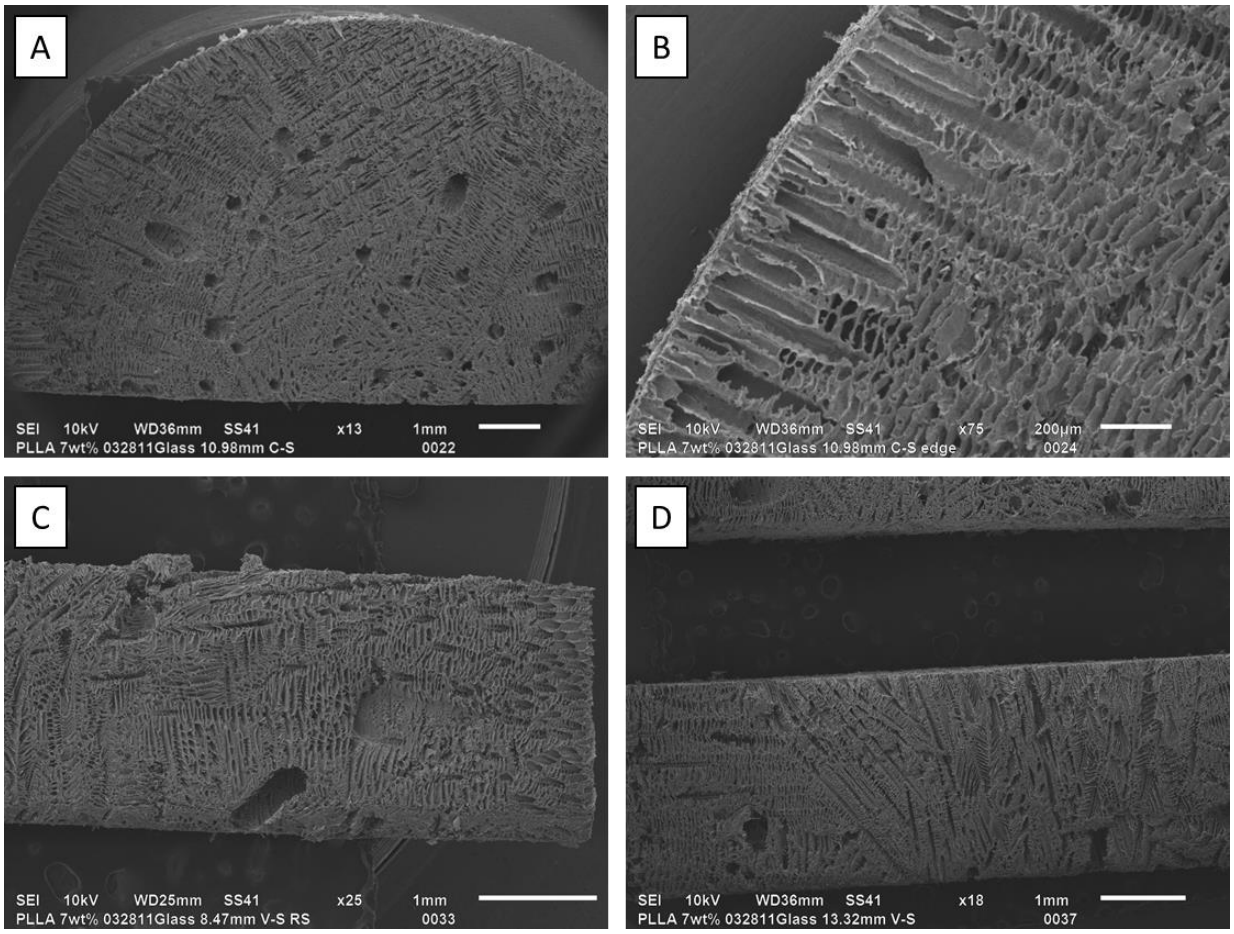

Figure 2.12. SEM image of scaffolds made from glass vials representing the cross-section perpendicular to the axis (A, B) and vertical section parallel to the axis (C, D)

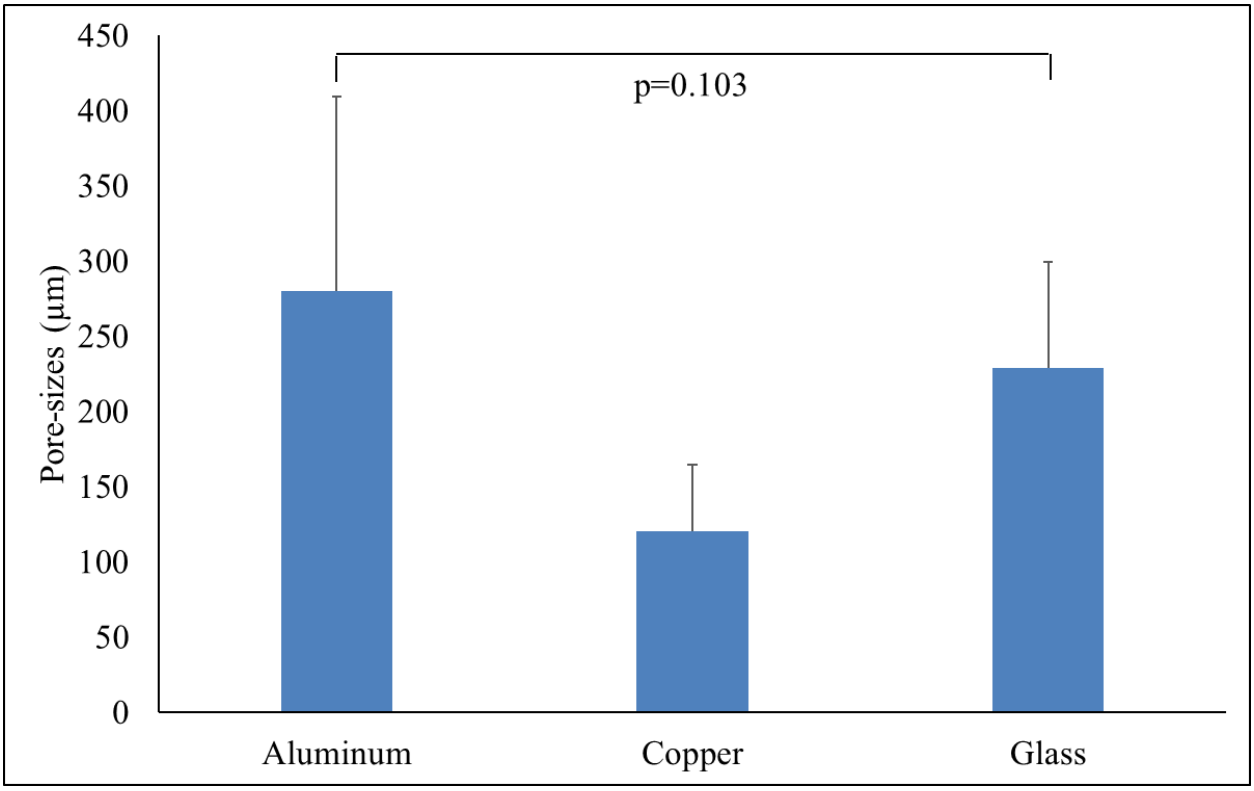

Figure 2.13. Comparison of mean pore-sizes of scaffolds made from Al, Cu and glass

Pore-sizes were measured from the SEM images on both vertical and horizontal sections. For spherical pore shapes pore-sizes were measured at random direction. For spindle shaped pore structures, the lengths of the pores were measured as this would influence the connectivity and resulting cell growth in that cavity. The mean pore-size of scaffolds made from aluminum vials had the highest of 279.91 µm. Scaffolds made from glass and copper had a mean pore-size of 228.78 µm and 120.04 µm respectively. However, there was no significant difference between the pore-sizes of scaffolds from aluminum and glass vials. Standard deviations of all samples were relatively large due to irregularity of porous structures which is expected from any non-3D printed fabrication method.

2.3.5. Compression Testing

Cylindrical samples of 12 mm in diameter and 10 mm in height were cut from the bottom of the resulting scaffold after lyophilization process. These samples were compressed to ~ 90% of its original height in the axial direction using INSTRON 5900 Series – Advanced Mechanical Testing Systems Compression tester (Instron Industrial Products, Liberty Street, Grove City, PA, USA). Compression was programmed at a rate of 0.9 mm/min while instantaneously measuring the force applied (N) and real strain values. The axial stresses calculated from the force applied and cross-sectional area (the cross-sectional area remained the same before and after compression) are plotted with respect to the strain experienced by the scaffolds in Fig. 2.14. The compressive modulus was calculated by linear regression method and plotted in Fig 2.15.

In Fig. 2.14, scaffolds made from copper and aluminum vials shows similar stress-strain curves relative to scaffolds made from glass vials. The scaffolds made from glass vials has a higher compression modulus of 806 kPa compared to scaffolds made from copper and aluminum vials (481 kPa and 437 kPa respectively). The compressive strength of copper and aluminum varied largely among replicate samples primarily because of the inconsistent height of the vials above liquid nitrogen over the cooling time of 90 mins. Compressive modulus of aluminum and glass showed a statistical significance of $p = 0.01$ while other pairs of data were statistically insignificant. From Fig. 2.15, the imposed cooling rate could have an influence on the compressive modulus of the resulting scaffolds since the scaffolds made from glass vials with a cooling rate of 1.44°C/min has a higher compressive modulus of scaffolds made from copper and aluminum vials (0.4°C/min).

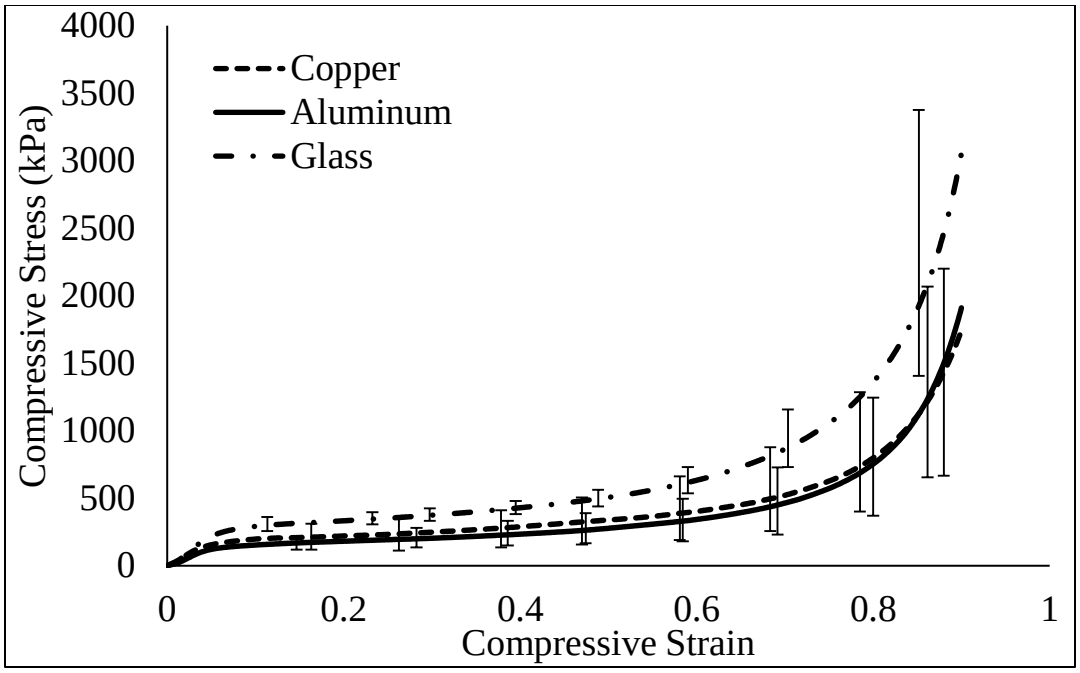

Figure 2.14. Compressive stress vs strain of scaffolds made from copper, aluminum and glass vials (n = 7)

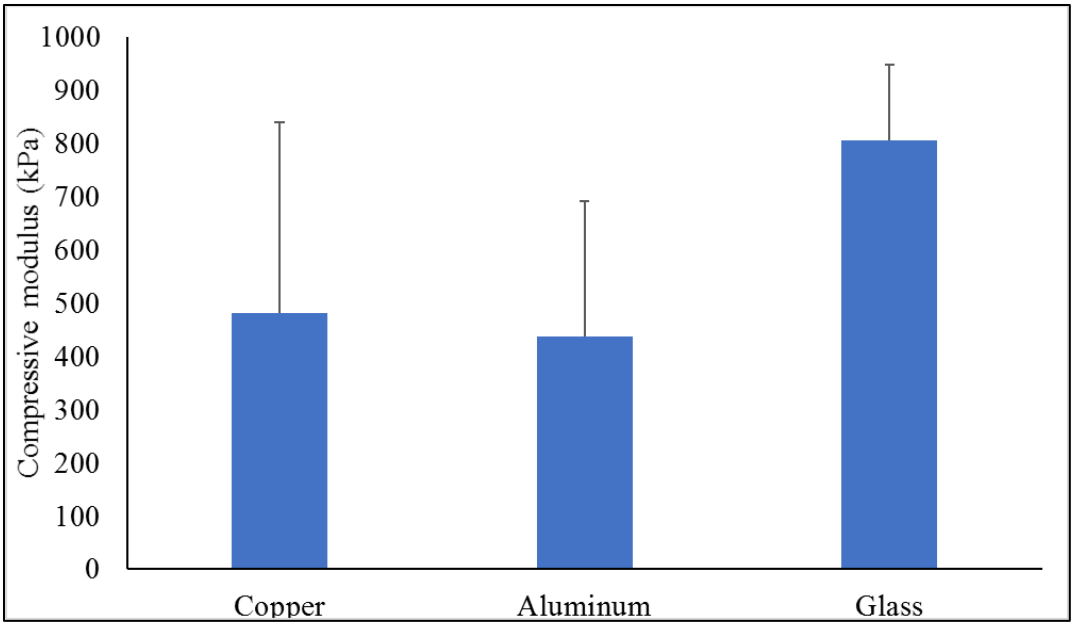

Figure 2.15. Compressive modulus of scaffolds made from copper, aluminum and glass vials (n = 7)

2.3.6. Effect of Initial Concentrations of PLLA on Structural Properties of Scaffolds

Glass vials were found to be ideal to impose a high cooling rate and to reach lower temperatures at the end of the freezing process. The effect of initial concentration of PLLA in dioxane on the structural properties were studied by repeating the freezing process using three different concentrations of 3, 5 and 7% (wt/v). For this study, 5 mL of solutions were used in every vial. This allows to have a thicker scaffold and to visualize the micro-porous structure above 10 mm from the bottom. Fig. 2.16 shows the cooling profile of the solutions with their maximum variations marked as error bars. It can be observed that the temperature profiles overlap each other and no significant trend is observed with increasing initial concentrations of PLLA in dioxane.

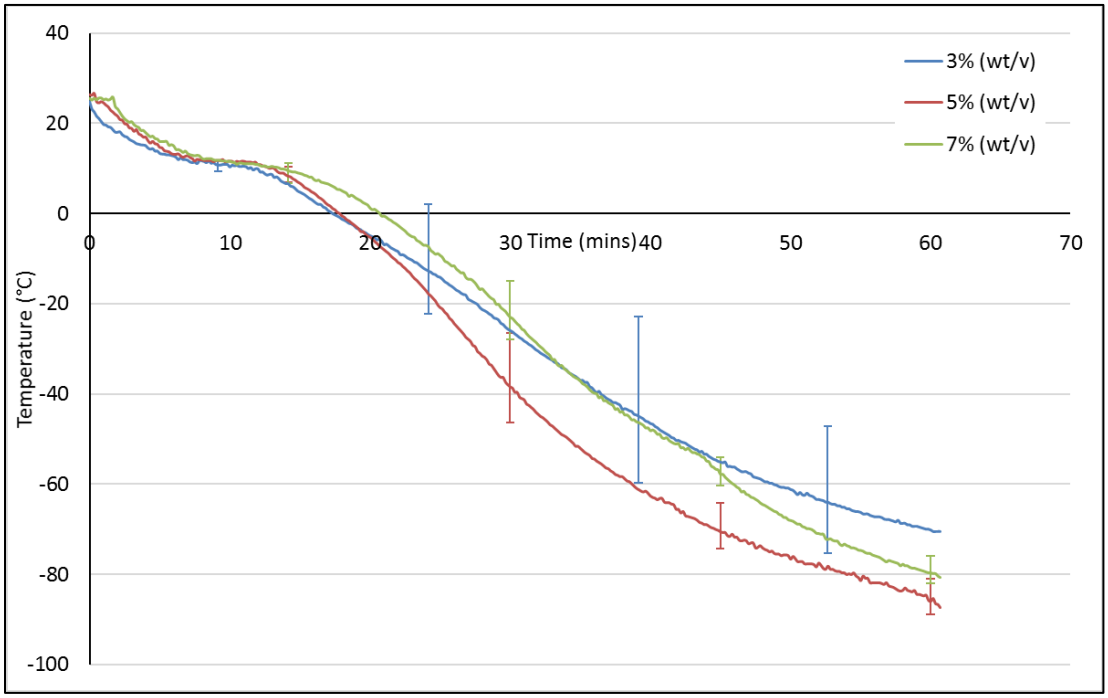

Figure 2.16. Temperature profile of PLLA/dioxane solutions at various concentrations with maximum temperature variations (n = 3)

The cooling rate of each of the solution concentrations from its nucleation point (10°C) to its final temperature was calculated and plotted in Fig 2.17. Highest effective cooling rate of 1.99°C/min was observed in 3% PLLA/dioxane. When 5% and 7% concentrations were used, the effective cooling rates were 1.19 and 1.45°C/min respectively. No significant change in cooling rates were observed between 3 and 7% concentrations. Effective cooling rates of 5 and 7% samples were also statistically insignificant with a p - value of 0.13. Thus, it can be concluded that the concentration of PLLA in dioxane does not play a significant role in deciding the in situ cooling rate of the solution.

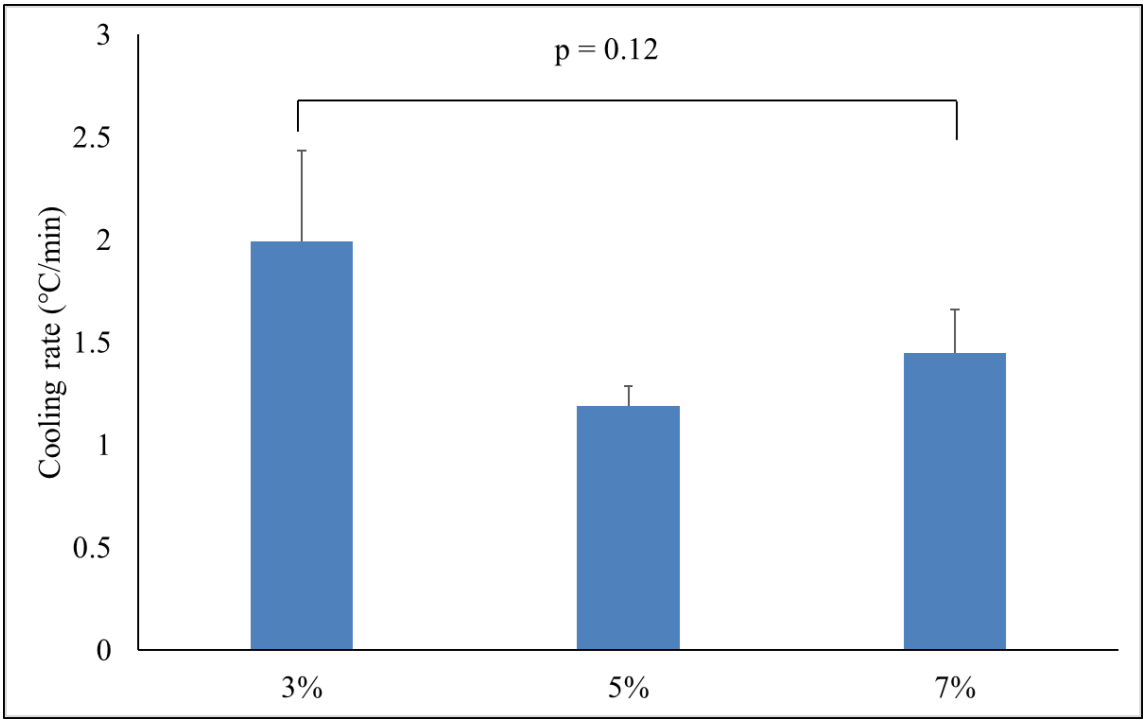

Figure 2.17. Cooling rates of the solution with increasing concentrations of PLLA

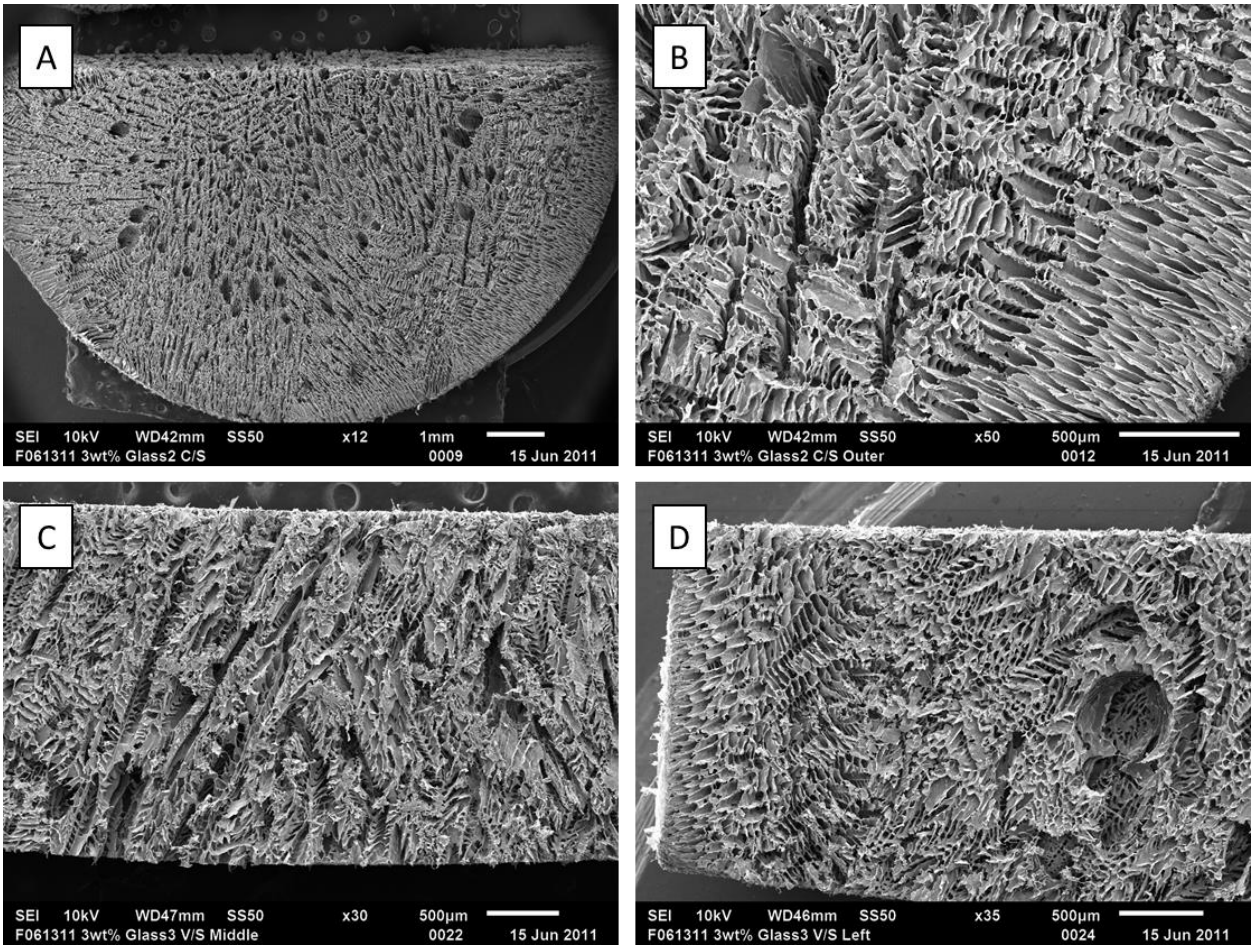

Figure 2.18. SEM image of scaffolds made from 3% (wt/v) PLLA/dioxane representing the cross-section perpendicular to the axis (A, B) and vertical section parallel to the axis (C, D)

Scaffolds made from 3% PLLA in dioxane were comprised of relatively irregular porous patterns in the central region. However, near the surface touching the vials while cooling, the porous structures were radially inward. This may be caused by relatively higher cooling rates of 1.99°C/min experienced by these scaffolds. The vertical sections show porous structures in the axial direction slightly tilting towards the periphery. These patterns were very similar to the scaffold micro-structure from 4mL of 7% (wt/v) solution in glass vials.

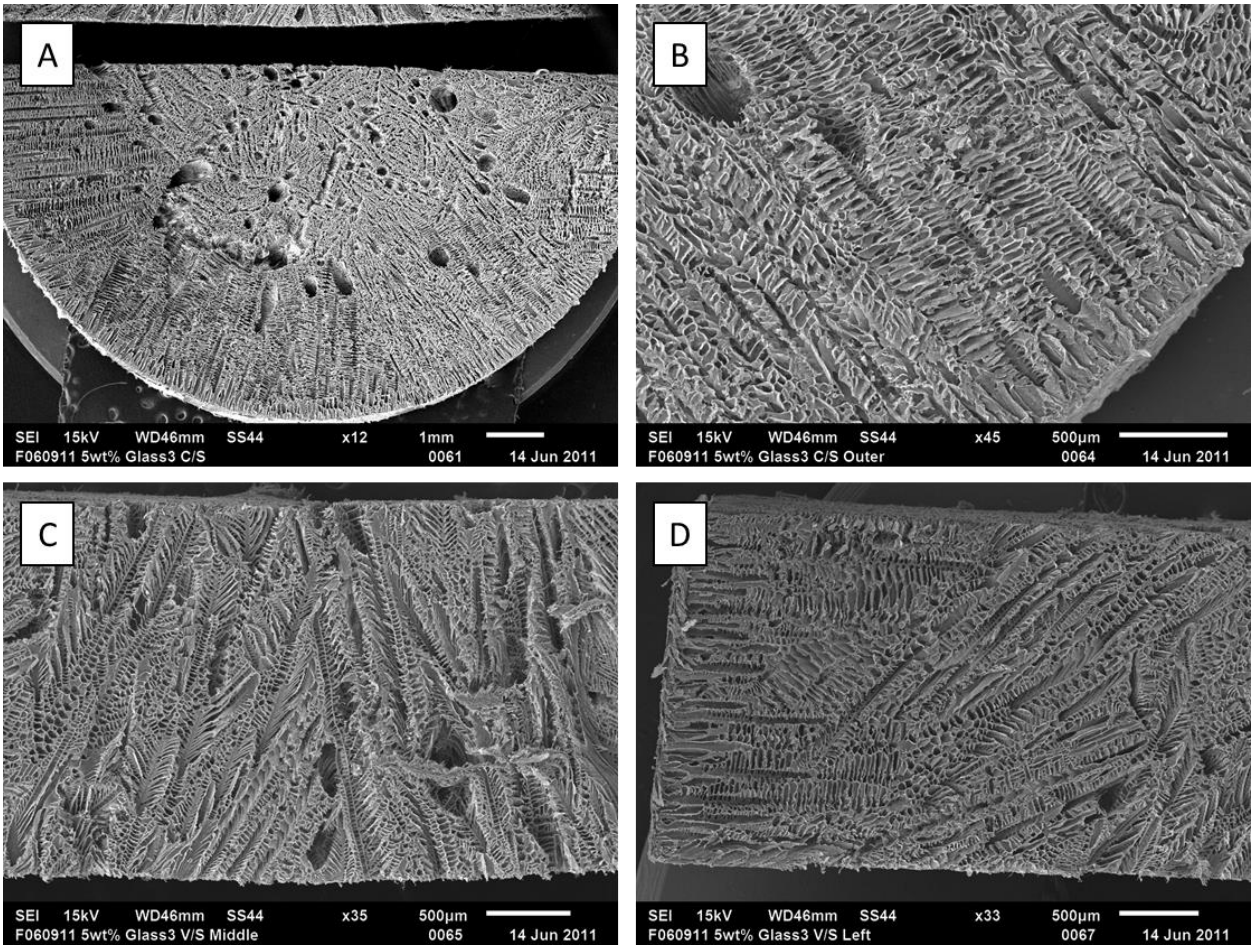

Figure 2.19. SEM image of scaffolds made from 5% (wt/v) PLLA/dioxane representing the cross-section perpendicular to the axis (A, B) and vertical section parallel to the axis (C, D)

The scaffolds made from 5% PLLA in dioxane had more regular porous patterns compared to the 3% samples. The extent of radial porous structures from the periphery were longer as observed in Fig 2.19 (C, D). This potentially increases the interconnectivity of pores and also the mean pore-size. The comparatively lower cooling rate did not cause any major changes in the pore structures generally observed.

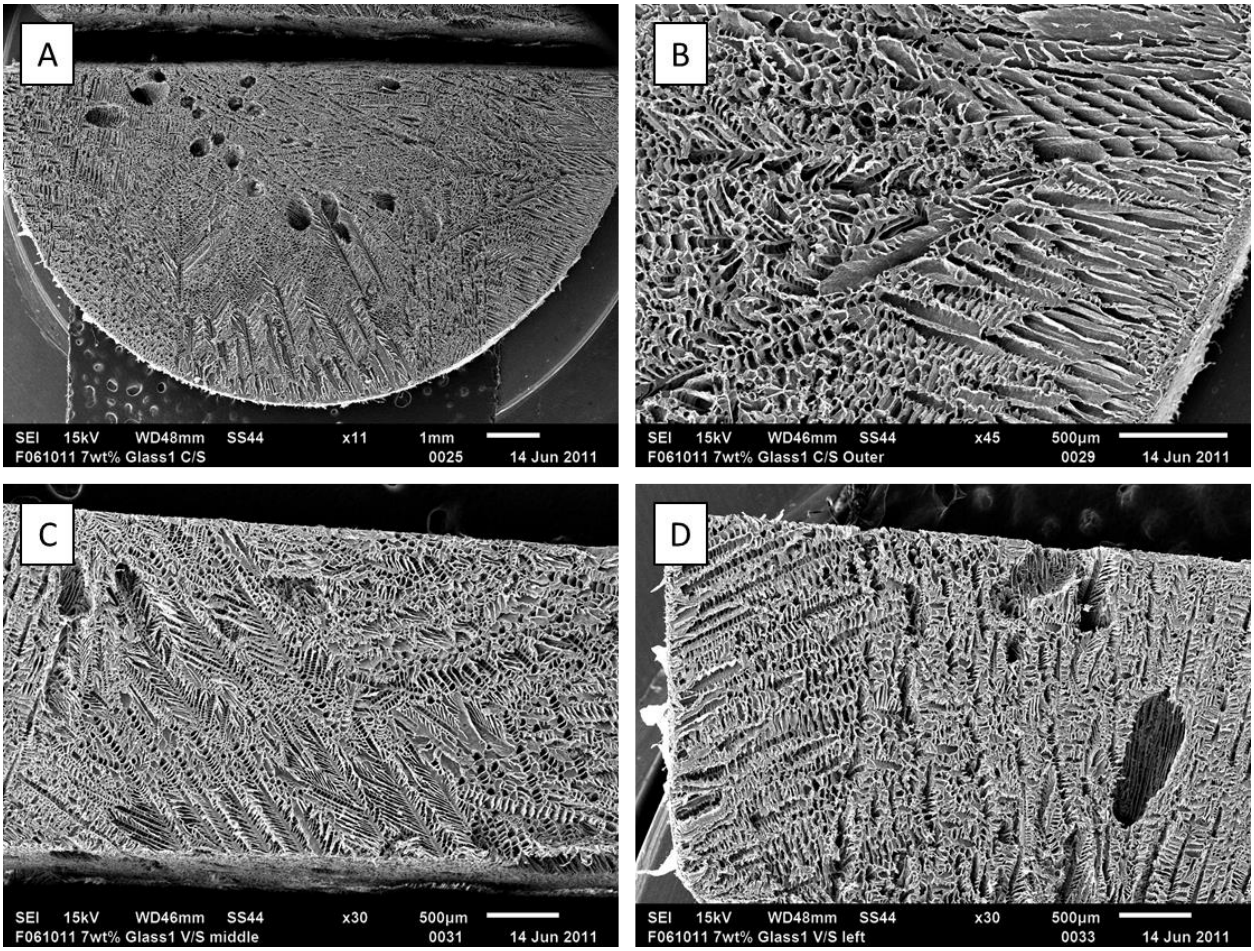

Figure 2.20. SEM image of scaffolds made from 5% (wt/v) PLLA/dioxane representing the cross-section perpendicular to the axis (A, B) and vertical section parallel to the axis (C, D)

When the initial PLLA concentration was increased to 7% (wt/v), the porous patterns were very similar to previously observed. However, the length of the radial pores increased a lot as observed in Fig 2.20 (B, D). The pore-sizes were measured using the JEOL JSM software. The mean-pore-size and their standard deviations are marked in Fig 2.21. The 7% (wt/v) PLLA/dioxane scaffolds had the highest mean pore-size of 212.6 µm. At the concentration of 3 and 5% (wt/v) PLLA in dioxane, the mean pore-sizes were 92.01 µm and 114.55µm respectively. However, there was no statistical significance between 3 and 5% concentrations.

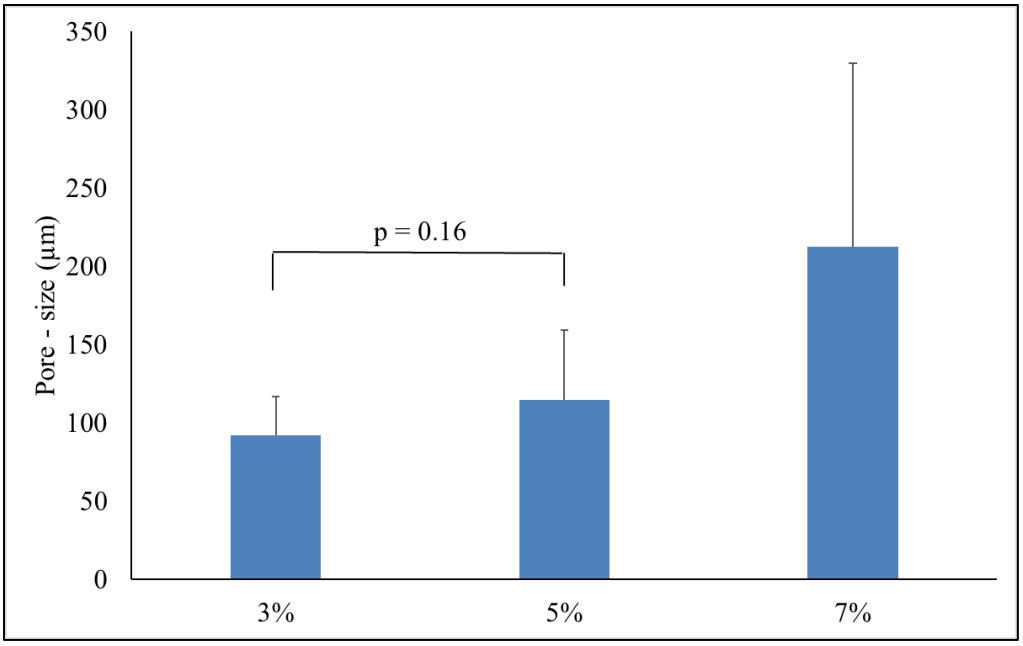

Figure 2.21. Mean pore-size of scaffolds with increasing concentrations of PLLA (n ~ 10)

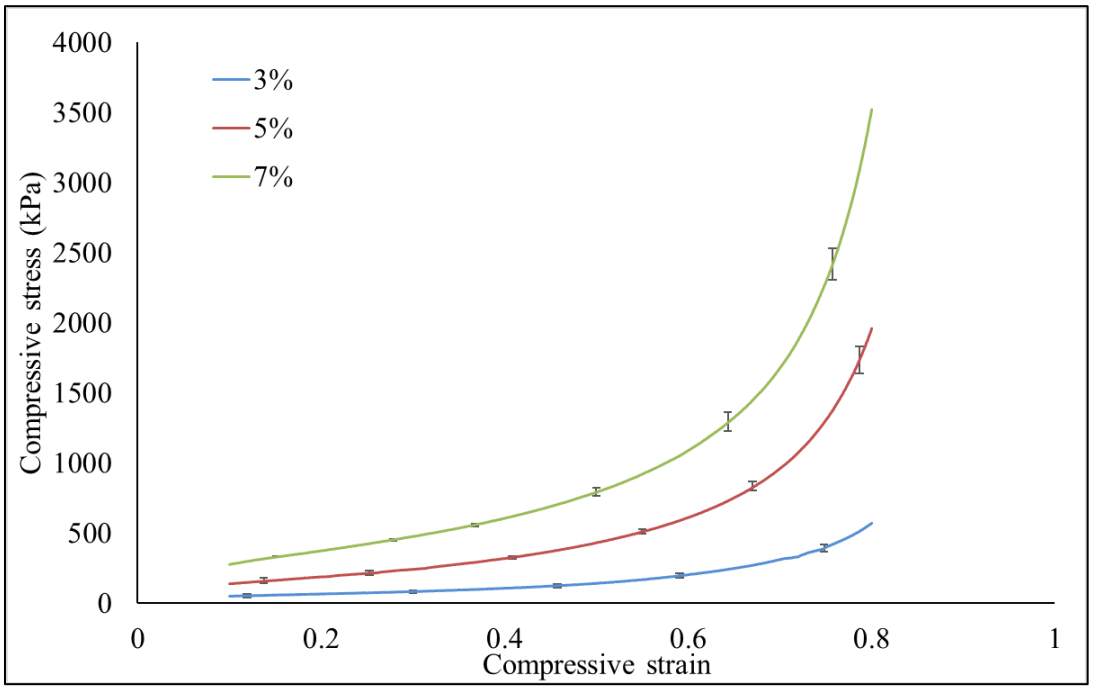

Figure 2.22. Real time stress strain curves of scaffolds made from 3, 5 and 7% (wt/v) PLLA in dioxane (n = 3)

From the instantaneous stress-strain values (Fig 2.22), using linear regression method, compressive modulus for each scaffold made from varying initial concentrations of PLLA was calculated and plotted in Fig 2.23. The compressive modulus were 273.07 kPa, 860.63 kPa and 1475.14 kPa for 3, 5 and 7% (wt/v) of initial concentrations respectively. Thus, there is a significant increase of compression strength when PLLA concentration was increased. However, the influence of imposed thermal profile (cooling rate) on the mechanical integrity of the resulting scaffolds is unknown as there was no control over the imposed cooling rate.

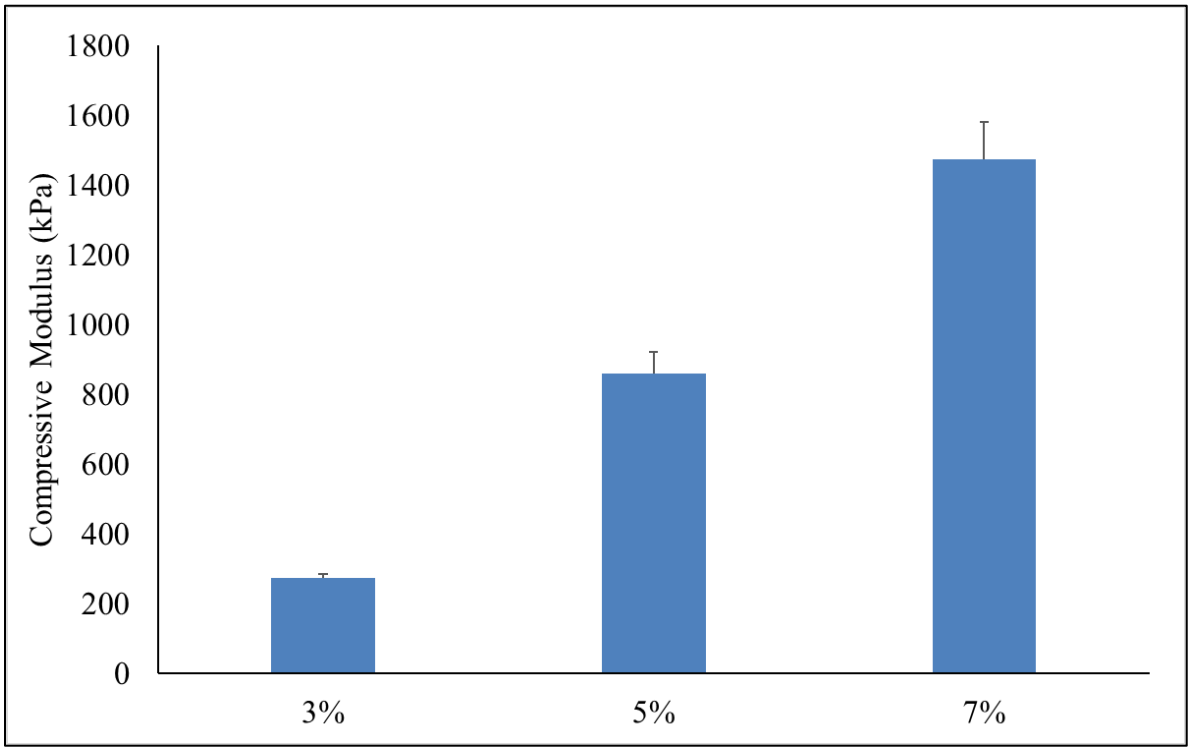

Figure 2.23. Compressive moduli of scaffolds made from 3, 5 and 7% (wt/v) PLLA in dioxane (n = 3)

2.3.7. Cooling Rate of Copper, Aluminum and Glass Vials in Dry Ice Bath

Throughout the 'effect of initial concentrations of PLLA' study, the cooling rate was uncontrolled and was in part determined by the EPS floating block's structure and the thermal property of the glass. The highest cooling rates ever achieved by above experiments was 1.99°C/min. Since quenching in liquid nitrogen (-196°C) was not a practical option as it broke the glass vials completely, dry ice bath (dry ice and ethanol) was used as a quenching medium. Copper, aluminum and glass vials were filled with 4 mL of 7% (wt/v) PLLA/dioxane solution. These vials were directly quenched in dry ice bath while simultaneously measuring the temperature. The cooling profiles are shown in Fig 2.24.

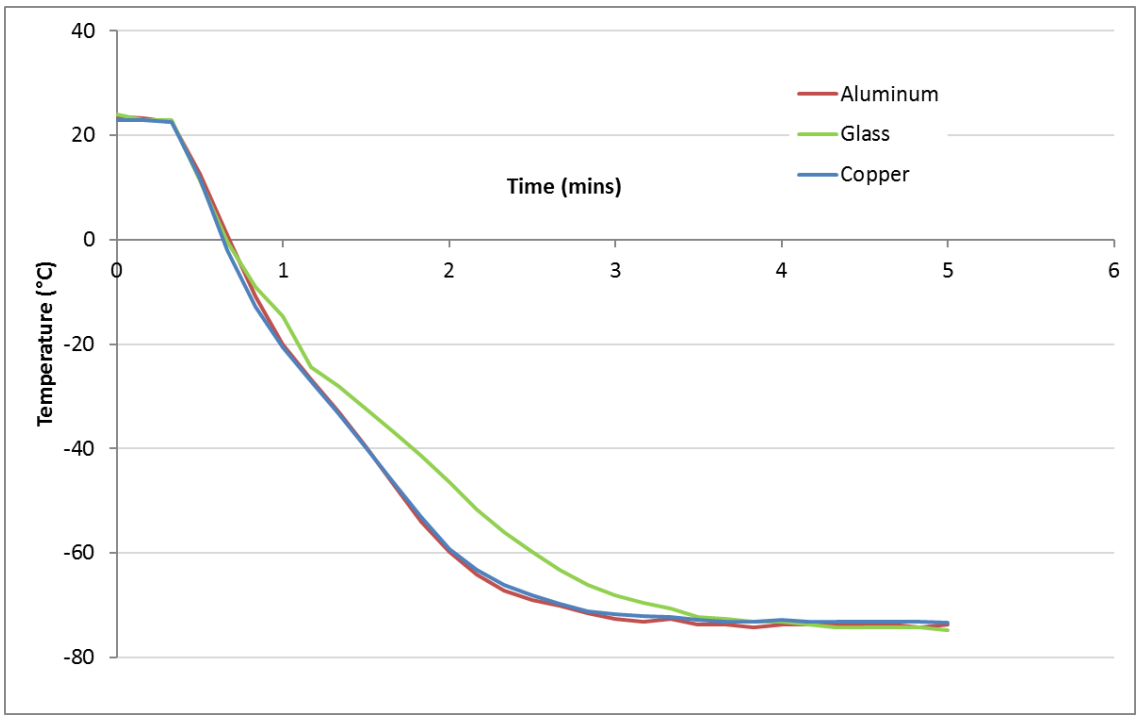

Figure 2.24. Temperature profile of 7% (wt/v) PLLA/dioxane solution in aluminum, copper and glass vials immersed in dry ice bath (-80°C)

The lowest temperature of -70°C was reached within 3 - 4 mins of immersion. The effective cooling rates from nucleation temperature to -70°C was calculated to be 34.67, 31.60 and 21.02°C/min for copper, aluminum and glass respectively. Though the cooling rates were higher by quenching in a liquid bath, all the vials had almost similar cooling rates. Therefore, quenching is not an ideal method to achieve a controlled cooling rate.

2.4. Conclusion

The experimental thermal profile of PLLA/dioxane in copper and aluminum vials were unexpected as the thermal conductivity of both the metals are significantly higher than glass. Though the structural difference in the metal vials could have played a role in limiting the thermal conduction of liquid nitrogen vapors, there could be an error in reading the temperature in situ. Galvanic corrosion between the thermocouple and metal vials could be possibility considering the presence of 1,4-dioxane in the solution. Also, glass vials were able to provide the lowest temperature at the end of 90 mins exposure to liquid nitrogen vapors. Copper and aluminum vials provided a minimum temperature of - 25°C and -30°C respectively, which is too high compared to the liquid nitrogen vapors at -160°C. The compressive modulus of scaffolds made from glass were significantly higher than that of scaffolds made from aluminum. Since mechanical integrity of a bone graft is of primal importance, though aluminum and glass vials provided a high mean pore-size with no significant difference, in future glass vials will be used to make scaffolds with equipment assisted imposition of varying thermal profiles.

Chapter 3 : Characterization of Scaffolds Made from Control Rate Freezer (CRF)

3.1. Introduction

There are many methods which have been used to fabricate 3D porous scaffolds of synthetic polymers, including solvent casting/particulate leeching techniques, gas-foaming process, electro-spinning method, and thermally induced phase separation (TIPS). The advantages of solvent casting method include: simple operation, ability to control pore size and porosity by varying the salt/polymer ratio and particle size of the added salt [38, 103, 104]. However, the scaffolds do not exhibit sufficient mechanical strength and the required material properties.33 Gas foaming allows the forming of 3D porous polymer structures with very high porosities (~90%) and pore sizes (~100 μm), however, the interconnectivity of pores is low, limiting the permeations of nutrients and cells into the scaffold matrix [39, 105, 106]. Electrospinning allows localized control on the micro-structure of the porous scaffold but is highly unsuitable and cumbersome to fabricate thick (mm size) 3D scaffolds [40, 107, 108]. TIPS is a simple procedure in which, the polymer dissolved in a solvent is frozen, subsequently the solvent is sublimated, resulting in a porous scaffold. The scaffolds fabricated using TIPS exhibit a compression moduli ~20 times higher than that of the scaffolds fabricated using other methods [41], while generating scaffolds with a pore size of 30–150 μm [93, 109, 110]. The pore morphology of the scaffolds varies depending on the concentration of the polymer solution as well as the induced thermal profile during freezing process. The objective of this study was to characterize the 3D porous Poly (l-lactic acid) (PLLA) scaffolds made in varying concentrations (3, 7 and 10% wt/vol) of PLLA in dioxane using three different freezing rates (1, 10 and 40°C/min to a final temperature of −60˚C). PLLA was chosen as the scaffold material due to its bio-compatibility and slower rate of degradation in vivo when compared to PLGA [99]. Furthermore, PLLA is FDA approved for in vivo research and has proven

to show more osteogenic properties than some ceramics. The fabricated scaffolds were analyzed to determine the structure-property relationship as a function of the polymer concentration and the imposed cooling rate.

3.2. Materials and Methods

3.2.1. Preparation of PLLA-dioxane/ethanol Solutions

PLLA (Mn: 100,000; density: 1.2 g/cm^3) was obtained from SurModics Pharmaceuticals (Birmingham, AL) with trade name '100 L 7A'. The PLLA-Dioxane solution was formed by dissolving 3, 7 and 10 % weight of PLLA in dehydrated 1,4-Dioxane solution or in 85% dioxane with 15% ethanol solution. The concentration Ethanol was limited to a maximum of 15% as that was the cloud-point concentration at room temperature. The mixture at 50 ˚C was stirred with a magnetic stirrer until a clear solution is formed. Approximately 5 mL of the PLLA-Dioxane solutions were transferred into cylindrical capsules of (internal) diameter of 13mm and stored at room temperature (27 to 30 ˚C).

3.2.2. Freezing process using Control Rate Freezer (CRF)

The cylindrical capsules (or vials) filled with PLLA/dioxane (: ethanol) solution were placed in the cooling chamber of a CRF (Planer PLC Group, Shepperton Surrey TW16 7HD, UK). The CRF was connected to a liquid nitrogen supply at 22 psi. The thermal profile of the chamber was programmed in the controller of the CRF as follows: Step (i): Cool from 20˚C to 10˚C at 10˚C/min; Step (ii): Hold at 10˚C for 1 min to nucleate 1,4 Dioxane (initial characterization experiments showed the phase change temperature of 1,4-Dioxane in PLLA to be ~10˚C); Step (iii): Cool from 10˚C to −60˚C at the pre-determined rate of cooling of either 1, 10 or 40 ˚C/min. The accuracy of the CRF was verified by measuring the temperature in the well plates, using type-T hypodermic

needle thermocouples (Omega Technologies, Stamford, CT, USA). Thermocouple voltages were read by a precision temperature data logger (Veriteq Instruments Inc, Richmond, BC, Canada) and transferred to a personal computer for further reduction and data analysis. The cooling rates imposed by the CRF was within 5% for cooling rates of ≤10 ˚C/min and within 10% for the highest cooling rates of 40 ˚C/min.

3.2.3. Freeze-drying Process

The frozen PLLA/dioxane (: ethanol) vials were immediately transferred to an ice pack (4°C) for transportation to the freeze dryer location (5mins) were the samples were placed in Labconco Fast-Freeze Flask. The Fast-Freeze Flask was connected to the FreeZone Plus 2.5 Liter Cascade Console Freeze Dryer (Labconco Corporation Kansas City, Missouri, USA) for 48 hours to sublimate the solvent (Dioxane or Dioxane-Ethanol). The console freeze dryer maintained the frozen PLLA-Dioxane/Ethanol vials at 0.037 bar and -55°C to generate 3D porous PLLA scaffolds. The frozen and freeze-dried porous scaffolds were extracted from the vials and typically range in size from 15 to 16 mm in height and approximately 12 mm in diameter (somewhat smaller than the internal diameter of the cylindrical capsule due to shrinkage during the sublimation process).

3.2.4. Compression Testing

INSTRON 5900 Series – Advanced Mechanical Testing Systems Compression tester (Instron Industrial Products, Liberty Street, Grove City, PA, USA) was used to compress the 3D porous PLLA scaffolds that were trimmed to 10 mm in length using a VWR razor blade. The cylindrical 3D porous scaffold samples (12 mm in diameter and 10 mm in length) were loaded onto the center of the compression anvil and the two jaws of the tester were adjusted to be in contact with the top

and bottom of the scaffold. The compression machine was programmed to compress the 3D porous PLLA scaffolds to 20% of its original length in the axial direction and to 66.67% of its original length in the radial direction, while simultaneously recording the instantaneous load applied (Fi) and the compressive strain (ϵi) experienced by the sample. From the instantaneous loads at each time point, compressive stress was calculated from which the Compressive Moduli was calculated as follows:

$$Instantaneous\ Stress\ (\sigma_i) = \frac{Instantaneous\ Load\ Applied\ (F_i)}{Cross-sectional\ area\ of\ scaffold}$$

$$Compressive\ Modulus = \frac{\sum(\epsilon_i - \bar{\epsilon}) \cdot (\sigma_i - \bar{\sigma})}{\sum(\epsilon_i - \bar{\epsilon})^2}$$

3.2.5. Micro-structural Characterization

The cross-sectional microstructure of the frozen and freeze-dried porous scaffolds was analyzed using Scanning Electron Microscopy (SEM) at a distance of 5 mm from the bottom scaffold surface. Additionally, the microstructures of the frozen and freeze-dried porous scaffolds were also obtained along the vertical cross sections. The surfaces of the 3D porous scaffolds to be characterized were coated with 15 nm's of Platinum using EMXS550X Sputter Coater (Electron Microscopy Sciences, Industry Road, Hatfield, PA, USA). JEOL JSM-6610LV Scanning Electron Microscope (Jeol, Dearborn Rd, Peabody, MA, USA) was then used to scan and capture the scaffold micro-structural images.

3.2.6. Pore Diameter and Porosity

Pore-sizes were measured at various random locations (~20) from the SEM images using JEOL JSM-6610LV software. Known volume of scaffolds (5 mm in height and 12 mm in diameter; 0.5655 cm^3) were weighted to obtain the density of scaffold ($\rho_{scaffold}$). The density of pure PLLA is known as 1.25 g/cm^3. Porosity of the scaffold was calculated by gravimetric method as follows [102]:

$$Scaffold\ density\ \left(\rho_{scaffold}\right) = \frac{mass}{volume}$$

$$Porosity\ (\%)\ = \left[1 - \frac{\rho_{scaffold}}{\rho_{PLLA}}\right] \times 100$$

3.2.7. Inter-connectivity of pores

Cylindrical scaffolds of 10 mm in height were fixed to the bottom of a 50 mL Pyrex® graduated measuring cylinder (Sigma-Aldrich, USA) using 1% agarose gel. This step was done to neglect the effects of buoyant forces when the measuring cylinder was filled with 100% ethanol up to 50 mL mark. The scaffolds were allowed to soak the 100% ethanol for 1 hour. Ethanol was used as a soaking medium, since PLLA is hydrophobic in nature with a water contact angle of higher than 120°. After an hour, the drop in the volume of ethanol was measured by refilling ethanol to reach the closest 50 mL mark using a combination of 100 and 1000 µL Eppendorf® Reference® 2 Variable Volume Pipettors (Sigma-Aldrich, USA). This excess volume absorbed by the scaffolds gives a measure of interconnected porous volume as isolated, closed pores will not absorb any ethanol. The interconnected region within a 10 mm height scaffold construct was expressed as

percentage by calculating the ratio of interconnected porous volume within a scaffold to the toal volume of the scaffold (1.13 cm^3).

3.3. Results and discussion

In Fig.3.1 micro-porous structure of scaffolds made from PLLA dissolved in 100% dioxane is shown according to the percentage of PLLA used and cooling rate imposed.

The porous structures looked more spherical in scaffolds made from 3% PLLA especially at cooling rates 1 and 10°C/min. No significant change in morphology was found between vertical and cross-sections at this PLLA concentration. Scaffolds made from 7 and 10% PLLA showed spindle-shaped pore structures. In general, the micro-porous structures became more regular with increase in cooling rates and proportion of PLLA used. However, in the case of 3% PLLA, porous structures were irregular even with increased cooling rates. With increasing concentrations of PLLA the pores were highly compartmentalized suggesting relatively poor interconnectivity.

Both macro-pores (>50 μm) and micro-pores (10-50 μm) were found in scaffolds made using 10% PLLA for all cooling rates. Combinations of pore-sizes in these ranges have reported to show better cell proliferation, vascularization and bone formation *in vivo* for ceramic scaffolds [111]. Though it was impossible to achieve a localized control on the micro-structure of scaffolds as reported in 3D printing [112-114] or have a high degree of interconnectivity as electro-spinning technique [40, 91, 115-117], regulating cooling thermal profile on different PLLA concentrations using TIPS method may help to achieve the necessary micro-structure in the scaffolds.

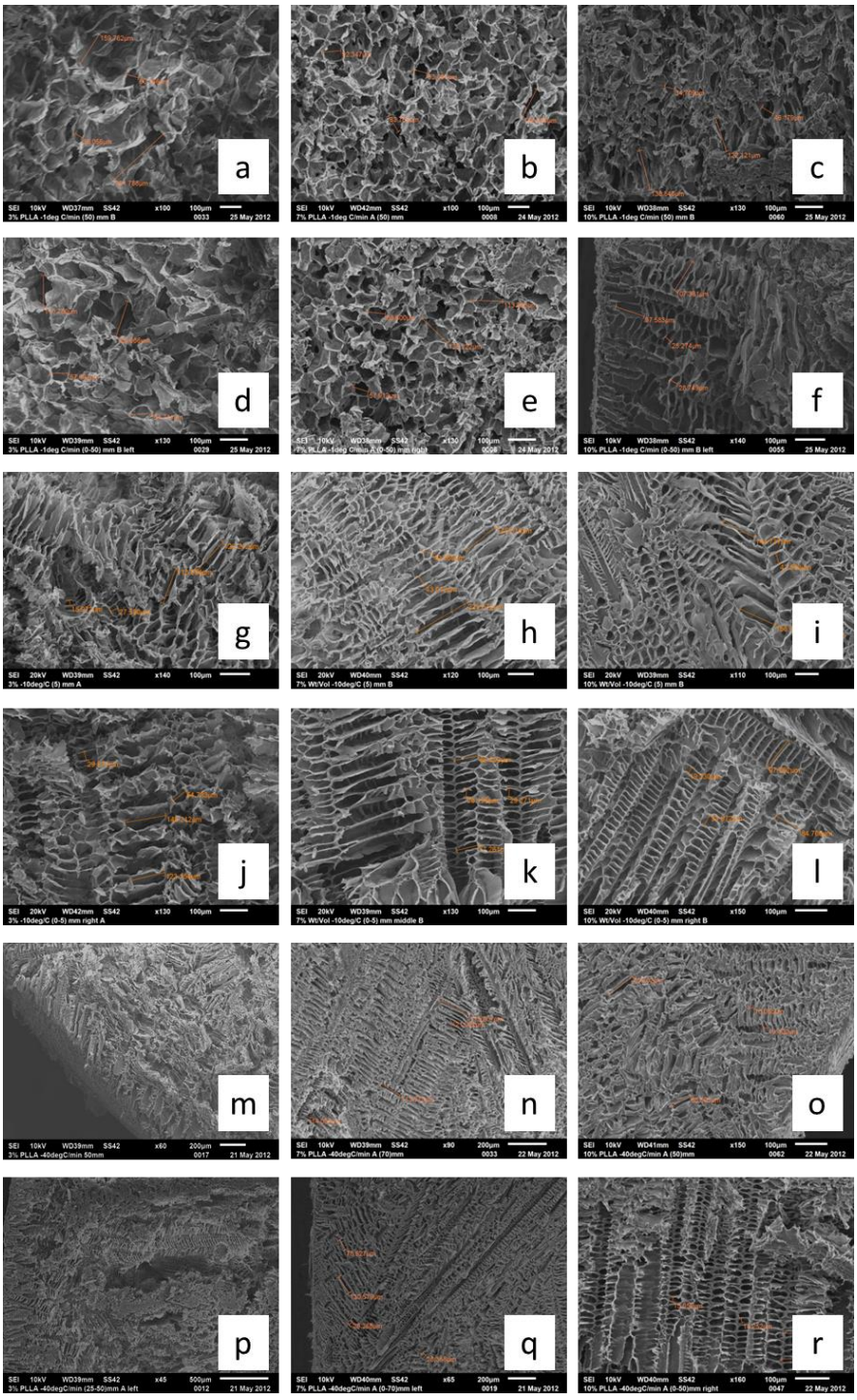

Figure 3.1. SEM images showing the micro-structures of the cross-section at 5 mm from the bottom of PLLA scaffolds made by cooling at 1°C/min (a, b and c), 10°C/min (g, h and i) and 40°C/min (m, n and o). Micro-structure of the vertical section in the region 0 – 5 mm for scaffolds cooled at 1°C/min (d, e and f), 10°C/min (j, k and l) and 40°C/min (p, q and r). All images arranged according to increasing PLLA concentrations in dioxane from left to right

Pore-sizes (n ~ 20) were measured at random from the SEM images and the mean pore size was plotted along with their standard deviations in Fig.3.2. Scaffolds made from 3% PLLA showed a decreasing trend of mean sizes such as 93.87 μm, 81.34 μm and 69.31 μm when cooled at 1, 10 and 40°C/min. However, none of these values were significantly different from each other due to relatively high standard deviations. Scaffolds made from 7% PLLA had a mean pore size of ~ 93 μm when cooled at 1 and 40°C/min, but when cooled at 10°C/min it shows a significant decrease to 74.05 μm. In scaffolds made from 10% PLLA, highest mean pore size of 90.42 μm was achieved when frozen at 10°C/min. Other mean pore sizes were 66.85 and 75.24 μm when cooled at 1 and 40°C/min respectively. In the case of 7% and 10% scaffolds, the length of the spindle structured pores were measured as the pore-size. This was done since the spindle structured hASCs were found to grow aligning along these structures with longer culture periods as observed in 42nd day (Chapter 4). Standard deviations of pore-sizes were found to improve with increasing PLLA concentrations for all cooling rates. High standard deviations in 3% PLLA scaffolds suggest irregular pore-structures as observed in SEM images.

Highest mean porosity of 96.65% was obtained in 3% PLLA scaffolds at cooling rate 1°C/min. When 7% PLLA was used, the porosity drops to ~92% as shown in Fig. 3.3. Both 3% and 7% scaffolds showed a very slight decrease in % porosity, linearly proportional to the logarithm (to the base 10) of the cooling rate used. The decrease in % porosity with respect to the increasing cooling rates was not significant (p-value > 0.05) for 3 and 7% PLLA scaffolds. In 10% scaffold, the highest porosity (90.36%) was obtained when cooled at 10°C/min. When cooled at 1 and 40°C/min, it was 89.3% and 88.22% respectively.

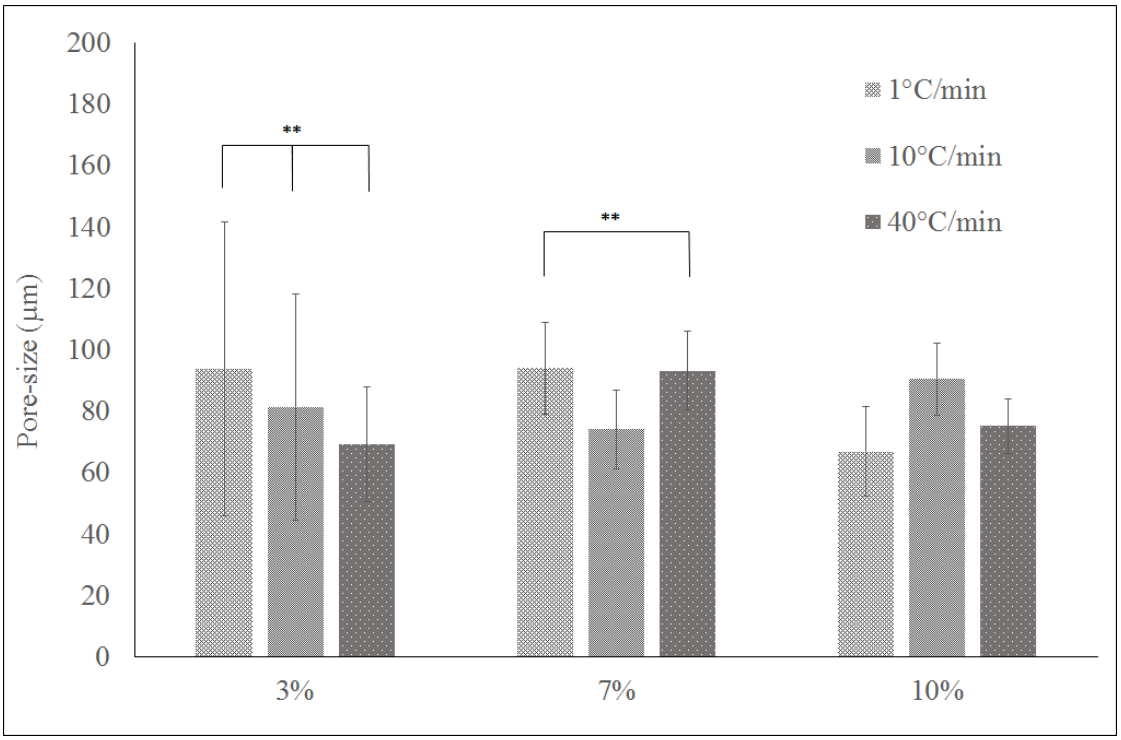

Figure 3.2. Mean pore diameter and standard deviations of scaffolds made from 3, 7 and 10 (wt/vol) % PLLA in Dioxane, measured randomly from SEM images (16-20 values per sample), and plotted corresponding to increasing cooling rates. ** indicates not significant (p-value > 0.1) (n ~ 20)

The red lines drawn at 97, 93 and 90% represents the theoretical porosity values of the initial concentrations (3, 7 and 10% respectively) of PLLA. Mean porosity of scaffolds made from 3 and 7% initial concentrations of PLLA were slightly lower than the theoretical values. This could be attributed due to the shrinkage of the PLLA/dioxane solution when cooled at higher cooling rates. Also, the shape of scaffolds after lyophilization process was similar to a negative imprint of a right conical structure from the top, suggesting movement of the PLLA/dioxane solution towards the walls of cylindrical capsules during freezing process. The porosity (%) of resulting scaffolds were calculated to determine the significance of this change of shape. However, it was found that there

was no significant change of porosity from the theoretical values for all initial concentrations and the change of porosity with increasing cooling rates were statistically insignificant.

Using TIPS to make 3D synthetic polymer scaffolds, high values of % porosity was achieved, which is vital for intrinsic vascularization of bone implants *in vivo* [118, 119].

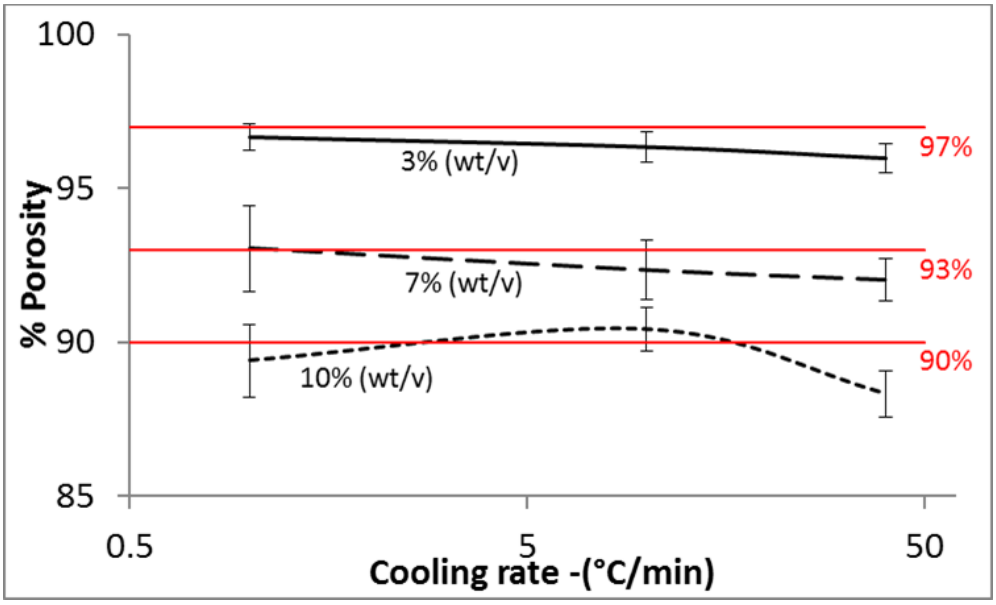

Figure 3.3. Percentage porosities of scaffolds made by dissolving 3, 7 and 10 (wt/vol) % PLLA in Dioxane, measured by void fraction method and are plotted against increasing cooling rates on a $\log_{10}$ scale (n = 4)

When compared to ceramic scaffolds which usually has porosity ranging 25 - 80 % [48, 49, 120, 121], our PLLA scaffolds had very high porosity (88 – 96 %) which is comparable to synthetic polymer scaffolds made by other methods like super-critical drying, gas-foaming, salt-leeching or a combination of these methods [122-131]. These values are closer to the 90% porosity of a

cancellous bone in human adult skeleton [62-64]. Higher porosity values and regular distribution of pores facilitate better degradation *in vivo* [132-136].

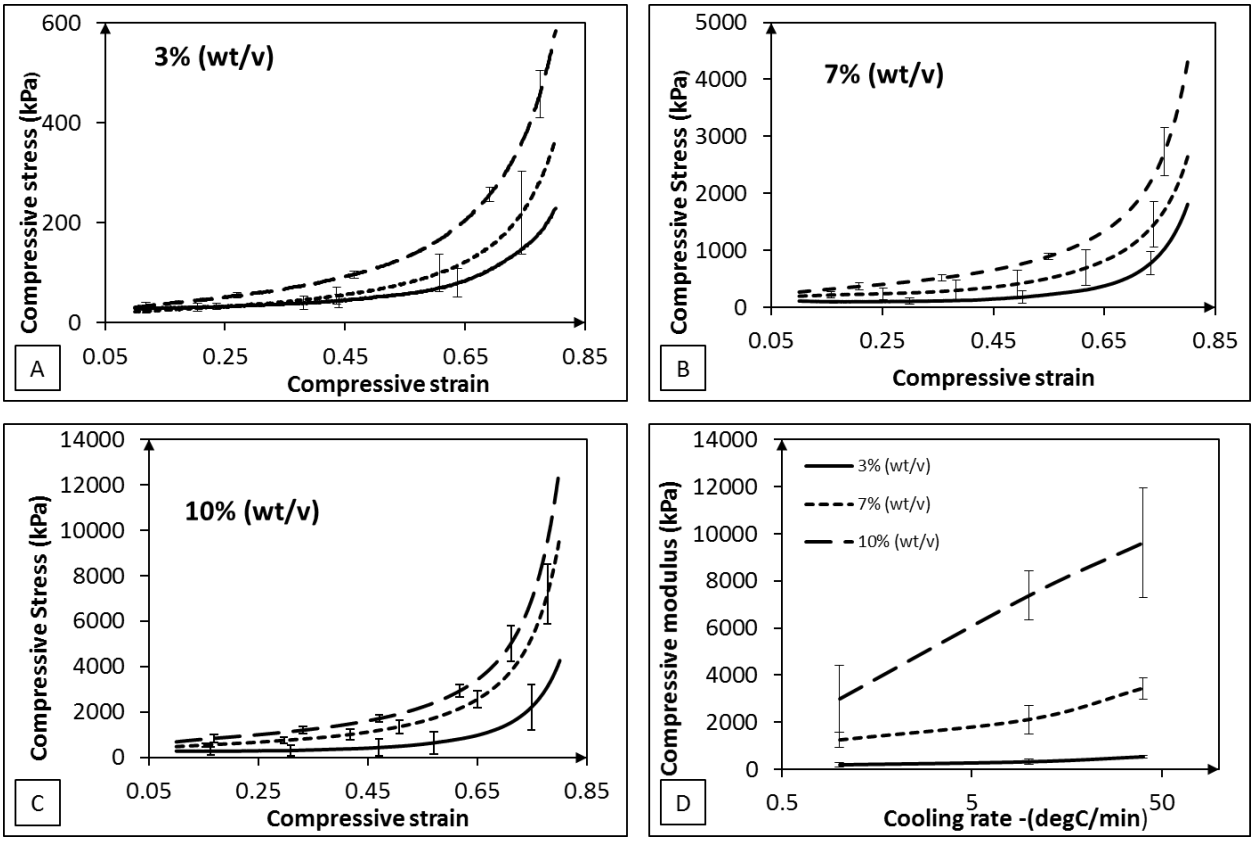

Figure 3.4. Real time axial stress strain curves of scaffolds made by dissolving (A) 3 (wt/vol) % (B) 7 (wt/vol) % and (C) 10 (wt/vol) % PLLA in dioxane, showing increasing compressive strength with increasing cooling rates. (D) Compressive Moduli of 3, 7 and 10 (wt/vol) % samples plotted along increasing cooling rates on log10 scale (n = 6)

Axial stress-strain curves of 3%, 7% and 10% scaffolds in Fig. 3.4 shows increased compressive strength with increasing cooling rates for all PLLA concentrations. The compressive modulus calculated by linear regression method increases linearly to logarithm (to the base 10) of the imposed cooling rate for each concentration of PLLA in solvent. Compressive moduli of 3%, 7%

and 10% PLLA scaffolds increased from 185.83 to 522.72 kPa, 1248.92 to 3426.29 kPa and 2989.05 to 9606.11 kPa respectively with increasing cooling rates. Also, the rate of increase in compressive modulus with respect to the logarithm (to the base 10) of cooling rate, increases significantly (~ 6 times from 3 to 7% PLLA and ~4 times from 7 to 10% PLLA) with increase in PLLA concentration.

The stress values along the mid-section perpendicular to the plane of loading was calculated from the known cross-sectional area (12 × 10 mm^2). The cross-sectional area of the midsection was measured to be same before and after the compression test. Stress-strain curves of 3% scaffolds shows a similar trend to that of the axial direction with increasing cooling rates as shown in Fig 3.5. However, the overall compressive modulus decreased more than 100 times (185 kPa to 1.1 kPa) in the radial direction when cooled at 1°C/min, about 160 times (316 kPa to 1.97 kPa) when cooled at 10°C/min and about 175 times (522 kPa to 2.97 kPa) when cooled at 40°C/min. The stress-strain curves of scaffolds made from 7 and 10% PLLA in dioxane solutions showed no change in the compressive strength with increasing cooling rates. The mean compressive modulus of 7% scaffolds cooled at 1°C/min was 14.1 kPa and when cooled at 10 and 40°C/min the compressive modulus was about 8.8 kPa. In the case of scaffolds made from 10% PLLA in dioxane the compression moduli were 28.4, 23.46 and 22.02 kPa when cooled at 1, 10 and 40°C/min respectively. However, there was no statistical significance of compressive modulus with increasing cooling rates for 7 and 10% scaffolds. This huge difference in compressive modulus of scaffolds between the axial and radial direction maybe influenced by the porous structures propagating in the radial direction is shifted towards the bottom of the capsule during the cooling process. Thus, the scaffold microstructure provides more resistance to axial loads than radial loads. As the cooling rate increases more number of pores are formed along this shifted direction as

observed in Fig 3.1 e, f, k, l, q and r. This combined with the porous formation in the axial direction from the bottom of the capsules may contribute to the substantial increment of axial compressive modulus with increasing cooling rates. Thus, the relative alignment of porous structures in the scaffold contribute to the fate of compressive modulus with varying cooling rates in any given direction.

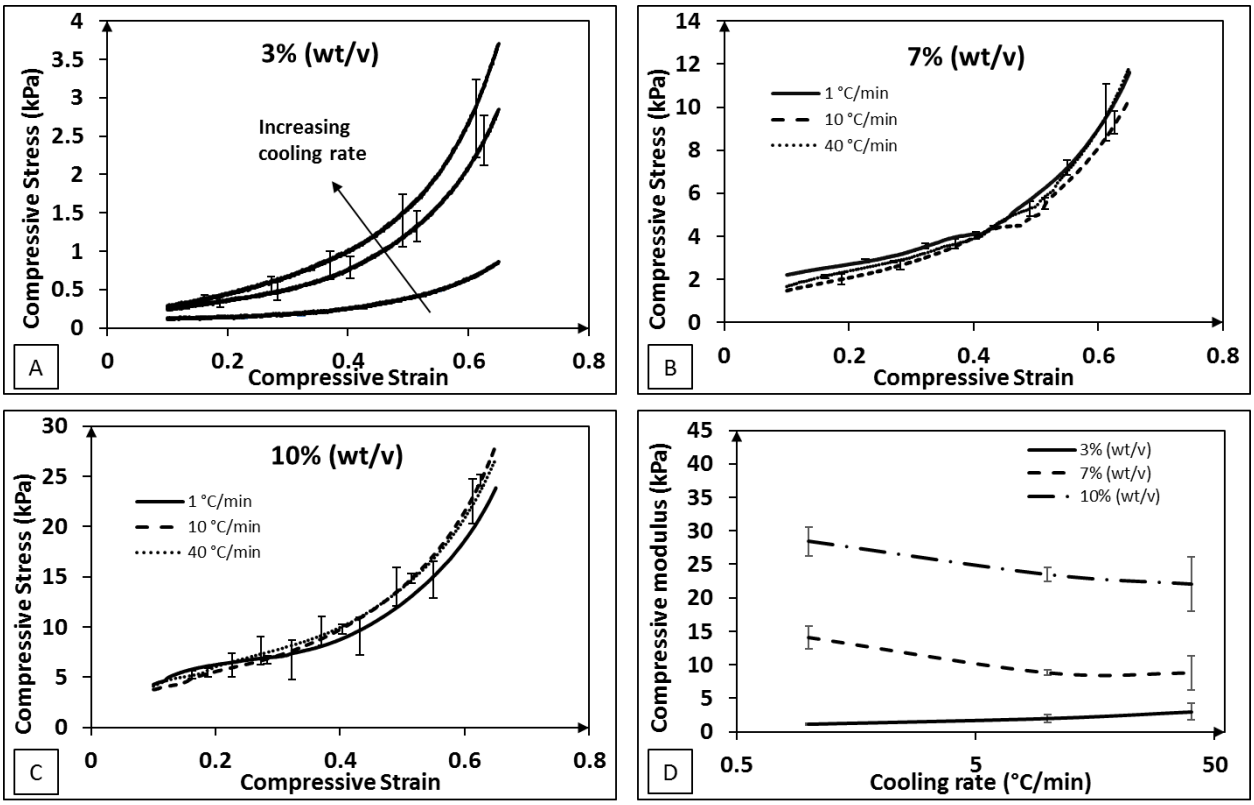

Figure 3.5. Real time radial stress strain curves of scaffolds made by dissolving (A) 3 (wt/vol) % (B) 7 (wt/vol) % and (C) 10 (wt/vol) % PLLA in dioxane, showing increasing compressive strength with increasing cooling rates. (D) Compressive Moduli of 3, 7 and 10 along the perpendicular mid-section to the loading direction (n = 4)

Table 3.1. Comparison with characteristics of scaffolds made from other studies

Scaffold material / Fabrication method	Pore-size		Porosity (%)		Compressive Modulus (MPa)	
	Min	Max	Min	Max	Min	Max
Non-3D printed ceramic scaffolds [47-49, 119-121, 137, 138]	30 μm	1 mm	25	80	3	50
Polymers / Gas foaming [50, 51, 106]	10 μm	100 μm (439 μm with salt leeching)	67	97	0.15	0.3
Ceramics / Gas foaming [52, 53]	100 μm	400 μm	46.8	78.4	100	1800
Polymers / Electro-spinning [40, 54, 55, 107]	0.11 μm (fiber dia)	1.19 μm (fiber dia)	-	-	1.09	20
Polymers / TIPS [56, 57, 110, 139]	50 μm	100 μm	71	91	0.15	6.2
PLLA / TIPS (present study)	30 μm	240 μm	88.22	98.22	0.101	9.61

The maximum compressive modulus of ~10MPa was achieved when 10% PLLA was dissolved in 100% dioxane and cooled at 40°C/min. This is about 100 times lower than the compressive modulus of pure PLLA (1GPa) and about 3500 times lower than the young's modulus of cortical bone (35 GPa) [61, 140] and about 5 times lower than the least young's modulus of a human cancellous bone (50-500 MPa) [48, 61]. Considering that the % porosity (90%) [62, 63] and pore size (~ 50 μm) [64] of a human cancellous bone is comparable to the scaffolds made from 10%

PLLA in pure dioxane and cooled at 10 and 40°C/min. Consequently, they could be an ideal scaffold for developing TE cancellous bone graft which could be implanted *in vivo* using acrylic cement for additional mechanical strength [141, 142].

For fair comparison, 3D ceramic (Hydroxyapatite / β-tricalcium phosphate) constructs which were fabricated using cost efficient methods like thermal extrusion, gas-foaming processes or commercially available products are considered in Table 3.1 (modified from Table 1.2 to compare characteristic values from present study).

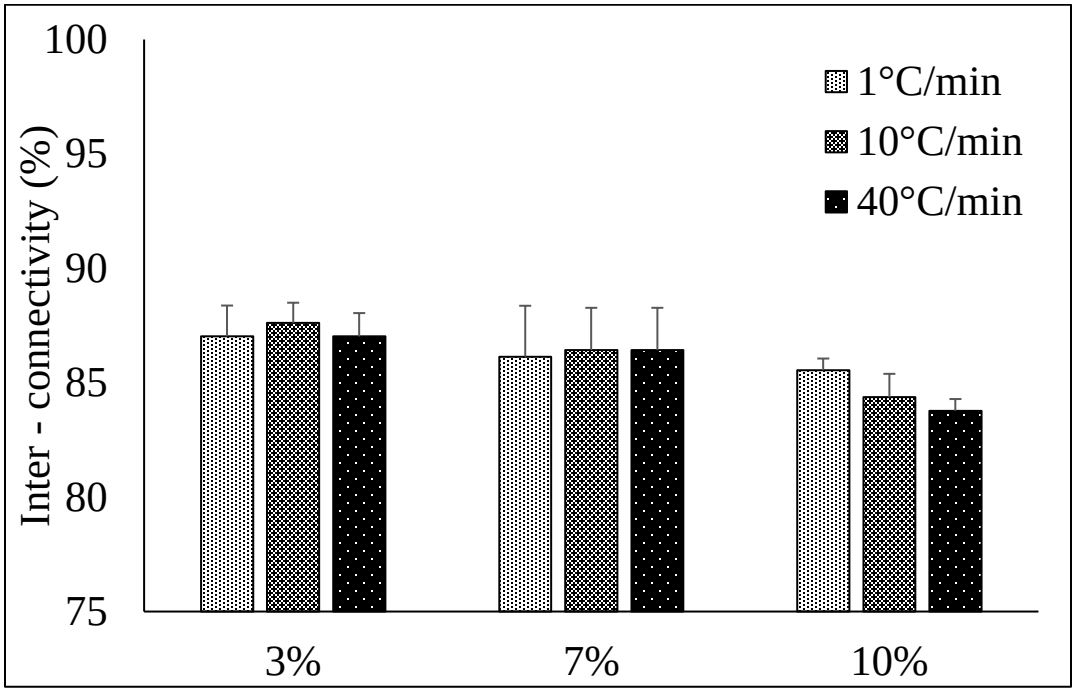

Figure 3.6. Volumetric percentage of inter-connected pores (n = 3)

These ceramic scaffolds have highest pore-sizes and compressive moduli, but very low % porosity. This could hinder intrinsic vascularization and bio-degradation *in vivo*. In the case of polymeric

scaffolds, comparatively high % porosities and compression moduli was obtained using TIPS technique. No data for % porosity was available for scaffolds made using electro-spinning method. This may be due to the inability to obtain a 3D construct using this method. In this study, by controlling the cooling rates in TIPS technique, even higher values of % porosities and compression moduli were achieved.

The percentage of interconnected volume varies within a tight range of 83% to 87%. No statistical significance was observed for any pairs of data sets except between 10% initial concentration cooled at 1 and 40°C/min, between 3% and 10% cooled at 10°C/min and between 3% and 10% cooled at 40°C/min.

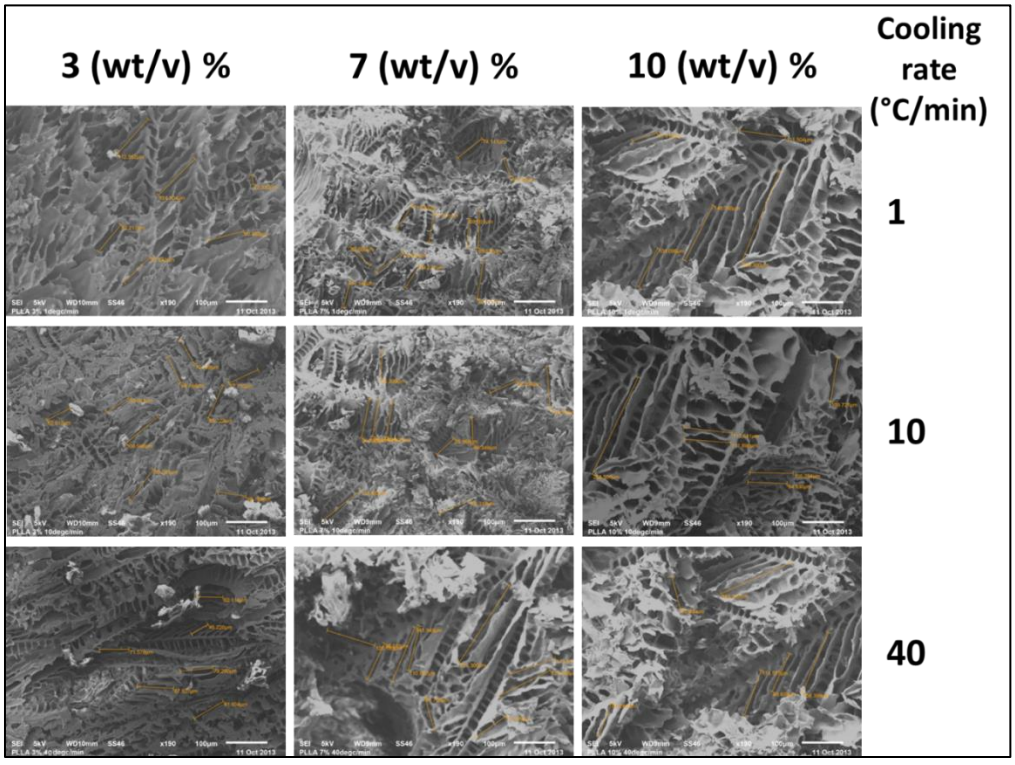

Figure 3.7. SEM images showing the porous micro-structures of PLLA scaffolds made by cooling each of the 3, 7 and 10 (wt/vol) % PLLA in Dioxane : Ethanol (0.85 : 0.15) solution at 1, 10 and 40°C/min using Control Rate Freezer (CRF).

In Fig 3.7 micro-porous structure of scaffolds made from PLLA dissolved in 85% dioxane and 15% ethanol is shown according to the percentage of PLLA used and cooling rate imposed. The porous structures of all the samples were irregular when compared to Fig.1. However, pore-sizes of scaffolds made by dissolving 7 and 10% PLLA in dioxane : ethanol (0.85 : 0.15) were larger than 100% dioxane. When compared to PLLA in pure dioxane, the inter-connectivity of pores seemed to increase when ethanol was used in the solvent. The anisotropic pore structures found in scaffolds made from PLLA in 100% dioxane was absent when ethanol was used. Both vertical and cross-sectional porous structures looked identical.

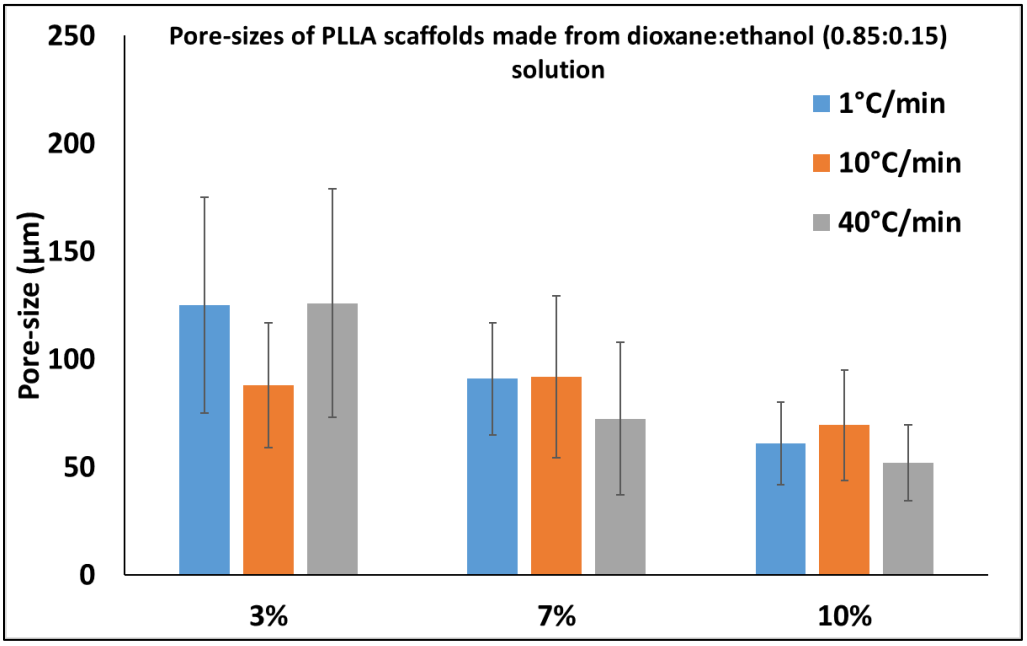

Figure 3.8. Mean pore diameter and standard deviations of 3, 7 and 10 (wt/vol) % PLLA in Dioxane : Ethanol (0.85 : 0.15) solution measured randomly from SEM images, and plotted corresponding to increasing cooling rates (n ~ 20)

Mean pore-sizes of scaffolds made using dioxane : ethanol solution showed decreasing trend with 3% PLLA and increasing trend with 7% PLLA with increasing cooling rates (Fig 3.8). Scaffolds made from 10% PLLA gave a constant mean pore-diameter of ~135µm for 1 and 10°C/min. When cooled at 40°C/min the pore-diameter dropped to ~120µm. Standard deviations of all the samples were very high (~40%) suggesting irregular porous structures.

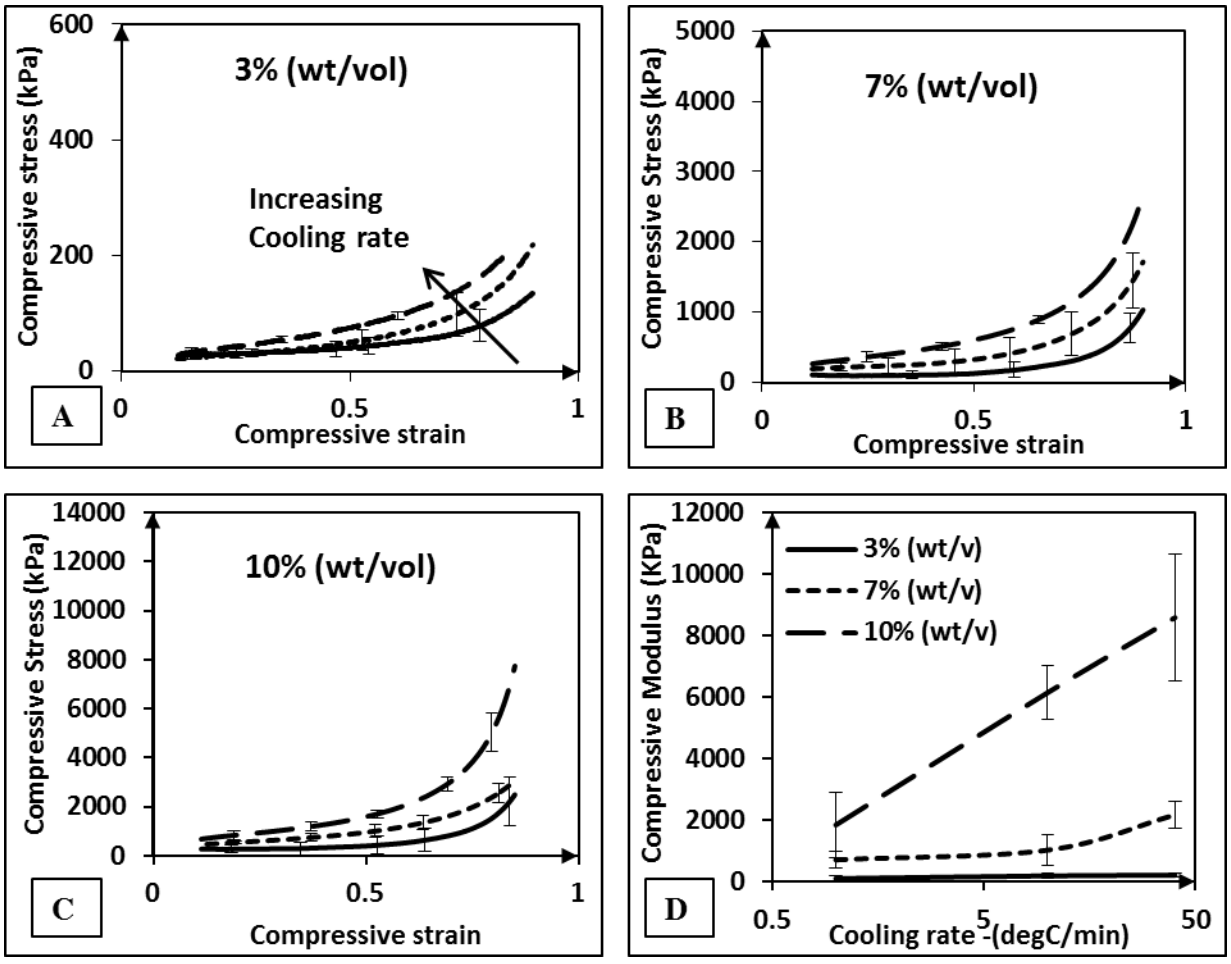

Figure 3.9. Real time axial stress strain curves of scaffolds made by dissolving (A) 3 (wt/vol) % (B) 7 (wt/vol) % and (C) 10 (wt/vol) % PLLA in Dioxane : Ethanol (0.85 : 0.15) solution, showing increasing compressive strength with increasing cooling rates. (D) Compressive Moduli of 3, 7 and 10 (wt/vol) % samples plotted along increasing cooling rates on $\log_{10}$ scale (n = 4)

When PLLA was dissolved in dioxane : ethanol solution, scaffolds showed decreased compression strength (Fig. 5B) when compared to PLLA dissolved in 100% dioxane. The compressive modulus was also decreased for all the parameters. Compressive moduli of 3%, 7% and 10% PLLA scaffolds increased from 101.46 to 212.35 kPa, 712.57 to 2172.48 kPa and 1842.88 to 8585.32 kPa respectively with increasing cooling rates. The structural integrity was weaker under high strains ($\varepsilon > 0.6$) when compared to scaffolds made from PLLA in 100% dioxane solution. However, the compressive modulus was linearly proportional to the logarithm (to the base 10) of the imposed cooling rate for each concentration of PLLA in solvent, similar to the results of scaffold made using pure dioxane.

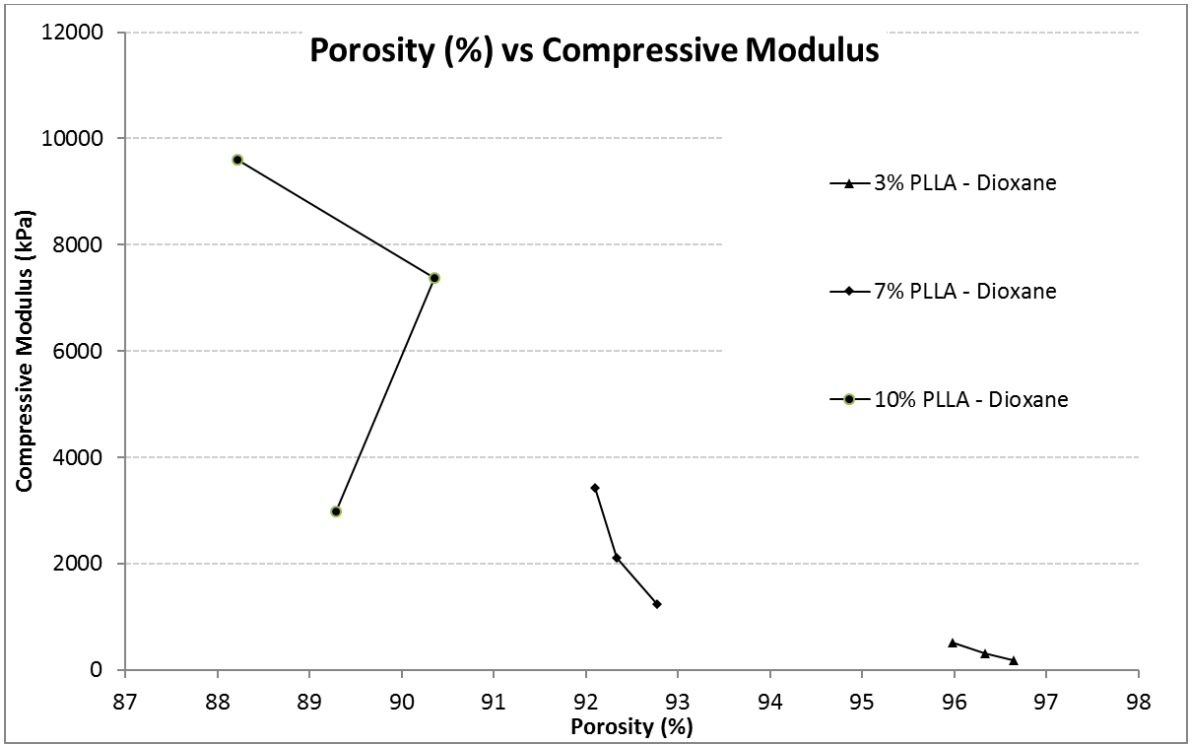

Figure 3.10. Variation of compressive modulus due to increasing cooling rates of PLLA scaffolds w.r.t. porosity (%)

In all other methods of scaffold fabrication, compression modulus was always compromised as an inverse function of the % porosity [48, 49, 123, 124, 128-130]. However, as stated earlier, high values for % porosity (~ 90%) and compression modulus (~ 10 MPa) are critical to foster the use of synthetic polymeric scaffolds. As described in this study, an analysis of the synthetic PLLA scaffolds fabricated using successively higher cooling rates (1 to 40 ˚C/min), irrespective of the PLLA : Dioxane concentration (ranging from 3 to 10%) resulted in the generation of scaffolds with regular micro-structure and consequently, these scaffolds showed increasing compression modulus while retaining a high % porosity (>88%) as shown in Fig.3.10.

3.4. Conclusion

Thermally Induced Phase Separation (TIPS) method was used to make porous three-dimensional PLLA scaffolds. The effect of imposed thermal profile during freezing of the PLLA in dioxane solution on the scaffold was characterized by their micro-structure, porosity (%), pore-sizes distribution and mechanical strength. The porosity (%) decreased considerably with increasing concentrations of PLLA in the solution, while a decreasing trend was observed with increasing cooling rates in both types of solvents. The mechanical strength increases with increase in PLLA concentration and also with increase in the cooling rate. Scaffolds made using higher concentrations of PLLA in solvent, showed better mechanical strength which improved relatively with increasing cooling rates in each case of initial PLLA concentration. This phenomenon of enhanced structural integrity with increasing cooling rates was more prominent in scaffolds made from higher initial PLLA concentrations. Therefore, by having a critical control over the imposed thermal profile during the freezing process of TIPS, mechanical strength of the scaffold can be controlled while maintaining relatively consistent (%) porosity.

Chapter 4 : Human Adipose Derived Stem Cells (hASCs) Isolation, Loading and Culture on PLLA Scaffolds Prepared using Thermally Controlled Methods

4.1. Introduction

Engineered tissues (grafts) a combination of scaffolds and cells could provide an alternative to the auto- and allo-grafts described earlier. The "perfect" graft material would provide the following properties [143, 144]: (i) *Mechanical support:* stabilizes the surgical site; (ii) *Osteoconductive*: facilitates the ingrowth and integration of adjacent bone; (iii) *Osteoinductive*: recruit and stimulate the formation and growth of bone from cells that may not naturally do so and; (iv) *Osteogenic*: contain cells that themselves are capable of forming new bone. Initially synthetic calcium phosphate (Ca-P) based hydroxyapatite (HA) was preferred as scaffold material for tissue engineered bone grafts, due to their abundant presence in the organic bone. Ca-P when used as a biomaterial in scaffolds also provides good osteo-conduction and bonds easily to the host bone [118]. In another study by Will et al.,[119] porous ceramic scaffolds with higher porosity favored rapid assimilation *in vivo*, while compromising on the mechanical resilience during surgery [145]. Subsequent studies explored the possibility of using biodegradable synthetic polymers like polyglycolides (PGA) and polylactides (PLA) [146]. Both PLA and PGA degrade *in vivo* by random hydrolysis of their ester bonds to form lactic acid which enters tricarboxylic acid cycle to be excreted as water and carbon dioxide from the body. PLA-PGA copolymers used in bone repair applications have shown to be biocompatible, non-toxic and non-inflammatory [132]. PLA/PGA copolymer implants accelerated the osseous defects in the tibia of rats. Many studies suggest that these polymers are sufficiently biocompatible [147]. In this study, human adipose derived stem cells (hASCs) derived from collagenase digestion of harvested subcutaneous adipose tissue

aspirates from liposuction procedures were used to measure and observe its response to PLLA scaffolds prepared by thermally controlled methods.

4.2. Materials and Methods

4.2.1. PLLA Scaffold Preparation and Selection

Crystalline PLLA was dissolved in 1,4 Dioxane at 3, 7 and 10 (wt/vol) % to form a homogenous clear solution. By thermally induced phase separation (TIPS) method, these solutions were each frozen to a low temperature (-60°C), at 1, 10 and 40°C/min cooling rates (C.R.). The frozen solutions were lyophilized (freeze-dried) to remove the frozen solvent resulting in the final scaffold, which was 3D porous PLLA structure. Based on characterization data of these scaffolds and practical handling, scaffolds made from 3 (wt/vol) % PLLA in dioxane was rejected for cell culture experiments due to poor mechanical integrity.

4.2.2. Human Adipose Tissue Derived Adult Stem Cells (hASCs) Isolation, Collection and Culture

All human protocols were reviewed and approved under the appropriate Louisiana State University Institutional Review Board (#E9119) protocols. Subcutaneous adipose tissue liposuction aspirates were provided by plastic surgeons in Baton Rouge, LA. All procedures were conducted under aseptic conditions according to a modification of methods outlined in [148, 149]. Tissue samples (100 to 200 ml) were washed 3-4 times in phosphate buffered saline (PBS) pre-warmed to 37 ˚C, suspended in PBS supplemented with 1% bovine serum albumin and 0.1% collagenase (Type I, Worthington Biochemicals, Lakewood, NJ), and digested with gentle rocking for 45-60 min at 37 ˚C. The digests were centrifuged for 5 min at 1200 r/min (300Xg) at room temperature, re-

suspended, and the centrifugation step repeated. The supernatant was aspirated and the pellet re-suspended in stromal medium (DMEM high glucose, 10% fetal bovine serum, 100 IU penicillin/mL, 100 μg streptomycin/ml, and 25 μg amphotericin/mL). The cell suspension was plated at a density equivalent to 0.125 mL of liposuction tissue per cm^2 of surface area, using a 35 mL volume of Stromal Medium per T225 flask. Cells were cultured for 48 hrs, in a 5% CO_2, humidified, 37 ˚C incubator. At which time, the adherent cells were rinsed once with pre-warmed PBS and the cells fed with fresh Stromal Medium. The cells were fed with fresh stromal medium every 2-3 days until they reached approximately 75-80% confluence. The medium was then aspirated; the cells were rinsed with pre-warmed PBS, and harvested by digestion with 0.05% trypsin solution (5-8 mL per T225 flask) for 3 to 5 min at 37 ˚C. The cells were suspended in stromal medium, centrifuged for 5 min at 1200 r/min (300 X g), the pellet re-suspended in a volume of 10 mL of stromal medium, and the cell count determined by trypan blue exclusion. These cells were identified as Passage 0 (P0) and were optimally cryopreserved [150, 151]. The stored PO cells were thawed and passaged as described through two successive passages (P1 to P2). hASCs from Passage 2 (P2) were used in the subsequent scaffold-cell interaction studies. Note that there is extensive data suggesting that these adherent cells exhibit multiple lineages when culture *in vitro* [152-162].

4.2.3. hASC-scaffold Loading and Culture

Based largely on the mechanical integrity and the regularity of micro-porous structures from SEM images, scaffolds made from 7 and 10% PLLA in dioxane at all cooling rates (average pore-size ~82 μm) were chosen for cell culture. Indeed, the scaffolds made from 3% PLLA at any cooling rate, lacked the mechanical integrity required for cell culture. These scaffolds of 12 mm in diameter were trimmed to a height of 1 mm for DNA quantification and 2 mm for Live/Dead staining, to fit

inside the wells of a 6 – well culture plate (Corning, USA) and affixed to the bottom of the plate using ~250 μL of 1% Agarose gel. This setup was done to counter the hydrodynamic floating of the scaffolds in stromal medium as PLLA is hydrophobic in nature. P2 cells were trypsinized (5 mL of 0.25% Trypsin-EDTA per T150 flask) and suspended in stromal media at a concentration of 1.5×10^6 cells/mL. Variable amounts of hASCs in stromal medium, calibrated according to specific assays were loaded on each scaffold's top surface as well as in the wells without scaffolds as control. These samples were cultured by feeding fresh stromal media (2 mL for control and ~ 6 mL for scaffold) every 2-3 days to quantify DNA and to observe the viability of hASCs on PLLA scaffolds and control at specific time points.

4.2.4. DNA Quantification

About $1 - 2 \times 10^5$ hASCs in stromal medium were loaded on each scaffold depending on the cell availability. For each experimental run, equal number of cells were plated on 6 - well plates as a control. The amount of DNA was measured at specific time points to quantify the hASC proliferation inside the scaffolds and control. The control samples and scaffolds were washed with PBS (Gibco, USA) thrice and treated with 3 mL of lysis buffer (0.2mg/mL sodium dodecyl sulfate (Thermo Fisher Scientific, USA) and 0.2mg/mL Proteinase K (Amresco, Ohio, USA)). The scaffolds were homogenized in a 7 mL Dounce tissue grinder (Sigma-Aldrich, USA) to lyse all the cells growing inside the three-dimensional construct. After incubation of 40 mins, 0.1 mL of lysates were transferred to 96-well plate and Quant-iT™ dsDNA Assay Kit (Thermo Fisher Scientific, USA) was used to calibrate and quantify the DNA according to the manufacturer's protocol.

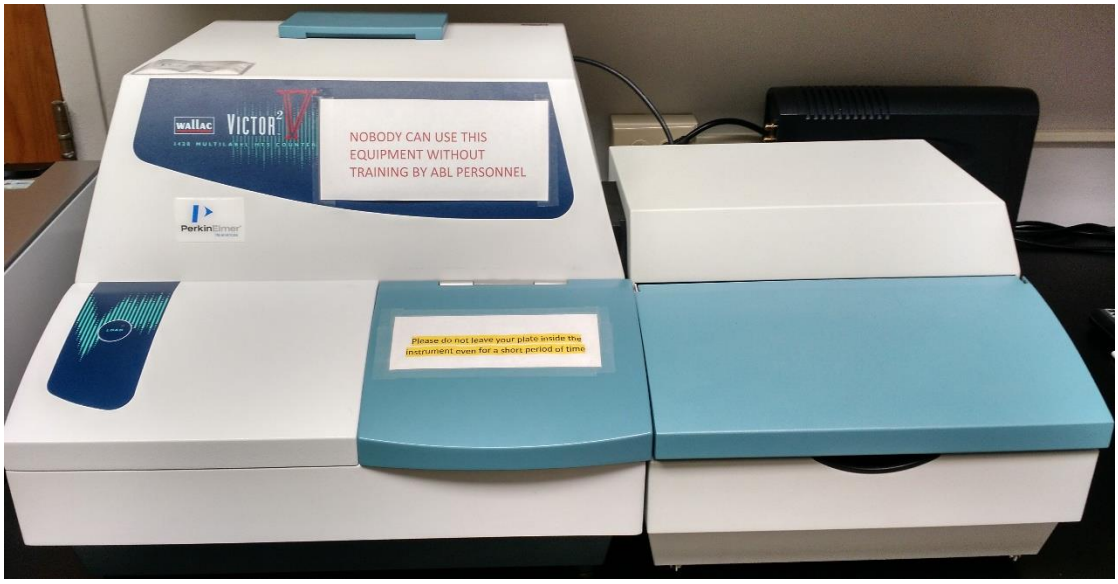

Figure 4.1. Perkin Elmer Wallac Victor 2 V Multi-label Counter 1420

4.2.5. Viability of hASCs

About 2×10^5 hASCs were loaded on each scaffold in stromal medium, while plating equal number of cells in 6 - well plate as a control. The samples were washed with PBS before incubating with Live/Dead staining solution (2 µM calcein AM and 4 µM ethidium homodimer-1) for 20 mins at 37°C to analyze the viability of hASCs on both scaffolds and culture plates. Cell-permeant, non-fluorescent calcein AM undergoes an enzymatic conversion to fluorescent calcein (Ex/Em: 495 nm/ 515 nm) in the presence of esterase activity in live cells. Ethidium homodimer-1 (EthD-1) (Ex/Em : 528 nm/ 617 nm) undergoes a 40-fold fluorescence enhancement when it binds with nucleic acids. Intact cell membranes of live cells prevent the entry of EthD-1. The images were captured using SteREO Lumar.V12 (Zeiss) fluorescent microscope. The green (live) pixels and red (dead) pixels were counted from each image after setting the threshold at the maximum

intensity (for red and green) in each image using ImageJ program. The % viability was calculated as the % of green pixels in total fluoresced pixels (green and red).

4.2.6. Three-dimensional Growth of hASCs in the Scaffolds

Human adipose stem cells were loaded at a concentration of 1×10^6 cells per sample and cultured in stromal medium. After specific time points of culturing hASCs and PLLA scaffold composites in the 6 - well plates, the samples were washed with PBS (Gibco, USA) thrice before incubating with 0.5 % (wt/v) osminum tetroxide solution (in PBS) for 12 hours. Osmium tetroxide is used as a fixing agent as well as a lipid stain in this process, where cell membranes are specifically stained. After 12 hours of incubation, the samples were washed with 6 mL of DI water 5 - 6 times. The stained, wet samples were air-dried for 2 - 3 days at room temperature. These samples were scanned using SKYSCAN 1074 Portable X-ray Microtomograph (Bruker, NJ, USA) equipped with a 50 kV X-ray source, in Radioisotope Imaging Laboratory (Physics Department, Louisiana State University). The heavy metal osmium, embedded on cells, create a contrast in X-ray scanning. The exposure time was calibrated to an ideal value of 480 ms for hASC - PLLA scaffold composites. X-ray images were scanned parallel to the axial plane at a rate of 400 scans per 360° rotation of the sample. The resolution of the scans were 37 μm and the device provides a filed view of 3 cm. These 400 scans were used to reconstruct an image set of horizontal sections (~160 images) using NRecon software (Bruker, NJ, USA). The NRecon software can be used to filter PLLA scaffold and osmium stained cellular regions due to their huge density difference. The Hounsfield Unit (HU) of PLLA scaffold varied from -850 HU to -600 HU, while the osmium varied from 1020 HU to 2660 HU. Thus, the two image sets were used to reconstruct a three-

dimensional image and scaffold and cellular regions were super-imposed using NIH ImageJ software.

Figure 4.2. SKYSCAN 1074 Portable X-ray Microtomograph

***Statistical Analysis*.** All values are indicated as mean ± SD. Two-tailed student's t-test was employed, with $p \leq 0.05$ considered to be statistically significant.

4.3. Results and Discussion

In Fig.4.1, quantity of DNA (ng) measured at time points 7, 14 and 21 days were normalized to the quantity of DNA at day 1 to avoid discrepancy in cellular attachment at this time point. Fold increase of DNA representing cell proliferation showed increased cell growth in all scaffolds compared to the control (1.55 fold) at 14 and 21 days. DNA growth of control remained constant at ~1.5 fold since it reached confluency at day 7. Mean fold increase of DNA for 7 and 10% PLLA scaffolds shows a similar trend as the mean pore sizes in Fig. 2. DNA increased to ~ 10.5 fold in

scaffolds made from 7% PLLA cooled at 1°C/min and 10% PLLA cooled at 10°C/min with no statistical significance (p-value = 0.29). Similarly, scaffolds made from 7% PLLA cooled at 40°C/min, 10% PLLA cooled at 1 and 40°C/min showed a DNA increase of ~ 7.75 fold with no statistical significance (p-value ~ 0.70) among any pair. There was weak statistical significance between two pairs of scaffolds: 7% PLLA cooled at 1 and 40°C/min with the DNA fold growth values at 10.03 and 8.01 respectively (p-value = 0.061); and between 7% PLLA cooled at 1°C/min and 10% PLLA cooled at 40°C/min (7.75 fold DNA) (p-value = 0.075). Interestingly, scaffolds made from 7% PLLA cooled at 10°C/min had the least cell growth with 5.28 fold DNA increase at day 21. Indeed, this scaffold had the least rate of growth (using data from day 7 and 14) with 0.25 fold DNA increase per day. The highest rate of cellular growth was recorded by 10% PLLA scaffold cooled at 10°C/min with 0.68 fold DNA increase per day. The % porosity of scaffolds does not seem to influence the cell growth in the scaffolds as both 7% and 10% PLLA scaffolds shows high DNA content for scaffolds that has a mean pore-size > 90 μm. The total DNA quantity representing the cellular growth on 10% PLLA : dioxane scaffolds shows a similar pattern to its mean pore-size with increasing cooling rates. When cooled at 10°C/min, the mean pore size was highest at 90 μm, whereas the other two cooling rates had a comparatively lower mean pore size of ~ 70 μm. Almost, 10 fold growth of cells over a period of 21 days do not suggest a comparative cell multiplication to the cells growing on a plate. This limitation maybe caused by the micro-scaled contours on the surface of the scaffold. No significant evidence of three-dimensional cellular growth was observed from live/dead staining. In particular, 10% PLLA scaffold cooled at 10°C/min displayed higher cell growth with its mean pore-size lower than 7% PLLA scaffolds by ~4μm.

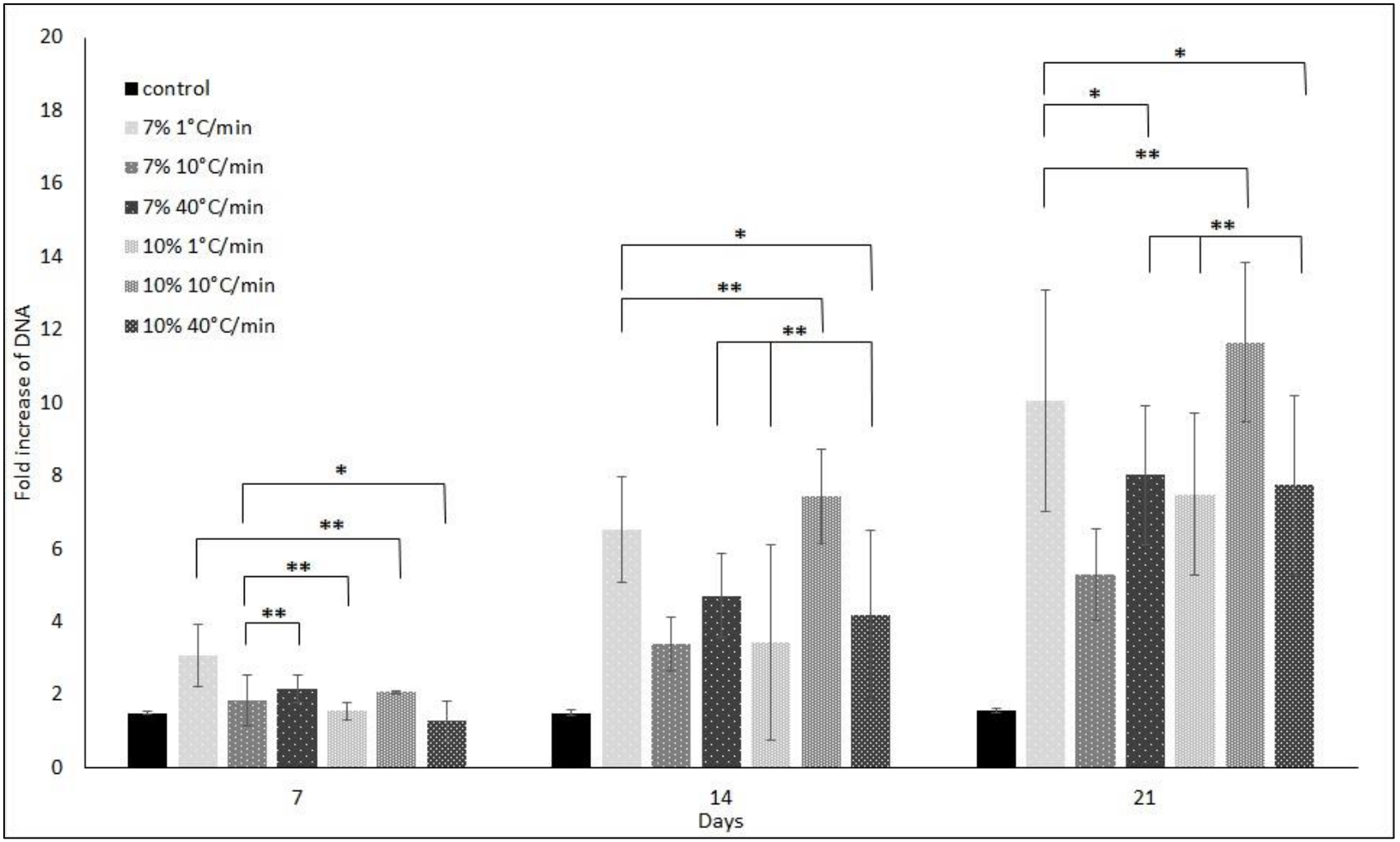

Figure 4.3. Fold increase of DNA representing cellular growth in PLLA scaffolds (7% and 10% cooled at 1, 10 and 40°C/min, 1 mm thick) at time points 7, 14 and 21 days relative to DNA quantity of initially loaded cells. *indicates weak statistical significance (0.05 < p-value < 0.1); **indicates not significant (p-value > 0.1) (n=9)

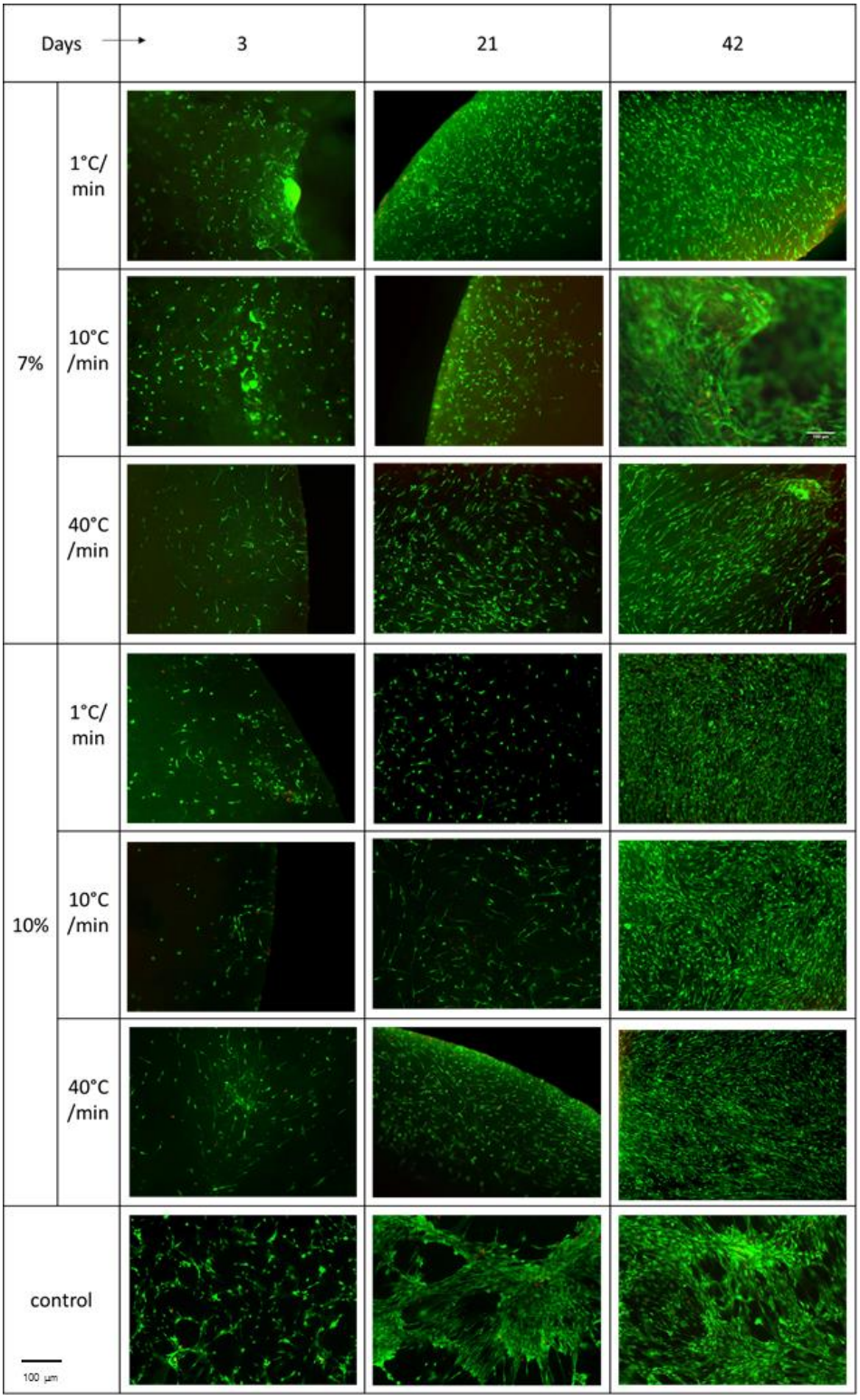

Figure 4.4. Live cells (green) and dead cells (red) in control and PLLA scaffolds (7% and 10% cooled at 1, 10 and 40°C/min, 2 mm thick) during time points 3, 21 and 42 days

Table 4.1. Viability (%) of human adipose stem cells

Days	7%			10%			control
	1° C/min	10° C/min	40° C/min	1° C/min	10° C/min	40° C/min	
3	96.64 %	93.09 %	96.23 %	97.95 %	93.79 %	96.78 %	99.78 %
21	98.10 %	96.76 %	98.90 %	99.58 %	96.36 %	98.72 %	99.96 %
42	99.75 %	99.36 %	99.11 %	99.78 %	99.97 %	99.36 %	99.98 %

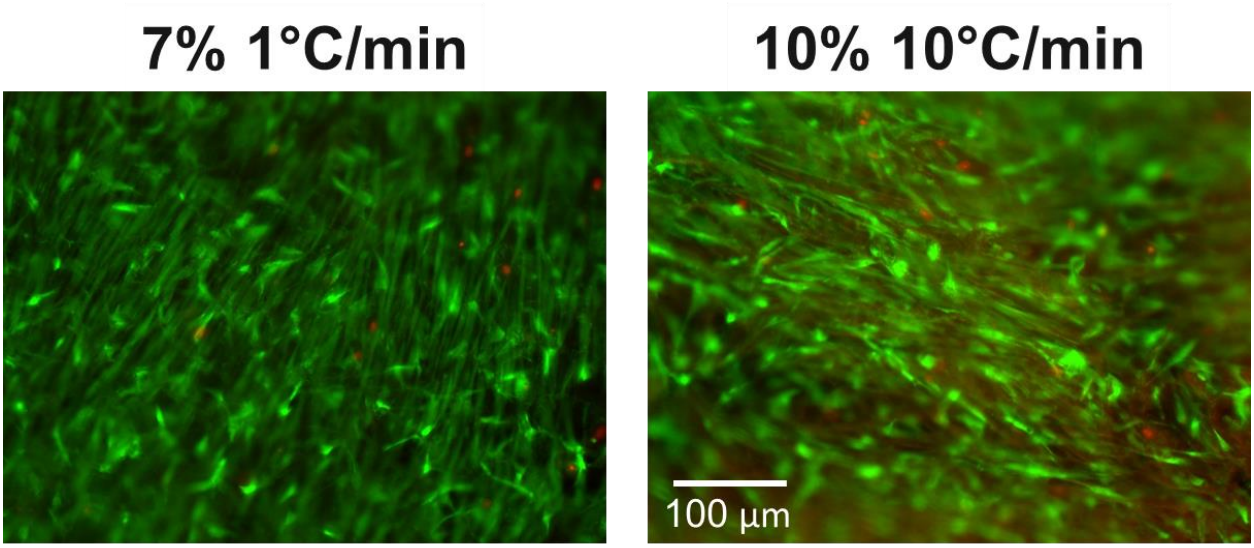

Figure 4.5. Zoomed-in image of live/dead staining showing both live (green) and dead (red) cells

Table 4.1, shows that the percentage viability increases consistently with time. Two- tailed student's t-test showed no significant difference between any of the scaffolds or control at a

particular time point. The relatively low % viability in scaffold at day 0 could be due to the initial difficulty in attachment of hASCs. However, as time progresses the % of live cells increases consistently to be on par with control at day 42. Also from Fig.4.2, we observe abundant cell growth three dimensionally on the scaffold at this time point.

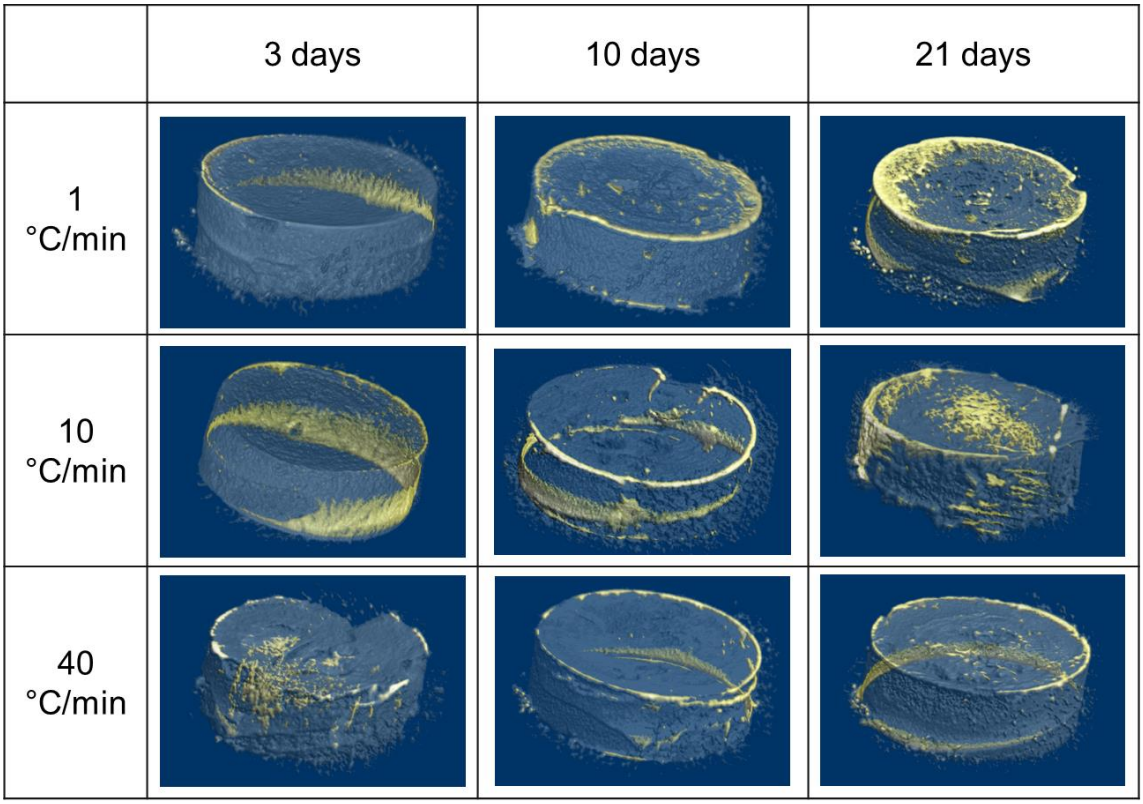

Figure 4.6. Three-dimensional cellular growth of hASCs (yellow) on scaffolds (transparent white) made using initial concentration of 7% (wt/v) PLLA/dioxane

Interestingly the cell growth was abundant around the edges of scaffolds as observed at day 21 in Fig.4.2 (shown for some scaffolds). This could be because of the relative long pore-sizes on the edges of the scaffold caused by higher thermal flux during the cooling process. Alternatively, it

could be because the cells preferred a location with more exposure to stromal medium. However, at day 42, homogenous growth of cells on the surface of the scaffolds was observed. At this time point the viability (%) of hASCs on all scaffolds were measured to be > 99%. Thus, PLLA scaffolds prepared by TIPS method with controlled cooling rate provide no cytotoxicity to hASCs. The hydrophobicity of PLLA does not hinder cell adhesion and proliferation.

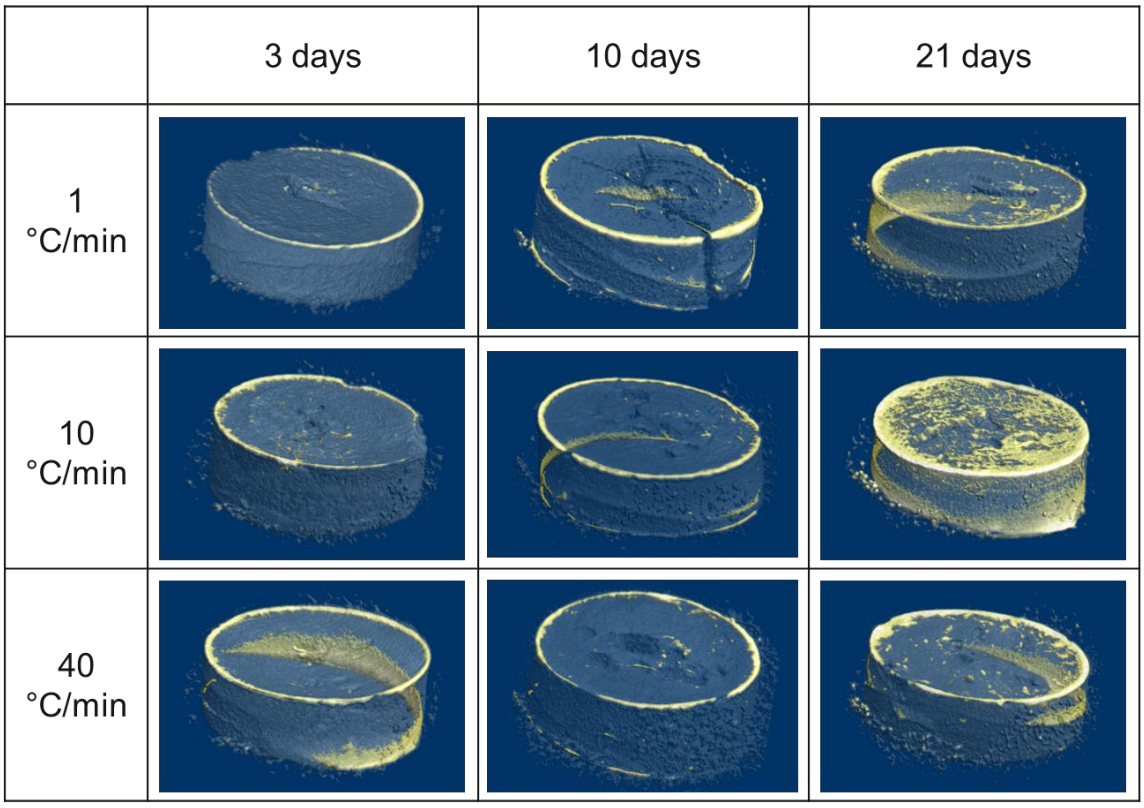

Figure 4.7. Three-dimensional cellular growth of hASCs (yellow) on scaffolds (transparent white) made using initial concentration of 10% (wt/v) PLLA/dioxane

Growth of hASCs within the three-dimensional constructs can be observed in Fig 4.6 and 4.7 with the passage of time. More confluence of cells was observed in the outer peripheral regions of the

scaffolds on the loading surface. The depth of cellular growth in the axial direction was approximately measured using NIH ImageJ software. The maximum growth in the axial region was about 1 mm in scaffolds made using 10% PLLA concentration and 10°C/min cooling rate. Although these measurements may not be accurate due to uneven scaffold surface during cutting before cell culture. Overall lack of cell penetration in the axial direction could be because of low mean pore-sizes. High confluence of cells was observed in the scaffolds made using 7% PLLA concentration cooled at 1°C/min and 10% PLLA concentration cooled at 10°C/min. This can be correlated with high cellular growth observed in DNA quantification for these scaffolds. It should also be noted that the SKYSCAN 1074 microtomograph has a resolution of 37 µm which is about 4 times smaller than the size of a hASC. Therefore, the regions detected by the scanner should be having a high confluence of cells, which were focused on the top surface.

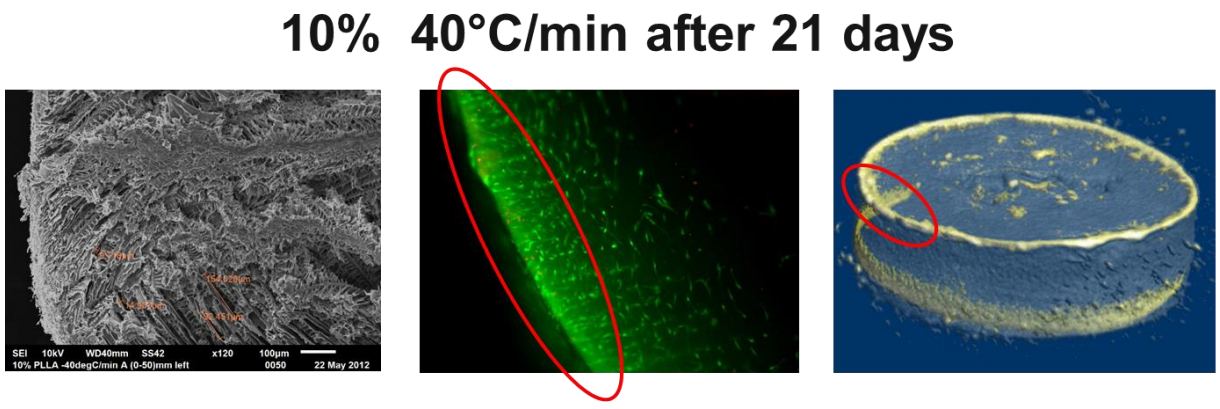

Figure 4.8. Preference of hASCs to the circumferential regions on a scaffold

Fig 4.8 represents a common trend observed in preference of hASCs to multiply rapidly at the outer circumferential regions of the top surface on the scaffolds. This trend was observed in scaffolds made using all parameters as shown in Fig 4.4, 4.6 and 4.7. As discussed in chapter 2 and 3, spindle shaped pores with larger lengths, propagating in the radial direction were found in the SEM images of the vertical section of scaffolds. Relatively larger pore sizes (>100 μm) could be one of the reasons why hASCs prefer the circumferential regions of a scaffold. Exposure of more surface to stromal medium could also be an additional factor causing this phenomenon.

4.4. Conclusion

Thus, this study compares the performance of PLLA scaffolds made by conducting extensive parametric TIPS fabrication. Human adipose derived stem cells were cultured on these scaffolds to measure the cell growth in the three dimensional PLLA constructs in terms of increase in DNA quantity. The intra-scaffold cell proliferation of hASCs suggests that the hydrophobicity of PLLA does not impede its bio-compatibility. Further, the viability increases consistently on the scaffold over a period of 42 days. This suggests that such optimally tailored PLLA scaffold could be a prime candidate for making surgically implantable tissue grafts *exvivo* [163, 164]. These tissue grafts could provide an efficient and viable alternative to current autologous bone grafting methods. Future osteogenic studies will be conducted on human adipose derived adult stem cells (ASCs) [125, 165, 166] in cohesion with optimally structured and strengthened PLLA scaffolds.

Chapter 5 : Osteogenesis of Human Adipose Derived Stem Cells on Cellular Responsive PLLA Scaffold

5.1. Introduction

There are three important features for an 'ideal' graft material used in a bone graft. (i) Osteoconductive: facilitates the ingrowth and integration of adjacent bone; (ii) Osteoinductive: undifferentiated pluripotent cells are stimulated to develop into the bone-forming cell lineage. One proposed definition is the process by which osteogenesis is induced and; (iii) Osteointegration: implanted bone graft get fused in the defect site homogenously [167-171]. Many synthetic polymer materials which has been studied in osteo-differentiation of precursor cells and reported to be 'osteo-inductive', have used chemical osteo-induction in the growth media. PLLA also has a similar fate where almost no in vitro study has been focused on whether PLLA as a material is osteo-inductive by itself. In this chapter, the osteo-inductivity of PLLA in relation to the chemical inductive differentiation is being reported.

5.2. Materials and Methods

5.2.1. Ideal Scaffold from Thermal Profile Variables

Varying the cooling rate and the PLLA concentration did produce significant difference in pore-sizes, porosity (%) and compressive modulus. But the real competence of a scaffold is proved by its cellular growth response. Due to its influence for robust cellular growth, scaffolds made by 10% (wt/v) PLLA/dioxane cooled at 10°C/min was used for osteogenic study. These scaffolds were trimmed to 1 mm in thickness for cell loading.

5.2.2. Cell Culture and Loading

After 2 passages, hASCs were trypsinized from T-150 flasks (Corning, USA) and suspended in stromal media (SM) at 10^6 cells / mL. About 500,000 cells were loaded on PLLA scaffolds (fixed on a 6-well plate by 1% agarose gel) and on 6-well plates as a control. The scaffolds and control were divided into two groups: one was cultured in stromal media (DMEM high glucose, 10% fetal bovine serum, 100 IU penicillin/mL, 100 μg streptomycin/ml, and 25 μg amphotericin/mL) and another group was cultured in osteogenic media (OM) (DMEM high glucose, 10% fetal bovine serum, 100 IU penicillin/mL, 100 μg streptomycin/ml, 25 μg amphotericin/mL, 50 μg/ml ascorbic acid, 10 mM β-glycerophosphate and 100 nM dexamethasone). All media were changed every 3 days and fresh media was prepared for each change.

5.2.3. Alizarin Red Staining

At time points 7, 14, 21 and 28 days the cells growing as control on 6-well plates were fixed with 70% ethanol in DPBS (without Ca, Mg) (Gibco, USA) at 4°C for 20 mins. Then washed with de-ionized water (DI H_2O). Then the samples were stained with 1mL of 40mM Alizarin Red S solution in DPBS (without Ca, Mg) per well, at room temperature for 20 mins. Alizarin red S can stain calcium deposits through interaction of its sulfonic acid and hydroxy groups with calcium ions [172, 173]. The staining solution was removed and washed with DI water until no further stain was washed away. At time points 7, 14 and 21 days, the scaffolds were washed with DPBS before fixing and staining with the same protocol mentioned above. The stained scaffold samples were washed with DI H_2O for 48 hrs on a rocker, changing the water every 12 hrs. After 48 hrs no further stain was removed from the scaffolds.

5.2.4. RNA Extraction

RNA extraction from PLLA scaffolds by commercial reagents TRI Reagent® (Sigma) or TRIzol RNA Isolation Reagents (Thermo Fisher Scientific) did not provide a high yield (< 10 ng) after 21 days in culture. Also, the $A_{260/280}$ and $A_{260/230}$ values were lower than one suggesting that the RNA in the template was not purified of other nucleic acids and other organelles respectively. An alternate product known as PureLink RNA Mini Kit (Thermo Fisher Scientific) provided the necessary purification equipment by means of spin cartridges. The membranes in the spin cartridges selectively binds to the RNA molecules, thus making further purification possible. After homogenizing the hASC - PLLA scaffold composites using 7 mL Dounce tissue grinder (Sigma-Aldrich, USA), with lysis buffer provided by the manufacturer, an extra centrifugation step was added to remove the debris from the scaffold. A calibration experiment was conducted to find an optimal centrifugation speed and time. Centrifugation was done using Minispin® Plus (Eppendorf, NY, USA). Five different centrifugation speeds were used for 5 min time period. Higher centrifugation speeds will cause higher heat generation which may lead to the degradation of nucleic acids and also affect the quality of the templates. It was found that the highest yield without compromising the quality was obtained at 5000 rpm. However, better quality maybe obtained when centrifuged for lower time periods. To test this hypothesis, the samples were centrifuged at 5000 rpm for 3 mins. It was found that the quality of the RNA template was compromised with other cellular debris indicated by $A_{260/230}$ value. Table 5.1 shows that the quality of RNA at 5000 rpm for 5 min was the highest. Ideal $A_{260/280}$ and $A_{260/230}$ values are 2.

Thus, after homogenization of PLLA scaffolds, an additional centrifugation for 5 mins at 5000 rpm was performed before following the manufacturer's protocol to obtain the final RNA template.

Table 5.1. Calibration of centrifugation step

Speed (rpm)	Time (min)	$A_{260/280}$	$A_{260/230}$	ng/µL
- (Lysis buffer added on top)		1.71	0.54	10.9
2,000	5	1.90	0.83	26.0
3,000	5	2.06	1.42	20.6
5,000	5	1.99	1.97	26.4
8,000	5	1.83	0.09	3.96
10,000	5	2.06	0.75	33.1
5,000	3	2.19	1.41	38.7

5.2.5. Quantitative Polymerase Chain Reaction (QPCR)

High-Capacity cDNA Reverse Transcription Kit (Applied Biosystems, CA, USA) was used for the transcription of RNA to cDNA template following manufacturer's protocol. Real-time qPCR was done to measure the upregulation of alkaline phosphatase (ALP) and Runt-related transcription factor 2 (Runx2). ALP and Runx2 are two important early expressing genes during osteogenic differentiation pathway. Runx2 is plays an important role during the differentiation of mesenchymal stem cell into an immature osteoblast. Peptidylprolyl isomerase B or cyclophilin B (PPIB) was used as a reference gene for relative quantification of ALP and Runx2 uptake. Power

SYBR Green PCR Master Mix (Applied Biosystems, CA, USA) reagent kit was used following the manufacturer's protocol in MiniOpticon Real-Time PCR System (Bio-Rad, CA, USA).

Table 5.2. Nucleotide sequence of the primers used

Gene	**Forward primer (5' - 3')**	**Reverse primer (5' - 3')**
ALP	CAAGGACGCTGGGAAATC	CGTCAATGTCCCTGATGTTAT
Runx2	GGACGAGGCAAGAGTTTC	GGGACACCTACTCTCATACT
PPIB	CTACAGGAGAGAAAGGATTTGG	AGCCGTTGGTGTCTTTG

5.3. Results and Discussion

In Fig. 5.1, it can be observed that there is an increase in the staining of alizarin red on scaffolds cultured in both stromal as well as osteogenic medium. The uptake of stain is more vigorous in scaffolds cultured in osteogenic media. In Fig. 5.2, it is found that the calcification takes 28 days to appear in hASCs cultured on plate and induced osteogenesis by chemicals (50 µg/ml ascorbic acid, 10 mM β-glycerophosphate and 10 nM dexamethasone). Alizarin red stains only the nodal calcium deposits among the osteoblast growth. This is the last stage of differentiation of hASCs into osteoblast phenotype. A significant uptake in PLLA scaffolds grown in OM is observed even at day 21 (7 days before OM induces osteogenesis in positive control). Therefore, it can be inferred that PLLA definitely plays a role in osteogenic induction of hASCs. Further evidence is given by

hASCs cultured on PLLA scaffolds with SM. Therefore, PLLA is definitely osteo-inductive without other methods of osteo-induction.

Days ↓	Scaffolds in SM	Scaffolds in OM
7		
14		
21		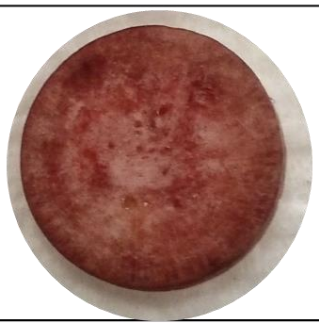

Figure 5.1. Alizarin red S staining of PLLA scaffolds cultured in stromal and osteogenic media

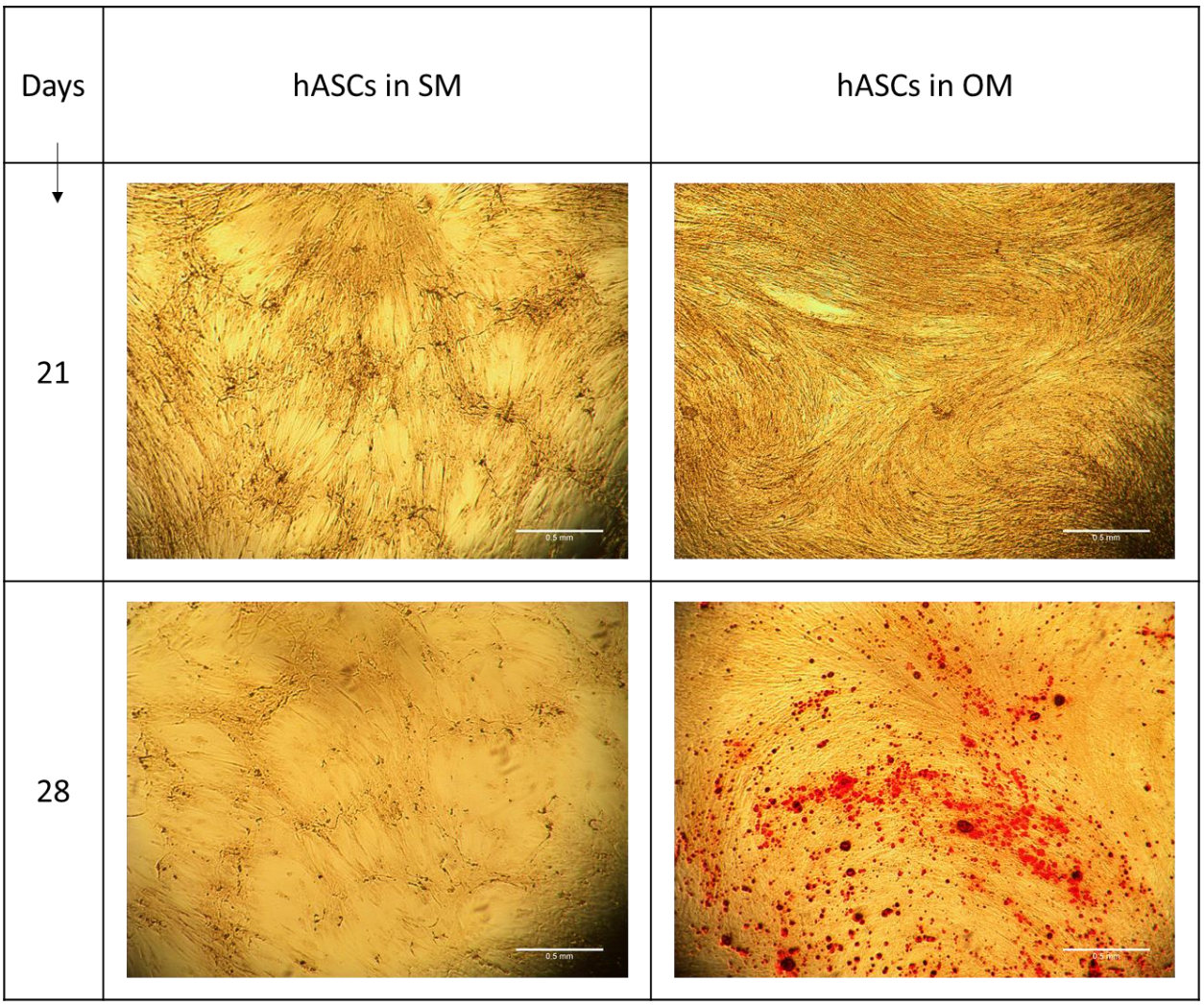

Figure 5.2. Alizarin red S stain of hASCs cultured in stromal and osteogenic media

The alizarin red stain from the samples were eluted using 10% cetylpyridinium chloride (CPC) in DI water. For positive and negative controls (hASCs in OM and hASCs in SM respectively), incubating the stained samples with 1 mL of 10% CPC at room temperature for 20 mins will successfully remove all the stains. For stained samples of PLLA scaffolds, the constructs were homogenized using a 7 mL Dounce tissue grinder with 1 mL of 10% CPC, incubated at room temperature for 20 mins. The solution was centrifuged at 1500 rpm for 2 mins to remove the PLLA

debris from homogenization and to obtain a clear supernatant with only CPC bound alizarin red. These CPC bound alizarin red solution were quantified using Wallac Victor2 Plate reader to measure the absorbance at 531 nm wavelength.

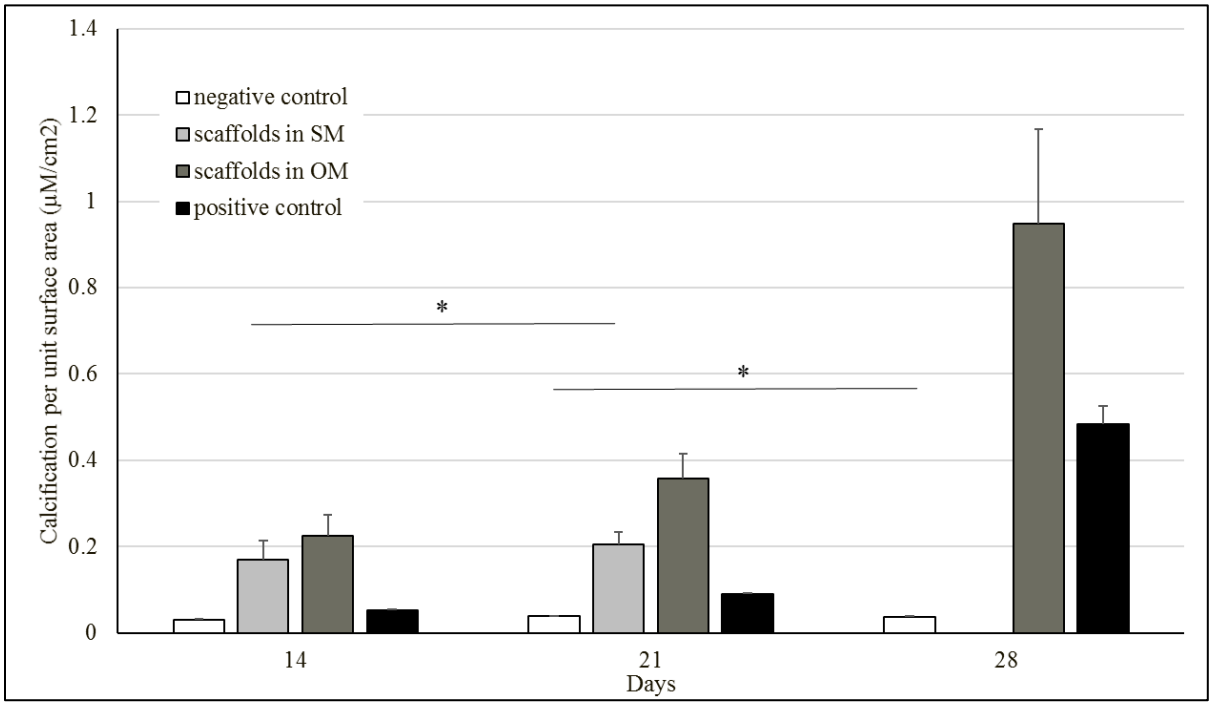

Figure 5.3. Quantification of alizarin red staining (n = 3)

The absorbance values were corresponded to a concentration of alizarin red using a known standard curve. The exact amount of alizarin red obtained was normalized with the surface area of scaffolds (exposed to growth medium) and controls, since most of the cell growth were on the outer surface of the scaffolds (as observed by three dimensional scans). Human adipose stem cells cultured on PLLA scaffolds with stromal medium showed no statistical increase from day 14 to day 21. However, the calcification concentration of scaffolds in SM (0.22 µM/cm^2) were higher

than the negative control (0.03 μM/cm^2) as well as the positive control (0.0522 μM/cm^2) at day 14. At day 21, there was increased calcification for all samples except the negative control (0.038 μM/cm^2). Calcification concentration of positive control was 0.09 μM/cm^2, scaffolds in SM was 0.2 μM/cm^2 and scaffolds in OM was 0.36 μM/cm^2. Continued increase in calcification was observed at day 28 suggesting that the hASC - PLLA scaffold composites are committing towards a bone graft formation.

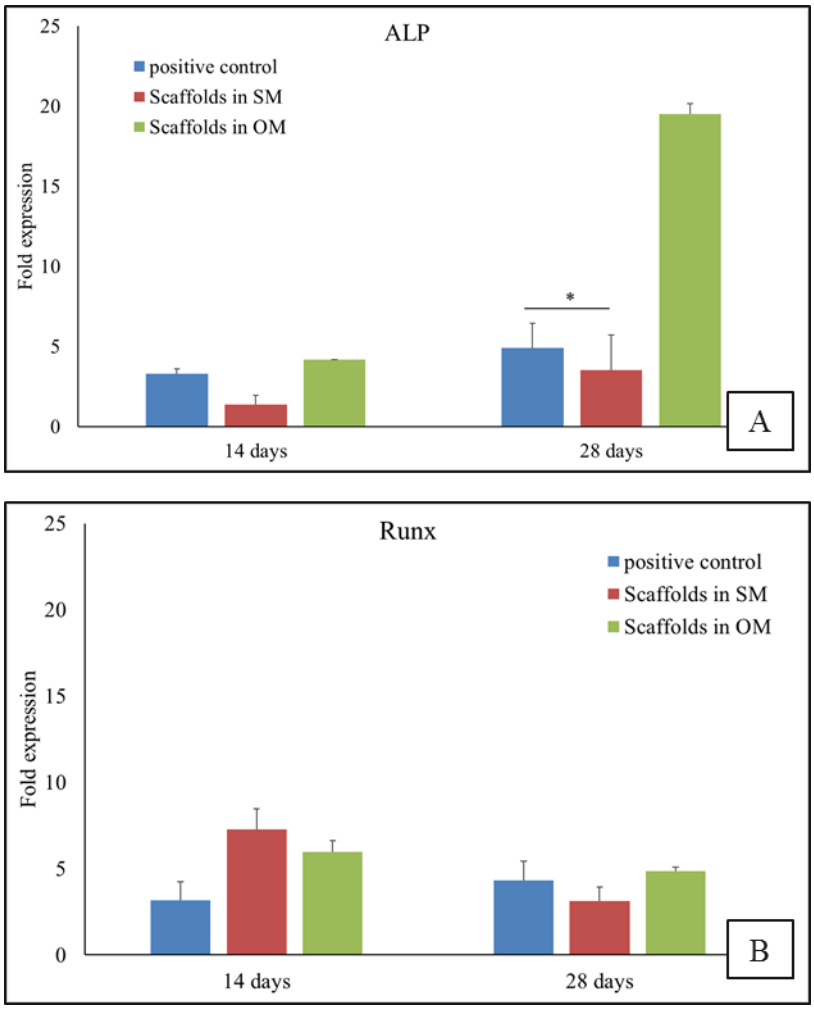

Figure 5.4. Expression of (A) ALP and (B) Runx2 genes at 14 and 28 days (n = 3)

The negative control was used to normalize and measure the up/down regulation of ALP and Runx2 at 14 and 28 day time points. The expression of ALP is increased from 3.27 ± 0.3 to 4.94 ± 1.5 fold in the positive control, from 1.36 ± 0.59 to 3.52 ± 2.18 fold in scaffolds in SM and from 4.16 ± 0.01 to 19.49 ± 0.66 fold in scaffolds in OM from day 14 to day 28. The expression of Runx2 was regulated as from 3.15 ± 1.07 to 4.32 ± 1.11 fold in the positive control, from 7.26 ± 1.12 to 3.14 ± 0.79 fold in scaffolds in SM and from 5.96 ± 0.65 to 4.86 ± 0.24 fold in scaffolds in OM from day 14 to day 28. The down regulation of Runx2 observed in scaffolds (cultured in both SM and OM) from 14 to 28 days suggests that the hASCs have crossed the immature osteoblastic stage during its differentiation pathway. Thus, suggesting that between 14 and 28 days mature osteoblasts are being formed. However more studies should be conducted to study the expression of other osteoblast specific genes like osteocalcin, osteopontin, SP7 etc., to exactly track the states of stem cells along the osteogenic pathway. The quantity of RNA and subsequently the cDNA was not enough to measure the expression of osteocalcin. About 10 ng of cDNA template was used for each reaction. Therefore, more number of cells should be loaded initially to obtain enough RNA template, to measure the expression of low sensitive, osteoblast specific genes in future studies.

5.4. Conclusion

A set of porous three-dimensional constructs made of PLLA was developed by varying thermal profiles and PLLA concentration. Based on the characterization an ideal parameter for making a robust viable scaffold was selected, particularly based on cellular proliferation in the three-dimensional construct. This scaffold was studied for osteogenic differentiation potential on hASCs. It was found that PLLA is osteo-inductive by nature without any external signaling. Hence, PLLA scaffolds combined with hASCs is an excellent method to form bone graft, which can be used for treatment procedures similar to Lendenckel et al [69].

The PLLA scaffolds supported uninhibited cellular growth as measured by DNA quantification over a period of 21 days. At longer periods of culture (42 days), the cytotoxicity was practically null relative to hASCs grown on control plates. However, more research should be done to encourage three-dimensional cellular growth as most of the scaffolds exhibited a resistance for cell permeation inside its construct. This could be because of relatively low pore-sizes (~90 μm). Further studies should be conducted to increase the mean pore size, by experimenting with alternate shapes/sizes of capsules to be used in controlled cooling methods. Viability of cells post cryo-preservation should be conducted to learn if the bone grafts are suitable for storage and future use.

Chapter 6 : Future Directions for Making Ex-vivo Tissue Engineered Bone Grafts

Current concepts of making tissue engineered bone grafts incorporates osteoblast progenitor cells and a structural construct which serves a substrate for the cells to grow and also to withstand mechanical stresses experienced in a host bone in vivo. This study primarily investigates using Poly (l-lactic acid) as a material to fabricate a three-dimensional porous construct using thermally induced phase separation method. Human adipose stem cells were used as the progenitor cells due to their simple extraction procedures and abundant availability. Future studies should be conducted to study the structure-property out comes of scaffolds made using vials different shaped vials like UV-Transparent Spectrophotometry Cuvettes (VWR, TX, USA). Vials of smaller dimensions (5 - 6 mm diameter) would be a rational option as abundant cellular growth was observed in regions on the scaffolds nearest to the glass contact. However, using glass vials should be preferred over other materials for practical reasons. Using copper, aluminum or polystyrene had practical issues of removing the scaffold after lyophilization.

Other biodegradable, FDA approved polymer materials like poly (glycolic acid) (PGA), poly (lactic-co-glycolic acid) (PLGA), Polycaprolactone (PCL) should be used to make scaffolds adopting a similar procedure to study its structure-property results and bio-responsivity in terms of cellular growth and osteoinduction. Polymer-ceramic composite materials should be considered for future studies as ceramics compounds like hydroxyapatite and calcium phosphate cements would increase the mechanical strength of the scaffolds. A tricalcium phosphate compound (βTCP) was used in conjunction with PLLA/dioxane solution at varying concentrations (10:90, 30:70 and 40:60 (PLLA:dioxane)). Following lyophilization, βTCP was lost in an imprecise manner due to lack of fusion between PLLA and βTCP. Therefore, ideal methods of fusing such ceramic compounds with polymer materials should be designed before using thermally controlled phase

separation method for scaffold fabrication. Also, some of the other solvents for most polymers like benzene, chloroform and cyclohexane should be used to make scaffolds using controlled, thermally induced phase separation method to study its structure-property outcomes. High toxicity of chloroform and benzene are the concerning factors in the context of cellular growth and cytotoxicity.

The greatest challenge in conducting cellular experiments on an opaque thermoplastic substance is the high adherence of hASCs on the scaffold material. Trypsin (0.05%) had to be used in higher quantities (> 6 mL per hASC - scaffold composite) for longer duration (> 10 mins) to remove hASCs from the scaffold substrate, damaging majority of the cells in this process. Finding a more efficient way to extract hASCs from the scaffold without causing major artifacts in the structure would lead to the possibility of many specific and quantitative assays like flow cytometry, alamar blue based metabolic assay, accurate quantification of RNA and protein expression. For osteoinduction medium, 100nM of dexamethasone was used in this study. However, recent studies have reported using 10nM of dexamethasone with earlier induction of osteogenesis on mesenchymal stem cells. Therefore, the osteogenic experiments should be conducted with 10nM concentration of dexamethasone to comparatively study advancement of osteogenesis (earlier expression of calcification and osteoblast specific RNA).

Effects of cryo-preservation of tissue engineered bone grafts should be studied in future. Various cryoprotectants such as dimethyl sulfoxide (DMSO), Polyvinylpyrrolidone (PVP), ethylene glycol and glycerol. These experiments should be focused on calibrating a suitable time for cryopreservation after loading hASCs on scaffolds. Early cryopreservable hASCs - scaffold composites would be ideal for industry specific needs. Viability, cellular growth and Osteoinductive potential of hASCs/osteoblasts before and after cryopreservation should be

studied. Such bio responsive bone grafts, post cryopreservation would enable patients to create and store customized bone grafts from their own stem cells in case of future requirements. Thus, successfully tissue engineered, cryopreservable bone grafts would be a major clinical breakthrough in terms of treating large scale skeletal defects requiring external bone graft implantation.

References

[1] T. T. Roberts and A. J. Rosenbaum, "Bone grafts, bone substitutes and orthobiologics: The bridge between basic science and clinical advancements in fracture healing," *Organogenesis,* vol. 8, pp. 114-24, Oct 1 2012.

[2] A. M. Thabet, D. Paley, M. Kocaoglu, L. Eralp, J. E. Herzenberg, and O. N. Ergin, "Periosteal Grafting for Congenital Pseudarthrosis of the Tibia: A Preliminary Report," *Clin Orthop Relat Res,* vol. 466, pp. 2981-94, Dec 2008.

[3] J. Gao, J. E. Dennis, L. A. Solchaga, A. S. Awadallah, V. M. Goldberg, and A. I. Caplan, "Tissue-engineered fabrication of an osteochondral composite graft using rat bone marrow-derived mesenchymal stem cells," *Tissue Eng,* vol. 7, pp. 363-71, Aug 2001.

[4] S. Saber-Samandari and S. Saber-Samandari, "Biocompatible nanocomposite scaffolds based on copolymer-grafted chitosan for bone tissue engineering with drug delivery capability," *Mater Sci Eng C Mater Biol Appl,* vol. 75, pp. 721-732, Jun 01 2017.

[5] S. D. Pals and R. M. Wilkins, "Giant cell tumor of bone treated by curettage, cementation, and bone grafting," *Orthopedics,* vol. 15, pp. 703-708, 1992.

[6] C. M. Murphy, M. G. Haugh, and F. J. O'Brien, "The effect of mean pore size on cell attachment, proliferation and migration in collagen–glycosaminoglycan scaffolds for bone tissue engineering," *Biomaterials,* vol. 31, pp. 461-466, 2010.

[7] H. H. de Boer, "The history of bone grafts," *Clin Orthop Relat Res,* pp. 292-8, Jan 1988.

[8] W. G. De Long, Jr., T. A. Einhorn, K. Koval, M. McKee, W. Smith, R. Sanders, *et al.*, "Bone grafts and bone graft substitutes in orthopaedic trauma surgery. A critical analysis," *J Bone Joint Surg Am,* vol. 89, pp. 649-58, Mar 2007.

[9] P. V. Giannoudis, H. Dinopoulos, and E. Tsiridis, "Bone substitutes: An update," *Injury,* vol. 36, pp. S20-S27, 11// 2005.

[10] A. Sood, S. Chung, P. J. Therattil, and E. S. Lee, "Reconstruction of a Complex Metacarpal Shaft Fracture With Segmental Bone Loss Using Autologous Iliac Crest Bone Graft," *Eplasty,* vol. 15, 2015.

[11] E. Truumees and H. N. Herkowitz, "Alternatives to autologous bone harvest in spine surgery," *The University of Pennsylvania Orthopaedic Journal,* vol. 12, pp. 77-88, 1999.

[12] R. Dimitriou, G. I. Mataliotakis, A. G. Angoules, N. K. Kanakaris, and P. V. Giannoudis, "Complications following autologous bone graft harvesting from the iliac crest and using the RIA: a systematic review," *Injury,* vol. 42 Suppl 2, pp. S3-15, Sep 2011.

[13] A. Gupta, N. Kukkar, K. Sharif, B. J. Main, C. E. Albers, and I. S. El-Amin, "Bone graft substitutes for spine fusion: A brief review," *World J Orthop,* vol. 6, pp. 449-56, Jul 18 2015.

[14] O. N. Nagi, M. S. Dhillon, V. R. Reddy, and K. Mathur, "Comparison of formalin preserved bone allograft in the form of a paste and as bone chips in fresh femoral shaft fractures with comminution," *Singapore Med J,* vol. 38, pp. 62-7, Feb 1997.

[15] K. U. Lewandrowski, V. Rebmann, M. Passler, G. Schollmeier, A. Ekkernkamp, H. Grosse-Wilde, *et al.*, "Immune response to perforated and partially demineralized bone allografts," *J Orthop Sci,* vol. 6, pp. 545-55, 2001.

[16] W. C. McGarvey and W. G. Braly, "Bone graft in hindfoot arthrodesis: allograft vs autograft," *Orthopedics,* vol. 19, pp. 389-94, May 1996.

[17] D. W. Hutmacher, J. T. Schantz, C. X. F. Lam, K. C. Tan, and T. C. Lim, "State of the art and future directions of scaffold-based bone engineering from a biomaterials perspective," *Journal of Tissue Engineering and Regenerative Medicine,* vol. 1, pp. 245-260, 2007.

[18] M. Bohner, "Calcium orthophosphates in medicine: from ceramics to calcium phosphate cements," *Injury,* vol. 31, pp. D37-D47, 2000/12/01 2000.

[19] C. Rey, C. Combes, C. Drouet, and D. Grossin, "1.111 - Bioactive Ceramics: Physical Chemistry A2 - Ducheyne, Paul," in *Comprehensive Biomaterials*, ed Oxford: Elsevier, 2011, pp. 187-221.

[20] J. H. Welch and W. Gutt, "874. High-temperature studies of the system calcium oxide-phosphorus pentoxide," *Journal of the Chemical Society (Resumed),* pp. 4442-4444, 1961.

[21] J. E. Fleming, Jr., C. N. Cornell, and G. F. Muschler, "Bone cells and matrices in orthopedic tissue engineering," *Orthop Clin North Am,* vol. 31, pp. 357-74, Jul 2000.

[22] L. S. Pryor, E. Gage, C. J. Langevin, F. Herrera, A. D. Breithaupt, C. R. Gordon, *et al.*, "Review of Bone Substitutes," *Craniomaxillofac Trauma Reconstr,* vol. 2, pp. 151-60, Oct 2009.

[23] A. R. Vaccaro, "The role of the osteoconductive scaffold in synthetic bone graft," *Orthopedics,* vol. 25, pp. S571-S578, 2002.

[24] H. R. Ramay and M. Zhang, "Preparation of porous hydroxyapatite scaffolds by combination of the gel-casting and polymer sponge methods," *Biomaterials,* vol. 24, pp. 3293-3302, 2003/08/01/ 2003.

[25] T. Fukasawa, M. Ando, T. Ohji, and S. Kanzaki, "Synthesis of porous ceramics with complex pore structure by freeze-dry processing," *Journal of the American Ceramic Society,* vol. 84, pp. 230-232, 2001.

[26] B. Seal, T. Otero, and A. Panitch, "Polymeric biomaterials for tissue and organ regeneration," *Materials Science and Engineering: R: Reports,* vol. 34, pp. 147-230, 2001.

[27] H. Tian, Z. Tang, X. Zhuang, X. Chen, and X. Jing, "Biodegradable synthetic polymers: preparation, functionalization and biomedical application," *Progress in Polymer Science,* vol. 37, pp. 237-280, 2012.

[28] P. A. Gunatillake and R. Adhikari, "Biodegradable synthetic polymers for tissue engineering," *Eur Cell Mater,* vol. 5, pp. 1-16, 2003.

[29] O. Jeon, J. W. Rhie, I.-K. Kwon, J.-H. Kim, B.-S. Kim, and S.-H. Lee, "In vivo bone formation following transplantation of human adipose–derived stromal cells that are not differentiated osteogenically," *Tissue Engineering Part A,* vol. 14, pp. 1285-1294, 2008.

[30] J. C. Middleton and A. J. Tipton, "Synthetic biodegradable polymers as orthopedic devices," *Biomaterials,* vol. 21, pp. 2335-2346, 12/1/ 2000.

[31] D. Garlotta, "A literature review of poly (lactic acid)," *Journal of Polymers and the Environment,* vol. 9, pp. 63-84, 2001.

[32] K. Rezwan, Q. Z. Chen, J. J. Blaker, and A. R. Boccaccini, "Biodegradable and bioactive porous polymer/inorganic composite scaffolds for bone tissue engineering," *Biomaterials,* vol. 27, pp. 3413-3431, 6// 2006.

[33] A. S. Dunn, P. G. Campbell, and K. G. Marra, "The influence of polymer blend composition on the degradation of polymer/hydroxyapatite biomaterials," *Journal of Materials Science: Materials in Medicine,* vol. 12, pp. 673-677, 2001.

[34] J. Y. Yoo, J. M. Kim, K. S. Seo, Y. K. Jeong, H. B. Lee, and G. Khang, "Characterization of degradation behavior for PLGA in various pH condition by simple liquid chromatography method," *Bio-medical materials and engineering,* vol. 15, pp. 279-288, 2005.

[35] G. G. Pitt, M. M. Gratzl, G. L. Kimmel, J. Surles, and A. Sohindler, "Aliphatic polyesters II. The degradation of poly (DL-lactide), poly (ε-caprolactone), and their copolymers in vivo," *Biomaterials,* vol. 2, pp. 215-220, 1981/10/01 1981.

[36] J. Rich, T. Jaakkola, T. Tirri, T. Narhi, A. Yli-Urpo, and J. Seppala, "In vitro evaluation of poly(epsilon-caprolactone-co-DL-lactide)/ bioactive glass composites," *Biomaterials,* vol. 23, pp. 2143-50, May 2002.

[37] C. Martin, H. Winet, and J. Y. Bao, "Acidity near eroding polylactide-polyglycolide in vitro and in vivo in rabbit tibial bone chambers," *Biomaterials,* vol. 17, pp. 2373-80, Dec 1996.

[38] P. X. Ma and R. Langer, "Fabrication of biodegradable polymer foams for cell transplantation and tissue engineering," *Tissue engineering methods and protocols*, pp. 47-56, 1999.

[39] A. I. Cooper, "Polymer synthesis and processing using supercritical carbon dioxide," *Journal of Materials Chemistry*, vol. 10, pp. 207-234, 2000.

[40] H. Yoshimoto, Y. M. Shin, H. Terai, and J. P. Vacanti, "A biodegradable nanofiber scaffold by electrospinning and its potential for bone tissue engineering," *Biomaterials*, vol. 24, pp. 2077-82, May 2003.

[41] P. X. Ma, R. Zhang, G. Xiao, and R. Franceschi, "Engineering new bone tissue in vitro on highly porous poly(α-hydroxyl acids)/hydroxyapatite composite scaffolds," *Journal of Biomedical Materials Research*, vol. 54, pp. 284-293, 2001.

[42] J. Bredt, A. C. M. E. T. Fan, K. S. Lee, B. Pruitt, and P. Williams, "Dimensional Printing: Rapid Tooling and Prototypes Directly from CAD Representation."

[43] R. Giordano, B. Wu, S. Borland, L. Cima, E. Sachs, and M. Cima, "Mechanical properties of dense polylactic acid structures fabricated by three dimensional printing," *Journal of biomaterials science. Polymer edition*, vol. 8, pp. 63-75, 1995.

[44] Z. Xiong, Y. Yan, S. Wang, R. Zhang, and C. Zhang, "Fabrication of porous scaffolds for bone tissue engineering via low-temperature deposition," *Scripta Materialia*, vol. 46, pp. 771-776, 6/7/ 2002.

[45] D. Puppi, F. Chiellini, A. M. Piras, and E. Chiellini, "Polymeric materials for bone and cartilage repair," *Progress in Polymer Science*, vol. 35, pp. 403-440, 4// 2010.

[46] J. Rouwkema, N. C. Rivron, and C. A. van Blitterswijk, "Vascularization in tissue engineering," *Trends in Biotechnology*, vol. 26, pp. 434-441, 8// 2008.

[47] S. B. Sulaiman, T. K. Keong, C. H. Cheng, A. B. Saim, and R. B. Idrus, "Tricalcium phosphate/hydroxyapatite (TCP-HA) bone scaffold as potential candidate for the formation of tissue engineered bone," *Indian J Med Res*, vol. 137, pp. 1093-101, Jun 2013.

[48] M. Houmard, Q. Fu, M. Genet, E. Saiz, and A. P. Tomsia, "On the structural, mechanical, and biodegradation properties of HA/beta-TCP robocast scaffolds," *J Biomed Mater Res B Appl Biomater*, vol. 101, pp. 1233-42, Oct 2013.

[49] A. Macchetta, I. G. Turner, and C. R. Bowen, "Fabrication of HA/TCP scaffolds with a graded and porous structure using a camphene-based freeze-casting method," *Acta Biomater*, vol. 5, pp. 1319-27, May 2009.

[50] L. D. Harris, B. S. Kim, and D. J. Mooney, "Open pore biodegradable matrices formed with gas foaming," *J Biomed Mater Res*, vol. 42, pp. 396-402, Dec 05 1998.

[51] X. H. Zhu, L. Y. Lee, J. S. Jackson, Y. W. Tong, and C. H. Wang, "Characterization of porous poly(D,L-lactic-co-glycolic acid) sponges fabricated by supercritical CO2 gas-foaming method as a scaffold for three-dimensional growth of Hep3B cells," *Biotechnol Bioeng,* vol. 100, pp. 998-1009, Aug 1 2008.

[52] W. Chen, H. Zhou, M. Tang, M. D. Weir, C. Bao, and H. H. Xu, "Gas-foaming calcium phosphate cement scaffold encapsulating human umbilical cord stem cells," *Tissue Eng Part A,* vol. 18, pp. 816-27, Apr 2012.

[53] W. Thein-Han and H. H. Xu, "Prevascularization of a gas-foaming macroporous calcium phosphate cement scaffold via coculture of human umbilical vein endothelial cells and osteoblasts," *Tissue Eng Part A,* vol. 19, pp. 1675-85, Aug 2013.

[54] M. M. Castillo-Ortega, A. G. Montano-Figueroa, D. E. Rodriguez-Felix, G. Prado-Villegas, K. P. Pino-Ocano, M. J. Valencia-Cordova, *et al.*, "Preparation by coaxial electrospinning and characterization of membranes releasing (-) epicatechin as scaffold for tissue engineering," *Mater Sci Eng C Mater Biol Appl,* vol. 46, pp. 184-9, Jan 2015.

[55] Q. Yu, S. Xu, H. Zhang, L. Gu, Y. Xu, and F. Ko, "Structure-property relationship of regenerated spider silk protein nano/microfibrous scaffold fabricated by electrospinning," *J Biomed Mater Res A,* vol. 102, pp. 3828-37, Nov 2014.

[56] H. Lo, S. Kadiyala, S. E. Guggino, and K. W. Leong, "Poly(L-lactic acid) foams with cell seeding and controlled-release capacity," *J Biomed Mater Res,* vol. 30, pp. 475-84, Apr 1996.

[57] P. X. Ma, R. Zhang, G. Xiao, and R. Franceschi, "Engineering new bone tissue in vitro on highly porous poly(alpha-hydroxyl acids)/hydroxyapatite composite scaffolds," *J Biomed Mater Res,* vol. 54, pp. 284-93, Feb 2001.

[58] S. Lee, M. Porter, S. Wasko, G. Lau, P.-Y. Chen, E. E. Novitskaya, *et al.*, "Potential bone replacement materials prepared by two methods," in *MRS Proceedings*, 2012, pp. mrsf11-1418-mm06-02.

[59] X. Wang and Q. Ni, "Determination of cortical bone porosity and pore size distribution using a low field pulsed NMR approach," *J Orthop Res,* vol. 21, pp. 312-9, Mar 2003.

[60] S. M. Richardson, J. M. Curran, R. Chen, A. Vaughan-Thomas, J. A. Hunt, A. J. Freemont, *et al.*, "The differentiation of bone marrow mesenchymal stem cells into chondrocyte-like cells on poly-l-lactic acid (PLLA) scaffolds," *Biomaterials,* vol. 27, pp. 4069-4078, 2006/08/01/ 2006.

[61] T. Kokubo, H. M. Kim, and M. Kawashita, "Novel bioactive materials with different mechanical properties," *Biomaterials,* vol. 24, pp. 2161-75, Jun 2003.

[62] R. Amirfeyz and G. Bannister, "The effect of bone porosity on the shear strength of the bone-cement interface," *Int Orthop,* vol. 33, pp. 843-6, Jun 2009.

[63] V. I. Sikavitsas, J. S. Temenoff, and A. G. Mikos, "Biomaterials and bone mechanotransduction," *Biomaterials,* vol. 22, pp. 2581-2593, 10/1/ 2001.

[64] D. C. Tancred, B. A. McCormack, and A. J. Carr, "A synthetic bone implant macroscopically identical to cancellous bone," *Biomaterials,* vol. 19, pp. 2303-11, Dec 1998.

[65] P. V. Giannoudis, H. Dinopoulos, and E. Tsiridis, "Bone substitutes: an update," *Injury,* vol. 36, pp. S20-S27, 2005.

[66] S. V. Dorozhkin, "Self-setting calcium orthophosphate formulations: cements, concretes, pastes and putties," *International Journal of Materials and Chemistry,* vol. 1, pp. 1-48, 2011.

[67] N. Alonso, G. H. Risso, R. Denadai, and C. E. Raposo-Amaral, "Effect of maxillary alveolar reconstruction on nasal symmetry of cleft lip and palate patients: a study comparing iliac crest bone graft and recombinant human bone morphogenetic protein-2," *J Plast Reconstr Aesthet Surg,* vol. 67, pp. 1201-8, Sep 2014.

[68] H. Fan, Y. Hu, C. Zhang, X. Li, R. Lv, L. Qin, *et al.*, "Cartilage regeneration using mesenchymal stem cells and a PLGA–gelatin/chondroitin/hyaluronate hybrid scaffold," *Biomaterials,* vol. 27, pp. 4573-4580, 9// 2006.

[69] S. Lendeckel, A. Jödicke, P. Christophis, K. Heidinger, J. Wolff, J. K. Fraser, *et al.*, "Autologous stem cells (adipose) and fibrin glue used to treat widespread traumatic calvarial defects: case report," *Journal of Cranio-Maxillofacial Surgery,* vol. 32, pp. 370-373, 12// 2004.

[70] A. M. Reitsma and J. D. Moreno, "Ethical regulations for innovative surgery: the last frontier?1," *Journal of the American College of Surgeons,* vol. 194, pp. 792-801, 6// 2002.

[71] R. Geesala, N. Bar, N. R. Dhoke, P. Basak, and A. Das, "Porous polymer scaffold for on-site delivery of stem cells–protects from oxidative stress and potentiates wound tissue repair," *Biomaterials,* vol. 77, pp. 1-13, 2016.

[72] R. Geesala, N. Bar, N. R. Dhoke, P. Basak, and A. Das, "Data on bone marrow stem cells delivery using porous polymer scaffold," *Data Brief,* vol. 6, pp. 221-8, Mar 2016.

[73] V. I. Sikavitsas, G. N. Bancroft, and A. G. Mikos, "Formation of three-dimensional cell/polymer constructs for bone tissue engineering in a spinner flask and a rotating wall vessel bioreactor," *J Biomed Mater Res,* vol. 62, pp. 136-48, Oct 2002.

[74] J. A. Burdick and K. S. Anseth, "Photoencapsulation of osteoblasts in injectable RGD-modified PEG hydrogels for bone tissue engineering," *Biomaterials,* vol. 23, pp. 4315-4323, 11// 2002.

[75] K. Uematsu, K. Hattori, Y. Ishimoto, J. Yamauchi, T. Habata, Y. Takakura, *et al.*, "Cartilage regeneration using mesenchymal stem cells and a three-dimensional poly-lactic-glycolic acid (PLGA) scaffold," *Biomaterials,* vol. 26, pp. 4273-4279, 7// 2005.

[76] H. J. Shin, C. H. Lee, I. H. Cho, Y. J. Kim, Y. J. Lee, I. A. Kim, *et al.*, "Electrospun PLGA nanofiber scaffolds for articular cartilage reconstruction: mechanical stability, degradation and cellular responses under mechanical stimulation in vitro," *J Biomater Sci Polym Ed,* vol. 17, pp. 103-19, 2006.

[77] Y.-C. Wu, S.-Y. Shaw, H.-R. Lin, T.-M. Lee, and C.-Y. Yang, "Bone tissue engineering evaluation based on rat calvaria stromal cells cultured on modified PLGA scaffolds," *Biomaterials,* vol. 27, pp. 896-904, 2// 2006.

[78] T. Ren, J. Ren, X. Jia, and K. Pan, "The bone formation in vitro and mandibular defect repair using PLGA porous scaffolds," *Journal of Biomedical Materials Research Part A,* vol. 74A, pp. 562-569, 2005.

[79] S. H. Oh, S. G. Kang, and J. H. Lee, "Degradation behavior of hydrophilized PLGA scaffolds prepared by melt-molding particulate-leaching method: Comparison with control hydrophobic one," *Journal of Materials Science: Materials in Medicine,* vol. 17, pp. 131-137, 2006.

[80] H. W. Ouyang, J. C. H. Goh, X. M. Mo, S. H. Teoh, and E. H. Lee, "The Efficacy of Bone Marrow Stromal Cell-Seeded Knitted PLGA Fiber Scaffold for Achilles Tendon Repair," *Annals of the New York Academy of Sciences,* vol. 961, pp. 126-129, 2002.

[81] J. Y. Kim and D.-W. Cho, "Blended PCL/PLGA scaffold fabrication using multi-head deposition system," *Microelectronic Engineering,* vol. 86, pp. 1447-1450, 4// 2009.

[82] Y. Zhang, F. Yang, K. Liu, H. Shen, Y. Zhu, W. Zhang, *et al.*, "The impact of PLGA scaffold orientation on in vitro cartilage regeneration," *Biomaterials,* vol. 33, pp. 2926-2935, 4// 2012.

[83] H. D. Kim, E. H. Bae, I. C. Kwon, R. R. Pal, J. D. Nam, and D. S. Lee, "Effect of PEG–PLLA diblock copolymer on macroporous PLLA scaffolds by thermally induced phase separation," *Biomaterials,* vol. 25, pp. 2319-2329, 5// 2004.

[84] H. H. Ahn, K. S. Kim, J. H. Lee, J. Y. Lee, B. S. Kim, I. W. Lee, *et al.*, "In vivo osteogenic differentiation of human adipose-derived stem cells in an injectable in situ–forming gel scaffold," *Tissue Engineering Part A,* vol. 15, pp. 1821-1832, 2009.

[85] X. Chen, S. E. Gleeson, T. Yu, N. Khan, R. W. Yucha, M. Marcolongo, *et al.*, "Hierarchically Ordered Polymer Nanofiber Shish Kebabs as a Bone Scaffold Material," *J Biomed Mater Res A,* Feb 15 2017.

[86] Y. Chen, A. F. T. Mak, M. Wang, J. Li, and M. S. Wong, "PLLA scaffolds with biomimetic apatite coating and biomimetic apatite/collagen composite coating to enhance osteoblast-like cells attachment and activity," *Surface and Coatings Technology,* vol. 201, pp. 575-580, 10/5/ 2006.

[87] S. S. Liao, F. Z. Cui, W. Zhang, and Q. L. Feng, "Hierarchically biomimetic bone scaffold materials: Nano-HA/collagen/PLA composite," *Journal of Biomedical Materials Research Part B: Applied Biomaterials,* vol. 69B, pp. 158-165, 2004.

[88] M. Bokhari, M. Birch, and G. Akay, "Polyhipe polymer: a novel scaffold for in vitro bone tissue engineering," *Adv Exp Med Biol,* vol. 534, pp. 247-54, 2003.

[89] J.-T. Schantz, A. Brandwood, D. W. Hutmacher, H. L. Khor, and K. Bittner, "Osteogenic differentiation of mesenchymal progenitor cells in computer designed fibrin-polymer-ceramic scaffolds manufactured by fused deposition modeling," *Journal of Materials Science: Materials in Medicine,* vol. 16, pp. 807-819, 2005.

[90] S.-S. Kim, M. Sun Park, O. Jeon, C. Yong Choi, and B.-S. Kim, "Poly(lactide-co-glycolide)/hydroxyapatite composite scaffolds for bone tissue engineering," *Biomaterials,* vol. 27, pp. 1399-1409, 3// 2006.

[91] Y. H. Lee, J. H. Lee, I.-G. An, C. Kim, D. S. Lee, Y. K. Lee, *et al.*, "Electrospun dual-porosity structure and biodegradation morphology of Montmorillonite reinforced PLLA nanocomposite scaffolds," *Biomaterials,* vol. 26, pp. 3165-3172, 6// 2005.

[92] G. Wei and P. X. Ma, "Structure and properties of nano-hydroxyapatite/polymer composite scaffolds for bone tissue engineering," *Biomaterials,* vol. 25, pp. 4749-4757, 8// 2004.

[93] Y. S. Nam and T. G. Park, "Porous biodegradable polymeric scaffolds prepared by thermally induced phase separation," *Journal of biomedical materials research,* vol. 47, pp. 8-17, 1999.

[94] P. Van de Witte, P. Dijkstra, J. Van den Berg, and J. Feijen, "Phase separation processes in polymer solutions in relation to membrane formation," *Journal of Membrane Science,* vol. 117, pp. 1-31, 1996.

[95] R. Bansil and G. Liao, "Kinetics of spinodal decomposition in homopolymer: Solutions and gels," *Trends in polymer science,* vol. 5, pp. 146-154, 1997.

[96] J. Mulder, *Basic principles of membrane technology*: Springer Science & Business Media, 2012.

[97] Y. Zhang, F. Yang, K. Liu, H. Shen, Y. Zhu, W. Zhang, *et al.*, "The impact of PLGA scaffold orientation on in vitro cartilage regeneration," *Biomaterials,* vol. 33, pp. 2926-2935, 2012.

[98] H. Do Kim, E. H. Bae, I. C. Kwon, R. R. Pal, J. Do Nam, and D. S. Lee, "Effect of PEG–PLLA diblock copolymer on macroporous PLLA scaffolds by thermally induced phase separation," *Biomaterials*, vol. 25, pp. 2319-2329, 2004.

[99] X. Liu and P. X. Ma, "Polymeric scaffolds for bone tissue engineering," 2004.

[100] V. La Carrubba, F. C. Pavia, V. Brucato, and S. Piccarolo, "PLLA/PLA scaffolds prepared via Thermally Induced Phase Separation (TIPS): tuning of properties and biodegradability," *International Journal of Material Forming,* vol. 1, pp. 619-622, 2008.

[101] F. J. Hua, G. E. Kim, J. D. Lee, Y. K. Son, and D. S. Lee, "Macroporous poly(L-lactide) scaffold 1. Preparation of a macroporous scaffold by liquid–liquid phase separation of a PLLA–dioxane–water system," *Journal of Biomedical Materials Research,* vol. 63, pp. 161-167, 2002.

[102] Q. L. Loh and C. Choong, "Three-dimensional scaffolds for tissue engineering applications: role of porosity and pore size," *Tissue Eng Part B Rev,* vol. 19, pp. 485-502, Dec 2013.

[103] A. G. Mikos, A. J. Thorsen, L. A. Czerwonka, Y. Bao, R. Langer, D. N. Winslow, *et al.*, "Preparation and characterization of poly(l-lactic acid) foams," *Polymer*, vol. 35, pp. 1068-1077, 1994/03/01 1994.

[104] R. C. Thomson, M. J. Yaszemski, J. M. Powers, and A. G. Mikos, "Fabrication of biodegradable polymer scaffolds to engineer trabecular bone," *J Biomater Sci Polym Ed,* vol. 7, pp. 23-38, 1995.

[105] L. D. Harris, B.-S. Kim, and D. J. Mooney, "Open pore biodegradable matrices formed with gas foaming," *Journal of Biomedical Materials Research,* vol. 42, pp. 396-402, 1998.

[106] D. J. Mooney, D. F. Baldwin, N. P. Suh, J. P. Vacanti, and R. Langer, "Novel approach to fabricate porous sponges of poly(d,l-lactic-co-glycolic acid) without the use of organic solvents," *Biomaterials,* vol. 17, pp. 1417-1422, 1996/07/01 1996.

[107] E. D. Boland, G. E. Wnek, D. G. Simpson, K. J. Pawlowski, and G. L. Bowlin, "TAILORING TISSUE ENGINEERING SCAFFOLDS USING ELECTROSTATIC PROCESSING TECHNIQUES: A STUDY OF POLY(GLYCOLIC ACID) ELECTROSPINNING," *Journal of Macromolecular Science, Part A,* vol. 38, pp. 1231-1243, 2001/11/30 2001.

[108] A. Moheman, M. S. Alam, and A. Mohammad, "Recent trends in electrospinning of polymer nanofibers and their applications in ultra thin layer chromatography," *Advances in Colloid and Interface Science,* vol. 229, pp. 1-24, 3// 2016.

[109] H. Lo, S. Kadiyala, S. Guggino, and K. Leong, "Poly (L-lactic acid) foams with cell seeding and controlled-release capacity," *Journal of Biomedical Materials Research Part A,* vol. 30, pp. 475-484, 1996.

[110] C. Schugens, V. Maquet, C. Grandfils, R. Jerome, and P. Teyssie, "Polylactide macroporous biodegradable implants for cell transplantation. II. Preparation of polylactide foams by liquid-liquid phase separation," *J Biomed Mater Res,* vol. 30, pp. 449-61, Apr 1996.

[111] S. F. Hulbert, S. J. Morrison, and J. J. Klawitter, "Tissue reaction to three ceramics of porous and non-porous structures," *J Biomed Mater Res,* vol. 6, pp. 347-74, Sep 1972.

[112] S. J. Hollister, "Porous scaffold design for tissue engineering," *Nat Mater,* vol. 4, pp. 518-24, Jul 2005.

[113] C. Y. Lin, N. Kikuchi, and S. J. Hollister, "A novel method for biomaterial scaffold internal architecture design to match bone elastic properties with desired porosity," *J Biomech,* vol. 37, pp. 623-36, May 2004.

[114] J. W. Lee, K. J. Kim, K. S. Kang, S. Chen, J. W. Rhie, and D. W. Cho, "Development of a bone reconstruction technique using a solid free-form fabrication (SFF)-based drug releasing scaffold and adipose-derived stem cells," *J Biomed Mater Res A,* vol. 101, pp. 1865-75, Jul 2013.

[115] Y. Liu, H. Cui, X. Zhuang, Y. Wei, and X. Chen, "Electrospinning of aniline pentamer-graft-gelatin/PLLA nanofibers for bone tissue engineering," *Acta Biomater,* vol. 10, pp. 5074-80, Dec 2014.

[116] R. Inai, M. Kotaki, and S. Ramakrishna, "Structure and properties of electrospun PLLA single nanofibres," *Nanotechnology,* vol. 16, pp. 208-13, Feb 2005.

[117] A. Moheman, M. S. Alam, and A. Mohammad, "Recent trends in electrospinning of polymer nanofibers and their applications in ultra thin layer chromatography," *Adv Colloid Interface Sci,* Dec 17 2015.

[118] H. Sun, F. Ye, J. Wang, Y. Shi, Z. Tu, J. Bao, *et al.*, "The upregulation of osteoblast marker genes in mesenchymal stem cells prove the osteoinductivity of hydroxyapatite/tricalcium phosphate biomaterial," *Transplant Proc,* vol. 40, pp. 2645-8, Oct 2008.

[119] J. Will, R. Melcher, C. Treul, N. Travitzky, U. Kneser, E. Polykandriotis, *et al.*, "Porous ceramic bone scaffolds for vascularized bone tissue regeneration," *J Mater Sci Mater Med,* vol. 19, pp. 2781-90, Aug 2008.

[120] A. Asti, G. Gastaldi, R. Dorati, E. Saino, B. Conti, L. Visai, *et al.*, "Stem Cells Grown in Osteogenic Medium on PLGA, PLGA/HA, and Titanium Scaffolds for Surgical Applications," *Bioinorg Chem Appl,* p. 831031, 2010.

[121] J. Y. Kim, T. J. Lee, D. W. Cho, and B. S. Kim, "Solid free-form fabrication-based PCL/HA scaffolds fabricated with a multi-head deposition system for bone tissue engineering," *J Biomater Sci Polym Ed,* vol. 21, pp. 951-62, 2010.

[122] L. Baldino, F. Naddeo, S. Cardea, A. Naddeo, and E. Reverchon, "FEM modeling of the reinforcement mechanism of Hydroxyapatite in PLLA scaffolds produced by supercritical drying, for Tissue Engineering applications," *J Mech Behav Biomed Mater,* vol. 51, pp. 225-36, Nov 2015.

[123] L. Budyanto, Y. Q. Goh, and C. P. Ooi, "Fabrication of porous poly(L-lactide) (PLLA) scaffolds for tissue engineering using liquid-liquid phase separation and freeze extraction," *J Mater Sci Mater Med,* vol. 20, pp. 105-11, Jan 2009.

[124] S. Cardea, L. Baldino, P. Pisanti, and E. Reverchon, "3-D PLLA scaffolds formation by a supercritical freeze extraction assisted process," *J Mater Sci Mater Med,* vol. 25, pp. 355-62, Feb 2014.

[125] P. C. Chang, B. Y. Liu, C. M. Liu, H. H. Chou, M. H. Ho, H. C. Liu, *et al.*, "Bone tissue engineering with novel rhBMP2-PLLA composite scaffolds," *J Biomed Mater Res A,* vol. 81, pp. 771-80, Jun 15 2007.

[126] L. He, B. Liu, G. Xipeng, G. Xie, S. Liao, D. Quan, *et al.*, "Microstructure and properties of nano-fibrous PCL-b-PLLA scaffolds for cartilage tissue engineering," *Eur Cell Mater,* vol. 18, pp. 63-74, 2009.

[127] J. Hu, X. Sun, H. Ma, C. Xie, Y. E. Chen, and P. X. Ma, "Porous nanofibrous PLLA scaffolds for vascular tissue engineering," *Biomaterials,* vol. 31, pp. 7971-7, Nov 2010.

[128] L. Lazzeri, M. G. Cascone, S. Danti, L. P. Serino, S. Moscato, and N. Bernardini, "Gelatine/PLLA sponge-like scaffolds: morphological and biological characterization," *J Mater Sci Mater Med,* vol. 18, pp. 1399-405, Jul 2007.

[129] Y. H. Lee, J. H. Lee, I. G. An, C. Kim, D. S. Lee, Y. K. Lee, *et al.*, "Electrospun dual-porosity structure and biodegradation morphology of Montmorillonite reinforced PLLA nanocomposite scaffolds," *Biomaterials,* vol. 26, pp. 3165-72, Jun 2005.

[130] C. Vaquette, C. Frochot, R. Rahouadj, and X. Wang, "An innovative method to obtain porous PLLA scaffolds with highly spherical and interconnected pores," *J Biomed Mater Res B Appl Biomater,* vol. 86, pp. 9-17, Jul 2008.

[131] B. M. Whited, J. R. Whitney, M. C. Hofmann, Y. Xu, and M. N. Rylander, "Pre-osteoblast infiltration and differentiation in highly porous apatite-coated PLLA electrospun scaffolds," *Biomaterials,* vol. 32, pp. 2294-304, Mar 2011.

[132] J. O. Hollinger, "Preliminary report on the osteogenic potential of a biodegradable copolymer of polyactide (PLA) and polyglycolide (PGA)," *J Biomed Mater Res,* vol. 17, pp. 71-82, Jan 1983.

[133] Y. S. Liu, Q. L. Huang, A. Kienzle, W. E. Muller, and Q. L. Feng, "In vitro degradation of porous PLLA/pearl powder composite scaffolds," *Mater Sci Eng C Mater Biol Appl,* vol. 38, pp. 227-34, May 1 2014.

[134] M. Therin, P. Christel, S. Li, H. Garreau, and M. Vert, "In vivo degradation of massive poly(alpha-hydroxy acids): validation of in vitro findings," *Biomaterials,* vol. 13, pp. 594-600, 1992.

[135] M. Vert, J. Mauduit, and S. Li, "Biodegradation of PLA/GA polymers: increasing complexity," *Biomaterials,* vol. 15, pp. 1209-13, Dec 1994.

[136] D. F. Williams and E. Mort, "Enzyme-accelerated hydrolysis of polyglycolic acid," *J Bioeng,* vol. 1, pp. 231-8, Aug 1977.

[137] A. M. Ng, K. K. Tan, M. Y. Phang, O. Aziyati, G. H. Tan, M. R. Isa, *et al.*, "Differential osteogenic activity of osteoprogenitor cells on HA and TCP/HA scaffold of tissue engineered bone," *J Biomed Mater Res A,* vol. 85, pp. 301-12, May 2008.

[138] C. Schopper, F. Ziya-Ghazvini, W. Goriwoda, D. Moser, F. Wanschitz, E. Spassova, *et al.*, "HA/TCP compounding of a porous CaP biomaterial improves bone formation and scaffold degradation--a long-term histological study," *J Biomed Mater Res B Appl Biomater,* vol. 74, pp. 458-67, Jul 2005.

[139] Y. S. Nam and T. G. Park, "Porous biodegradable polymeric scaffolds prepared by thermally induced phase separation," *J Biomed Mater Res,* vol. 47, pp. 8-17, Oct 1999.

[140] K. Rezwan, Q. Z. Chen, J. J. Blaker, and A. R. Boccaccini, "Biodegradable and bioactive porous polymer/inorganic composite scaffolds for bone tissue engineering," *Biomaterials,* vol. 27, pp. 3413-31, Jun 2006.

[141] W. R. Krause, W. Krug, and J. Miller, "Strength of the cement-bone interface," *Clin Orthop Relat Res,* pp. 290-9, Mar 1982.

[142] K. A. Mann, D. C. Ayers, F. W. Werner, R. J. Nicoletta, and M. D. Fortino, "Tensile strength of the cement-bone interface depends on the amount of bone interdigitated with PMMA cement," *J Biomech,* vol. 30, pp. 339-46, Apr 1997.

[143] K. Rezwan, Q. Chen, J. Blaker, and A. R. Boccaccini, "Biodegradable and bioactive porous polymer/inorganic composite scaffolds for bone tissue engineering," *Biomaterials,* vol. 27, pp. 3413-3431, 2006.

[144] T. Albrektsson and C. Johansson, "Osteoinduction, osteoconduction and osseointegration," *Eur Spine J,* vol. 10 Suppl 2, pp. S96-101, Oct 2001.

[145] R. L. Barrack, "Bone graft extenders, substitutes, and osteogenic proteins," *J Arthroplasty,* vol. 20, pp. 94-7, Jun 2005.

[146] P. A. Gunatillake and R. Adhikari, "Biodegradable synthetic polymers for tissue engineering," *Eur Cell Mater,* vol. 5, pp. 1-16; discussion 16, May 20 2003.

[147] T. Ren, J. Ren, X. Jia, and K. Pan, "The bone formation in vitro and mandibular defect repair using PLGA porous scaffolds," *J Biomed Mater Res A,* vol. 74, pp. 562-9, Sep 15 2005.

[148] Y. D. Halvorsen, D. Franklin, A. L. Bond, D. C. Hitt, C. Auchter, A. L. Boskey, *et al.*, "Extracellular matrix mineralization and osteoblast gene expression by human adipose tissue-derived stromal cells," *Tissue Eng,* vol. 7, pp. 729-41, Dec 2001.

[149] A. Sen, Y. R. Lea-Currie, D. Sujkowska, D. M. Franklin, W. O. Wilkison, Y. D. Halvorsen, *et al.*, "Adipogenic potential of human adipose derived stromal cells from multiple donors is heterogeneous," *J Cell Biochem,* vol. 81, pp. 312-9, Mar 26 2001.

[150] S. Thirumala, X. Wu, J. M. Gimble, and R. V. Devireddy, "Evaluation of polyvinylpyrrolidone as a cryoprotectant for adipose tissue-derived adult stem cells," *Tissue Eng Part C Methods,* vol. 16, pp. 783-92, Aug 2010.

[151] S. Thirumala, W. S. Goebel, and E. J. Woods, "Clinical grade adult stem cell banking," *Organogenesis,* vol. 5, pp. 143-54, Jul 2009.

[152] P. H. Ashjian, A. S. Elbarbary, B. Edmonds, D. DeUgarte, M. Zhu, P. A. Zuk, *et al.*, "In vitro differentiation of human processed lipoaspirate cells into early neural progenitors," *Plast Reconstr Surg,* vol. 111, pp. 1922-31, May 2003.

[153] H. A. Awad, M. Q. Wickham, H. A. Leddy, J. M. Gimble, and F. Guilak, "Chondrogenic differentiation of adipose-derived adult stem cells in agarose, alginate, and gelatin scaffolds," *Biomaterials,* vol. 25, pp. 3211-22, Jul 2004.

[154] D. A. De Ugarte, K. Morizono, A. Elbarbary, Z. Alfonso, P. A. Zuk, M. Zhu, *et al.*, "Comparison of multi-lineage cells from human adipose tissue and bone marrow," *Cells Tissues Organs,* vol. 174, pp. 101-9, 2003.

[155] J. Gimble and F. Guilak, "Adipose-derived adult stem cells: isolation, characterization, and differentiation potential," *Cytotherapy,* vol. 5, pp. 362-9, 2003.

[156] J. M. Gimble and M. E. Nuttall, "Bone and fat: old questions, new insights," *Endocrine*, vol. 23, pp. 183-8, Mar-Apr 2004.

[157] K. C. Hicok, T. V. Du Laney, Y. S. Zhou, Y. D. Halvorsen, D. C. Hitt, L. F. Cooper, *et al.*, "Human adipose-derived adult stem cells produce osteoid in vivo," *Tissue Eng*, vol. 10, pp. 371-80, Mar-Apr 2004.

[158] S. Lendeckel, A. Jodicke, P. Christophis, K. Heidinger, J. Wolff, J. K. Fraser, *et al.*, "Autologous stem cells (adipose) and fibrin glue used to treat widespread traumatic calvarial defects: case report," *J Craniomaxillofac Surg*, vol. 32, pp. 370-3, Dec 2004.

[159] H. Mizuno, P. A. Zuk, M. Zhu, H. P. Lorenz, P. Benhaim, and M. H. Hedrick, "Myogenic differentiation by human processed lipoaspirate cells," *Plast Reconstr Surg*, vol. 109, pp. 199-209; discussion 210-1, Jan 2002.

[160] K. M. Safford, K. C. Hicok, S. D. Safford, Y. D. Halvorsen, W. O. Wilkison, J. M. Gimble, *et al.*, "Neurogenic differentiation of murine and human adipose-derived stromal cells," *Biochem Biophys Res Commun*, vol. 294, pp. 371-9, Jun 7 2002.

[161] K. M. Safford, S. D. Safford, J. M. Gimble, A. K. Shetty, and H. E. Rice, "Characterization of neuronal/glial differentiation of murine adipose-derived adult stromal cells," *Exp Neurol*, vol. 187, pp. 319-28, Jun 2004.

[162] M. Q. Wickham, G. R. Erickson, J. M. Gimble, T. P. Vail, and F. Guilak, "Multipotent stromal cells derived from the infrapatellar fat pad of the knee," *Clin Orthop Relat Res*, pp. 196-212, Jul 2003.

[163] B. Barrilleaux, D. G. Phinney, D. J. Prockop, and K. C. O'Connor, "Review: ex vivo engineering of living tissues with adult stem cells," *Tissue Eng*, vol. 12, pp. 3007-19, Nov 2006.

[164] S. F. Kolle, A. Fischer-Nielsen, A. B. Mathiasen, J. J. Elberg, R. S. Oliveri, P. V. Glovinski, *et al.*, "Enrichment of autologous fat grafts with ex-vivo expanded adipose tissue-derived stem cells for graft survival: a randomised placebo-controlled trial," *Lancet*, vol. 382, pp. 1113-20, Sep 28 2013.

[165] A. Childs, U. D. Hemraz, N. J. Castro, H. Fenniri, and L. G. Zhang, "Novel biologically-inspired rosette nanotube PLLA scaffolds for improving human mesenchymal stem cell chondrogenic differentiation," *Biomed Mater*, vol. 8, p. 065003, Dec 2013.

[166] T. Ushida, K. Furukawa, K. Toita, and T. Tateishi, "Three-dimensional seeding of chondrocytes encapsulated in collagen gel into PLLA scaffolds," *Cell Transplant*, vol. 11, pp. 489-94, 2002.

[167] T. Albrektsson and C. Johansson, "Osteoinduction, osteoconduction and osseointegration," *European Spine Journal,* vol. 10, pp. S96-S101, 2001.

[168] P. Habibovic, U. Gbureck, C. J. Doillon, D. C. Bassett, C. A. van Blitterswijk, and J. E. Barralet, "Osteoconduction and osteoinduction of low-temperature 3D printed bioceramic implants," *Biomaterials,* vol. 29, pp. 944-953, 3// 2008.

[169] G. Daculsi, B. H. Fellah, T. Miramond, and M. Durand, "Osteoconduction, Osteogenicity, Osteoinduction, what are the fundamental properties for a smart bone substitutes," *IRBM,* vol. 34, pp. 346-348, 11// 2013.

[170] S. Fujibayashi, M. Neo, H.-M. Kim, T. Kokubo, and T. Nakamura, "Osteoinduction of porous bioactive titanium metal," *Biomaterials,* vol. 25, pp. 443-450, 2// 2004.

[171] Alfredo Pompili, Fabrizio Caroli, Livio Carpanese, Mauro Caterino, Laura Raus, Giancarlo Sestili, *et al.*, "Cranioplasty performed with a new osteoconductive, osteoinducing hydroxyapatite-derived material," *Journal of Neurosurgery*, vol. 89, pp. 236-242, 1998.

[172] M. Lievremont, J. Potus, and B. Guillou, "Use of alizarin red S for histochemical staining of Ca2+ in the mouse; some parameters of the chemical reaction in vitro," *Acta Anat (Basel),* vol. 114, pp. 268-80, 1982.

[173] H. Puchtler, S. N. Meloan, and M. S. Terry, "On the history and mechanism of alizarin and alizarin red S stains for calcium," *J Histochem Cytochem,* vol. 17, pp. 110-24, Feb 1969.

Vita

Harish Chinnasami is from the city of Coimbatore in the state of Tamil Nadu in India. He got his matriculation and higher secondary education in Carmel Garden Matriculation Higher Secondary School in Coimbatore. He was accepted by Anna University, Tamil Nadu, India to purse Bachelor of Engineering in Mechanical Engineering major based on meritorious credit in high school and Tamil Nadu Professional Courses Entrance Examination. He worked as a part-time lecturer at Government Polytechnic College, Coimbatore from the period of October 2009 to June 2010. In August 2010, he was accepted by Louisiana State university to pursue Masters in mechanical Engineering. Due to his interests in pursuing a research career and high academic standing he was accepted to pursue Doctoral program in Mechanical Engineering at LSU in June 2011. He is interested in pursuing a research oriented career in the field of biomechanics in the future. He intends to use his knowledge and experience gained during his doctoral program to provide productive contribution to real-life applications. He plays tennis as a recreation and has a passion for baking homemade pizza. He is an ardent fan of classical music and a beginner in playing violin.